A Density Functional Theory Study of the Structure and Chemistry of Zeolite Linde Type A (LTA)

A Major Qualifying Project:

Submitted to the Faculty

Of the

WORCESTER POLYTECHNIC INSTITUTE

in partial fulfillment of the requirements for the

Degree of Bachelor of Science

by

<student signature>

Junbo Chen

Date: May 17th 2017

Approved:

Professor N. Aaron Deskins

Abstract

Zeolites have been widely applied in several industries: water purification, catalysis, and hazardous containment. These aluminosilicate minerals (composed of Al, Si and O) possess micro-porous structures, which allow processes such as filtration, size-selective catalysis, and ion exchange. Zeolite LTA (Linde Type A) has three different sized pore windows and is the focus of this work. Via density functional theory, computational simulations were performed to model the effect of different cation substitutions. One of the objectives of this research was to determine the change in structure and chemistry when substituting the pure Si-O composition with Na^{+}/Al^{3+}, K^{+}/Al^{3+}, H^{+}/Al^{3+}, and Ca^{2+}/Al^{3+}, in Si/Al ratios of 23, 3 and 1. Pore sizes for the three pore windows were also calculated to determine the effect of different cations on molecular diffusion through the pores. Another objective of this research was to determine the most stable, i.e. lowest energy, positioning and sites for various cations. This project also investigated the adsorption of alkane and alcohol after entering the pore. The results of these simulations will shed some light on LTA zeolites as catalysts and ion-exchangers.

Table of Contents

List of Figures

List of Tables

1 Introduction

Zeolites, discovered in 1765 by a Swedish mineralogist Freidrich Axel Cronstedt, have been studied by chemists and chemical engineers ever since. With their microporous structures, zeolites were first discovered to adsorb large amount of steam from water. These microporous minerals are composed of aluminum silicate. Many zeolites occur as natural minerals, but it is the synthetic varieties which are among the most widely used sorbents, catalysts and ion-exchange materials in the world.(Cundy & Cox, 2003) When tested with different materials, zeolites were found to be able to filter and adsorb molecules. Various applications of zeolites were then devised: water purifier, catalysts, catalyst support, and laundry detergent additives. In 1992, 5.5 million tons of Zeolite A was consumed in Europe.(Fawer, Postlethwaite, & Klüppel, 1998) The effectiveness of zeolites has a direct impact on people's standard of living. Water purifiers, such as BRITA®, contain activated carbon and zeolites in a compressed block that reduces the water's Chlorine and Lead("Brita Natural Water Filtration Process," 2017). Zeolites can remove the odor and metal ions from tap water and improve the quality of water.

As of September 2016, 232 unique zeolite frameworks have been studied, 40 are naturally formed, whereas most of the rest are synthesized("Database of Zeolite Structures," 2017). Due to the microporous nature of zeolites, zeolites can accommodate various cations such as sodium, potassium, calcium, magnesium, etc. When substituting these cations into a specific zeolite framework, the structure of this zeolite is altered and will have different physical properties compared to before substitution.

In the 1960s, Nobel Prize winner Laurent Walter Kohn and colleagues developed density functional theory (DFT). DFT allows computational simulations to be performed on molecules in cooperation with computers. DFT therefore could shed new light onto the discovery of zeolite frameworks. DFT has become an essential tool for scientists to study the behaviors of various molecular structures.

This research is dedicated to the study of the behavior of zeolite framework LTA (Linde Type A). With the simulations generated by CP2K, a DFT program, LTA was studied for its structural change after substituting cations into the pure aluminum silicate zeolite framework. The pore openings on each site of the framework surface are determined to estimate the size of molecules that can be adsorbed into LTA's "supercage" structure. Various molecules are inserted into LTA to simulate their interaction to LTA and its cation derivatives.

2 Background

The background section includes knowledge that is essential to fully understand the goal and approach of this study. This chapter will introduce zeolite modeling, application, and density functional theory.

2.1 Zeolite synthesis

For zeolites that are not naturally formed, zeolite synthesis can lead to a vast variation in structure and composition, and therefore the function in adsorption and catalysis. According to a review by Cundy & Cox (2003), for aluminosilicate zeolites, the synthesis is usually developed under hydrothermal conditions from reactive gels in alkaline media at temperatures between 80 and 200 °C. In the 1960s, increasing use was made of organic compounds, such as quaternary ammonium salts. These salts become a template for zeolite synthesis because the zeolite structure appears to form around them. However, for quaternary salts, which also act as charge-balancing cations, the templates impose a restriction on the framework's charge density, resulting in products of increased Si/Al ratio (the ratio of silicon atom to aluminum). For most high-silica zeolites (Si/Al > 10), the organic templates must be removed in order to produce the open-pore materials for sorption and catalysis(Cundy & Cox, 2003).

In this study, the effect of varying Si/Al ratio will be examined, as such a parameter can vary during the synthesis of aluminosilicate zeolites. In Cundy & Cox's review, crystal growth rates tend to decrease as the Si/Al ratio increases so that the short preparation times (minutes to hours) become extended for the high-silica materials (hours to

days)(Cundy & Cox, 2003). By understanding the structures of zeolites, we can better understand the effect of zeolite's Si/Al ratio, which will directly affect the practicality of the zeolite synthesis.

2.2 Zeolite uses

After its discovery, zeolites have been widely applied in industries such as water purification and petroleum industry. The porous structure of zeolites allows selective activity of particular molecules in ion exchange and catalysis. The channels and cavities in zeolites can effectively lead to adsorption of the exchanging molecules.

2.2.1 Ion exchange and water softening

In water purification processes, a common application for zeolite is water softening. Zeolites for these applications will have lower charged cation, such as sodium (+1 charge). When zeolite exchanges with hard water (water with high mineral content, mostly caused by the existence of calcium), calcium's higher charge (+2 charge) will tend to displace the existing sodium that is located in the cage structure of the zeolite. Note that the sodium does not belong to the ring structure of the zeolite, as will be explained in section 2.3.1 of this paper. In Figure 1, the calcium ion in water, after exchange with sodium-exchanged

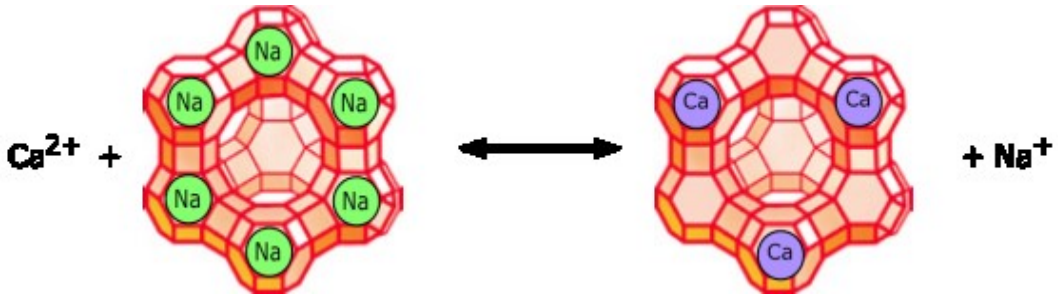

Figure 1 - An illustration shows the ion exchange between calcium ion in water and zeolite (Lower, 2013).

zeolite, is trapped in the zeolite. The sodium ion is released, which effectively removes the element that causes the hard water (the removal of the water's calcium).

2.2.2 Catalytic cracking

Cracking is the process in breaking up large hydrocarbon molecules into smaller and useful molecules. Without a catalyst, this process is often achieved with high pressures and temperatures, which makes the cracking process cost-inefficient. The main components in crude oil consist of large hydrocarbons. Cracking cuts a long carbon chain into smaller ones; for example, in Figure 2, it shows a linear chain of hydrocarbon ($C_{15}H_{32}$) being broken into a variety of different products such as double-bond alkenes, which are the byproducts from natural gas and crude oil cracking. Ethene[1] is the most important organic feedstock in the

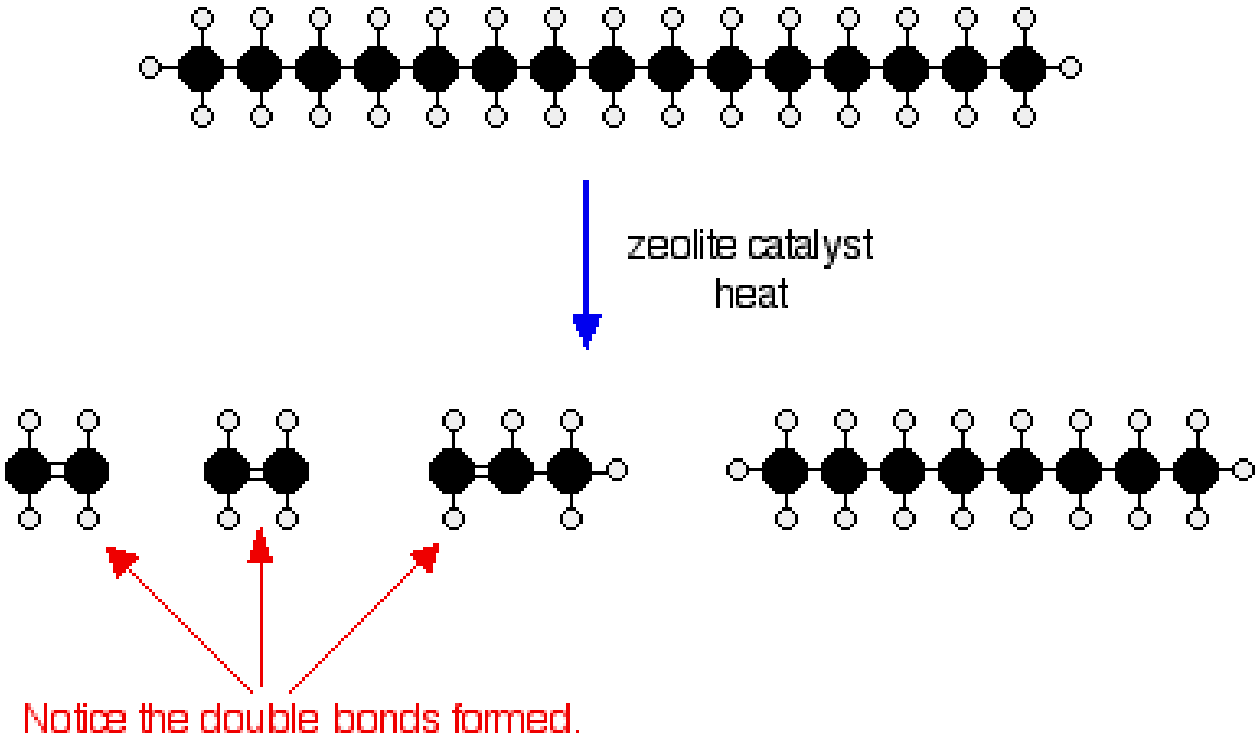

Figure 2 - An illustration of $C_{15}H_{32}$ in a cracking process by a zeolite catalyst and heat, producing smaller hydrocarbons, such as ethene, propene and octane. (Clark, 2002)

[1] Also known as ethylene.

chemical industry and in 2011 is approximately produced at 141 million metric tons worldwide, second in tonnage after sulfuric acid(True, 2012).

In a modern cracking process, cracking uses zeolites as catalysts. Zeolite catalysts have the advantage of removing hydrogen from alkanes at the zeolite's reaction sites (also known as the acidic sites, which will be introduced in section 2.4.2). In Figure 3, after interaction with the zeolite catalyst, the hydrocarbon forms a transition state (TS) which is a positive ion (carbocation) formed. As mentioned in Clark's introduction on zeolite catalysis, the operating conditions are usually at a temperature of about 500°C and relatively low pressures. This transition state will lead to the reorganization of the hydrocarbon chain and therefore creates various products. The zeolites used in catalytic cracking usually give high yields of hydrocarbons with between 5 and 10 carbon atoms, which is particularly useful for gasoline, and it produces branched alkanes and aromatics, such as benzene(J. Clark, 2002).

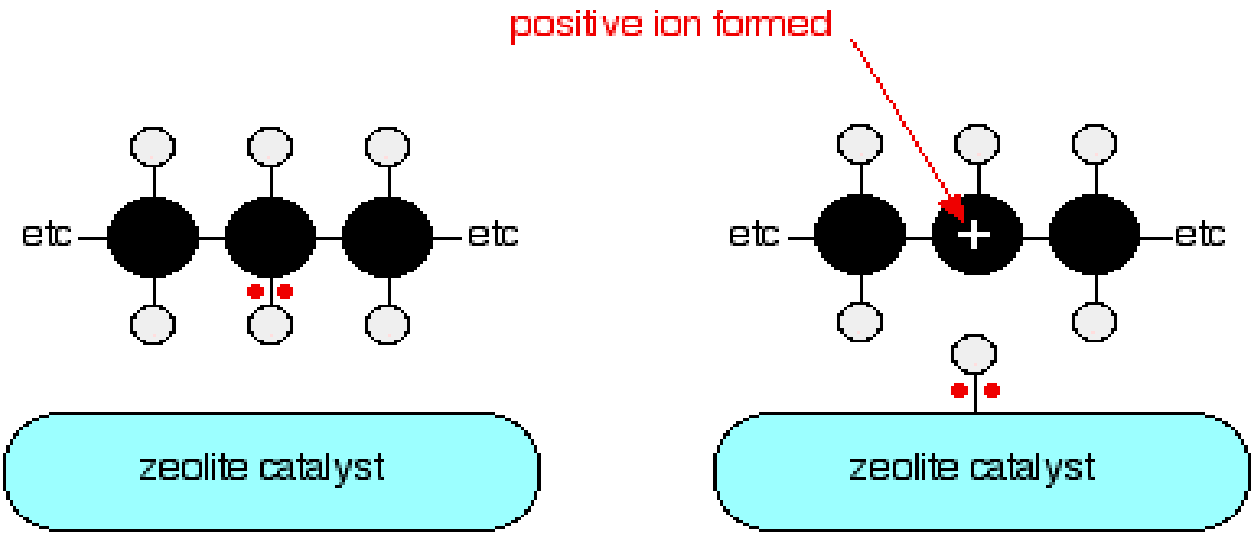

Figure 3 - An illustration showing alkane interacts with zeolite catalyst. The interaction leads to a positive ion formed on the alkane, which will lead to the formation of other products via reorganization(Clark, 2002).

2.3 Zeolite properties

Zeolites are commonly used for adsorbents. Due to their porous structures, zeolites allow various types of ion exchanges to occur within. After exchanged with positive ions such as sodium, potassium, calcium, etc., zeolites can form acid sites (Brønsted or hydrogen substitution) based on the charges exchanged. The structures of mesoporous zeolites are usually differentiated by geometries of aluminosilicate's arrangement. As of March 2017,

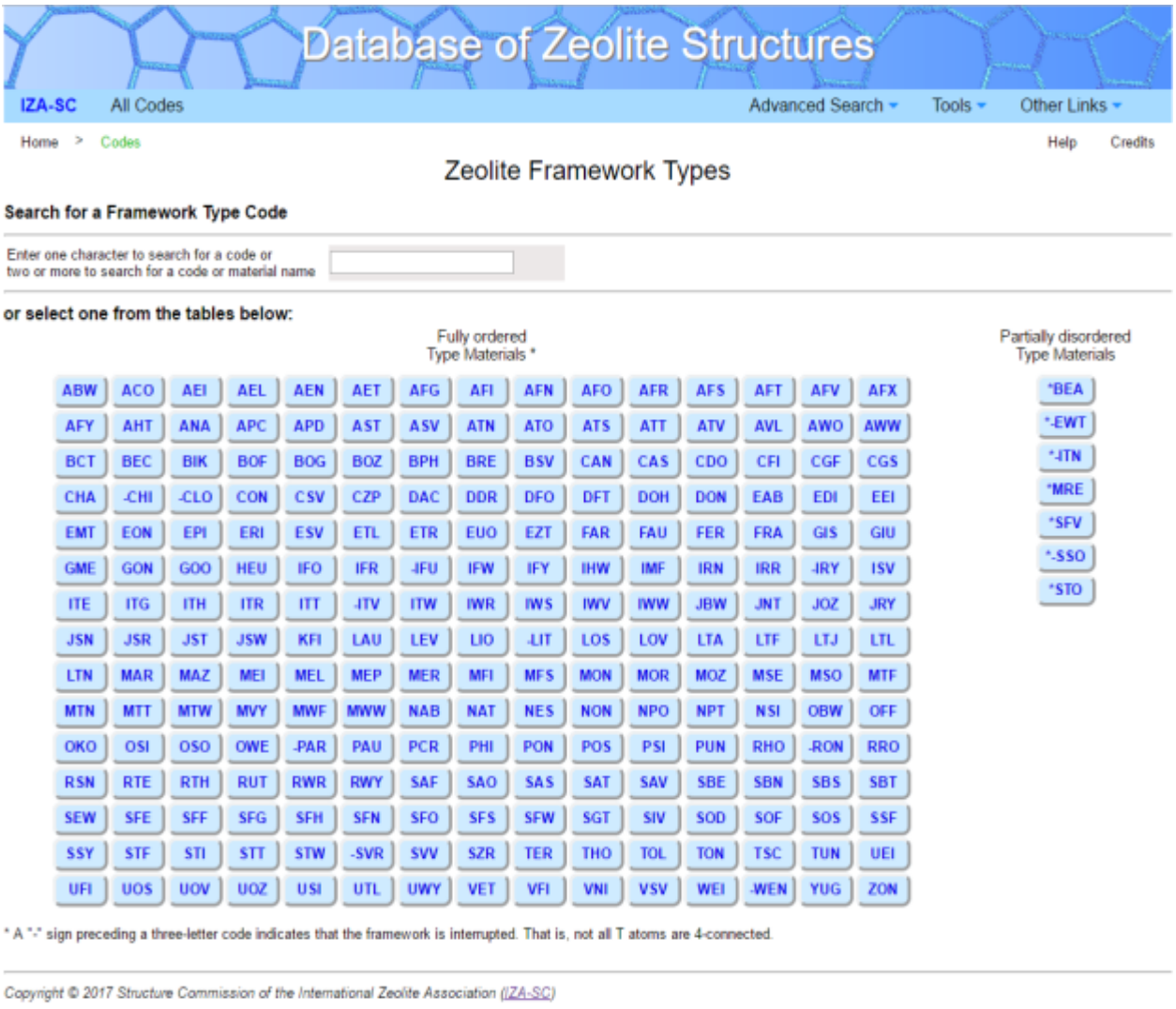

Figure 4 - Database of Zeolite Structures, which shows all 235 zeolite structure codes ("Database of Zeolite Structures," 2017).

235 unique zeolite frameworks were categorized, as shown in Figure 4, of which 40 types of zeolites occur naturally. In Figure 5, the framework type LTA is described in the database in terms of its cell parameters, ring sizes, maximum diameter of a sphere that can be included, etc. These parameters will be referenced in this study as the basis for understanding the unmodified zeolite LTA. Zeolites have tetrahedral building blocks consisting of one silicon atom binding with four oxygen atoms. Connecting all the

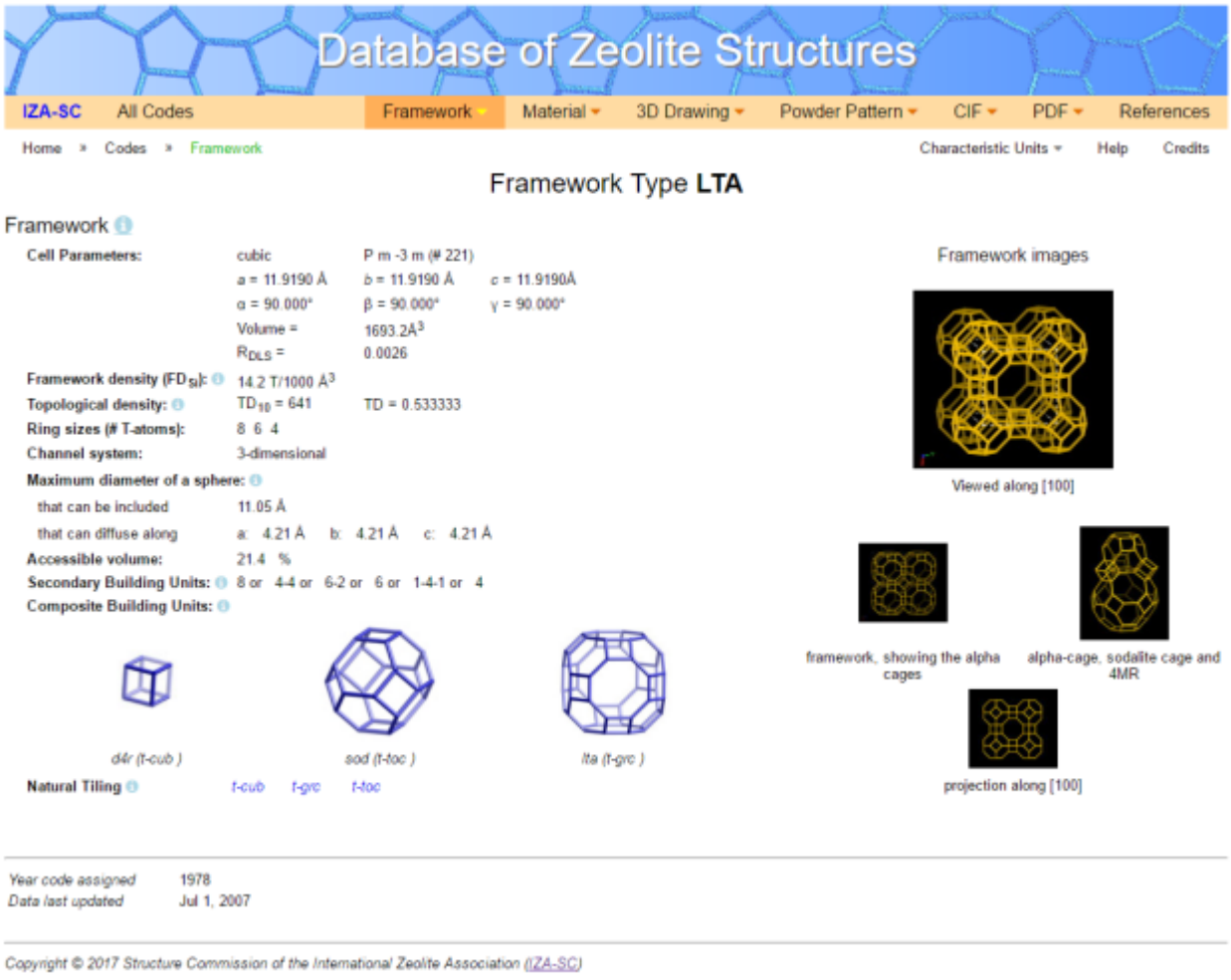

Figure 5 - Framework Type LTA in the database. This figure shows the parameters of the unit cell and other geometric information of this zeolite("Database of Zeolite Structures," 2017).

tetrahedrons of silicon-oxygen moieties can result in a network of molecular sieve. These sieve structures give zeolites the ability to selectively sort molecules based on their physical properties and size exclusion process. Therefore, varying the size of the pores in zeolite structures can change the selectivity of the molecular sieve for different types of zeolites. As shown in Figure 6, each silicon atom (grey) forms bonds with adjacent oxygen atoms (red) to form a network of three different size rings.

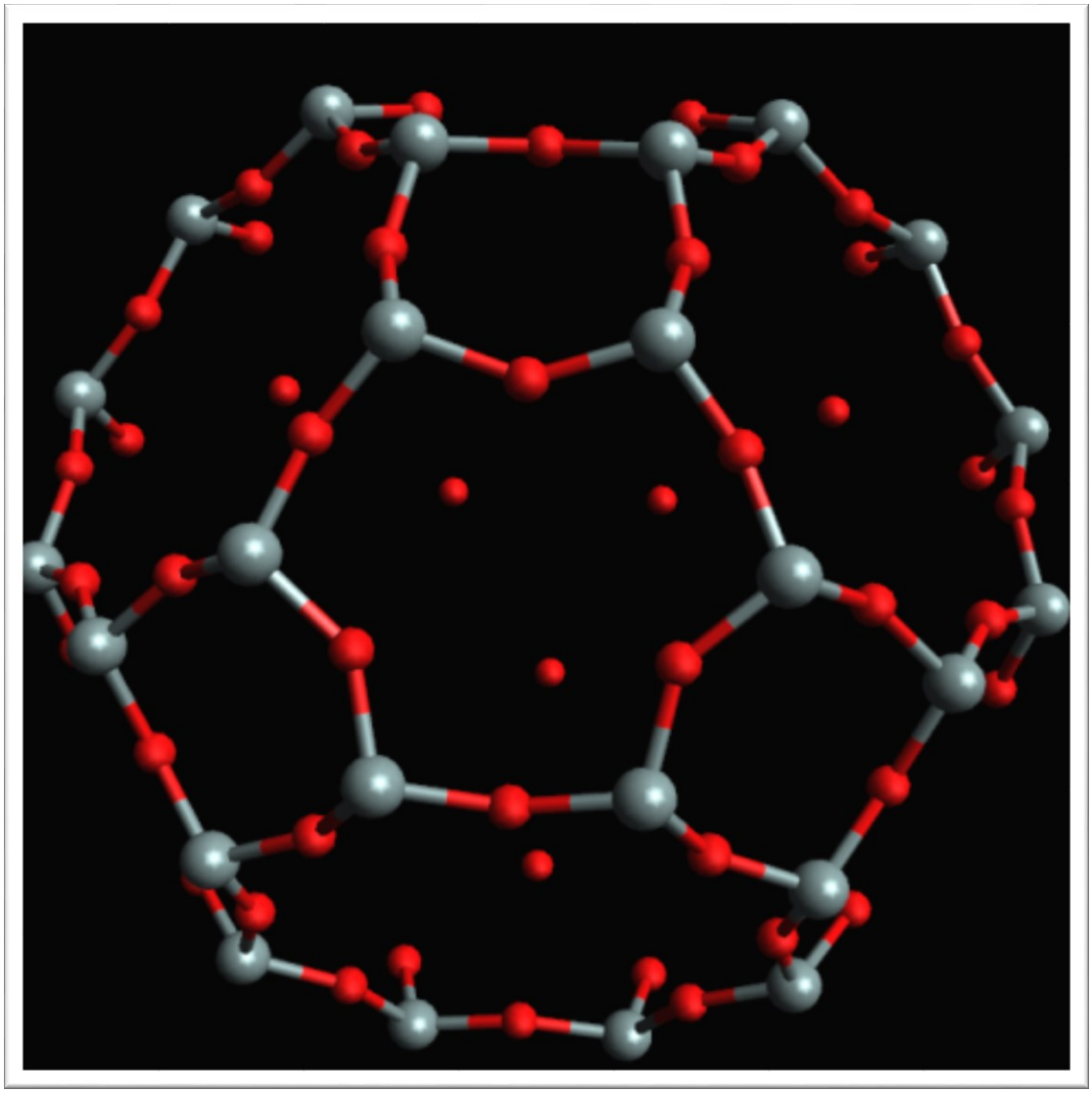

Figure 6 – A unit cell of LTA. Red spheres represent oxygen atoms and grey spheres represent silicon atoms. Some oxygen atoms appear alone because of the periodic boundary conditions. These atoms are in reality bound to Si atoms in neighboring cells.

2.3.1 Zeolite membered ring

A silicate zeolite ring is based on the shape of SiO_4 tetrahedra. In a 3-dimensional network, all four corners of the tetrahedra are shared, therefore producing a microporous material. In Figure 7, a 6-membered ring is represented in a hexagonal ring with each dot as a silicon atom. In LTA, there are three ring sizes. As shown in Figure 8, each membered ring resembles a shape that is defined by a Secondary Building Unit (SBU). The 4-membered

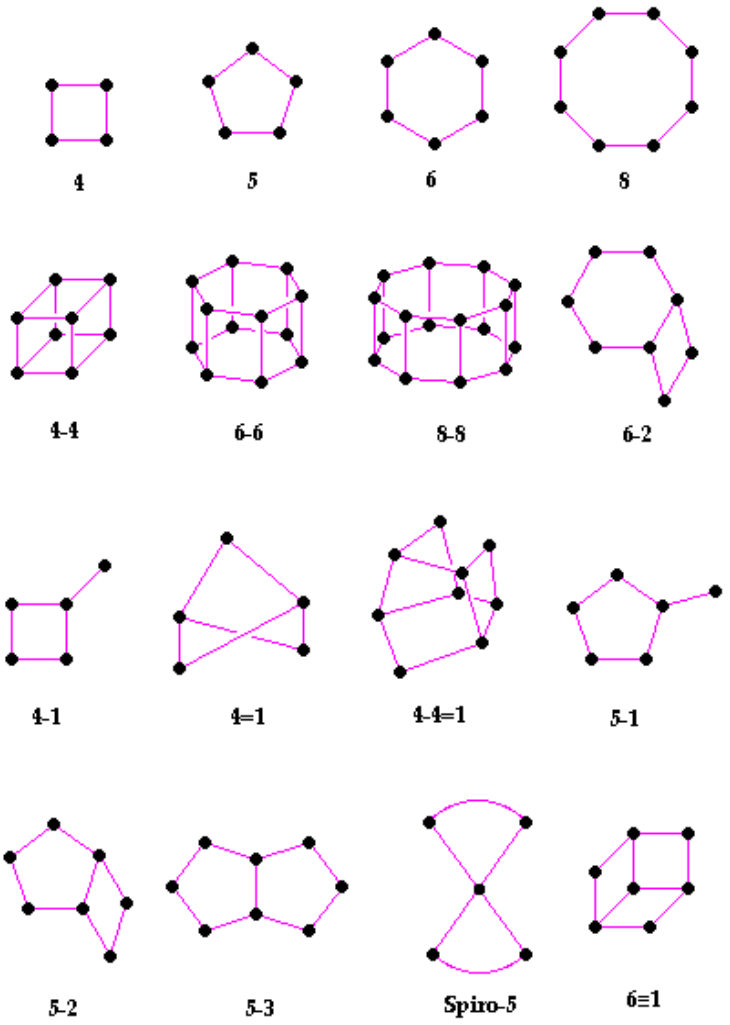

Figure 7 - Secondary Building Units (SBU's) in zeolites. The corners of the polyhedra represent tetrahedral atoms(“Structure - Zeolites,” 2017).

ring forms a square, 6-memebred a hexagon, and 8-memebered an octagon. These three

SBUs form the LTA unit cell in connection. In this structure, each unit cell then will be connected and repeated to form a sieve, which will be analyzed further in this study.

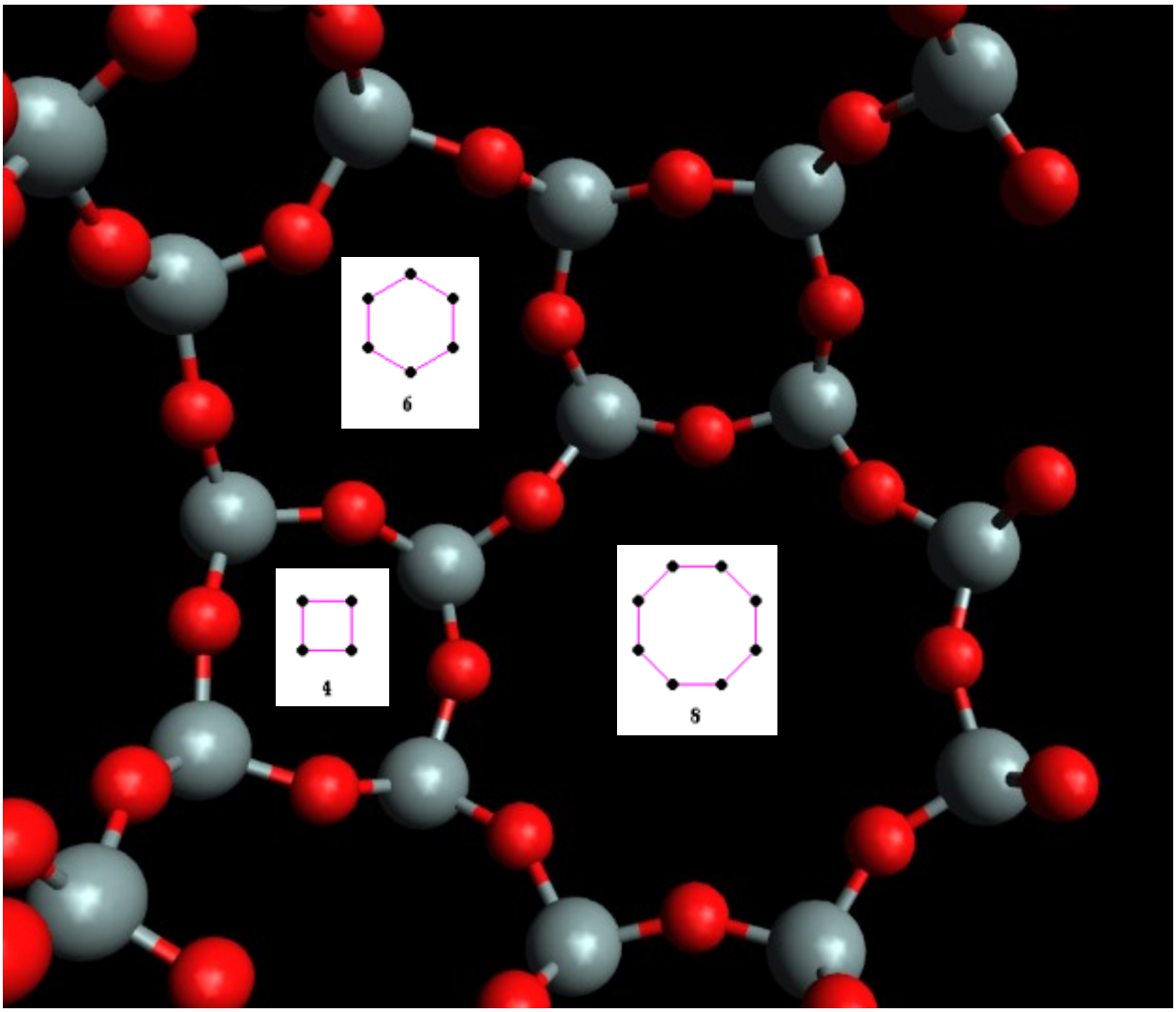

Figure 8 – A partial LTA cage unit cell with its four, six and eight membered rings indicated. Each SBU (Secondary Building Units) represents its ring's shape by the silicon atoms (grey) that form the ring.

2.3.2 Linde Type A (LTA)

Zeolite Linde Type A (LTA) has a 3-dimensional pore structure with pores running perpendicular to each other in the x, y, and z planes. Because each pore can be described with a diameter that fairly match the area of a ring, the ring diameter becomes a variable that can be altered by the types of atoms presenting on the ring. In Figure 9, the four yellow lines represent the four possible pore diameters for an 8-membered ring. The oxygen atoms are bent towards the center of the ring due to the covalent bonds between oxygen

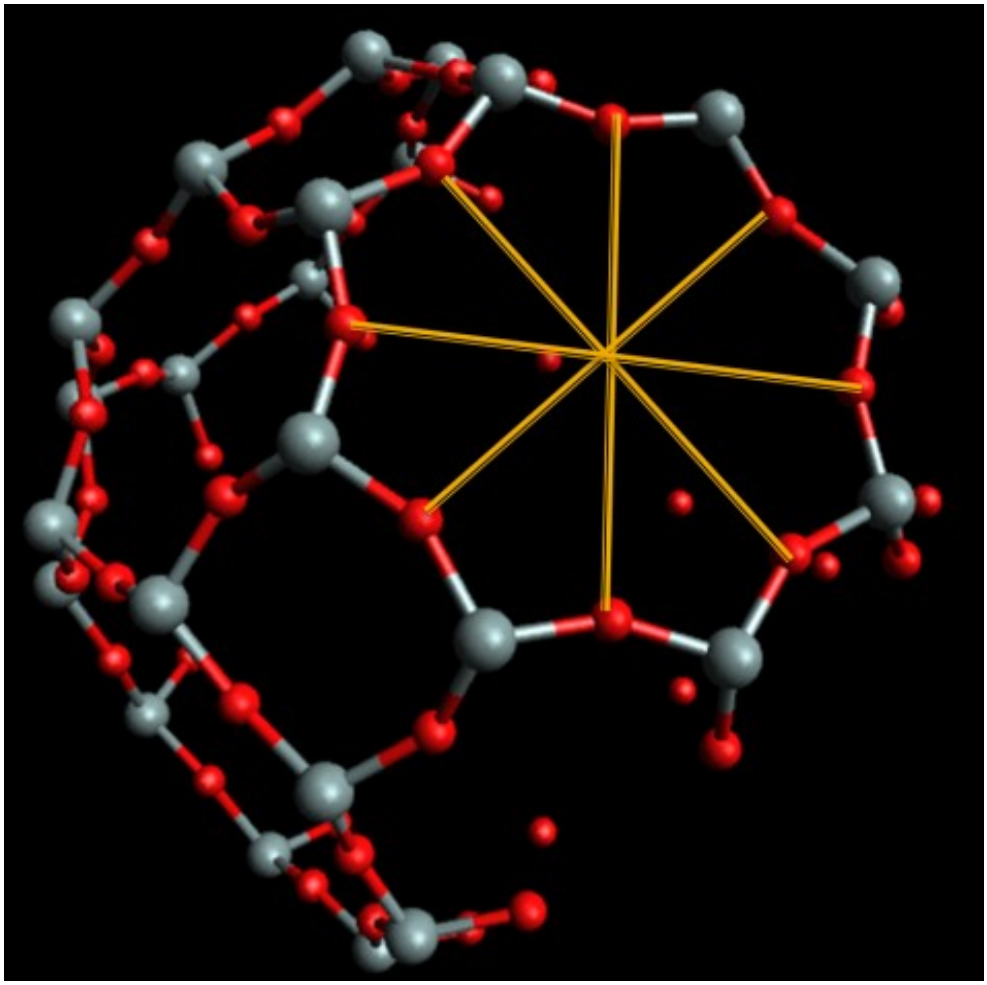

Figure 9 - An 8-membered ring in LTA, with its 3 possible pore diameters in the pore opening, depicted as the yellow lines. The red spheres represent oxygen atoms, and the grey spheres represent silicon atoms.

atom (red) and its adjacent silicon atoms (grey). As depicted in Figure 10, each silicon cation forms four covalent bonds with its adjacent four oxygen cations. Also because the strength of the covalent bonds, the covalent bonds are shorter and therefore causes the bent between the Si-O-Si bond. The charge balance is achieved by the continuous network of silicon and oxygen cations. A single SiO_4 molecule does not show a charge balance as shown in Figure 10 because an oxygen cation is -2 charge: the empirical formula for pure zeolite LTA is SiO_2. For cation substitution, the charge balancing equation is $Si^{4+} \rightarrow Al^{3+} + M^+$, where M is a metal cation (Na^+, for example) with a positive charge.

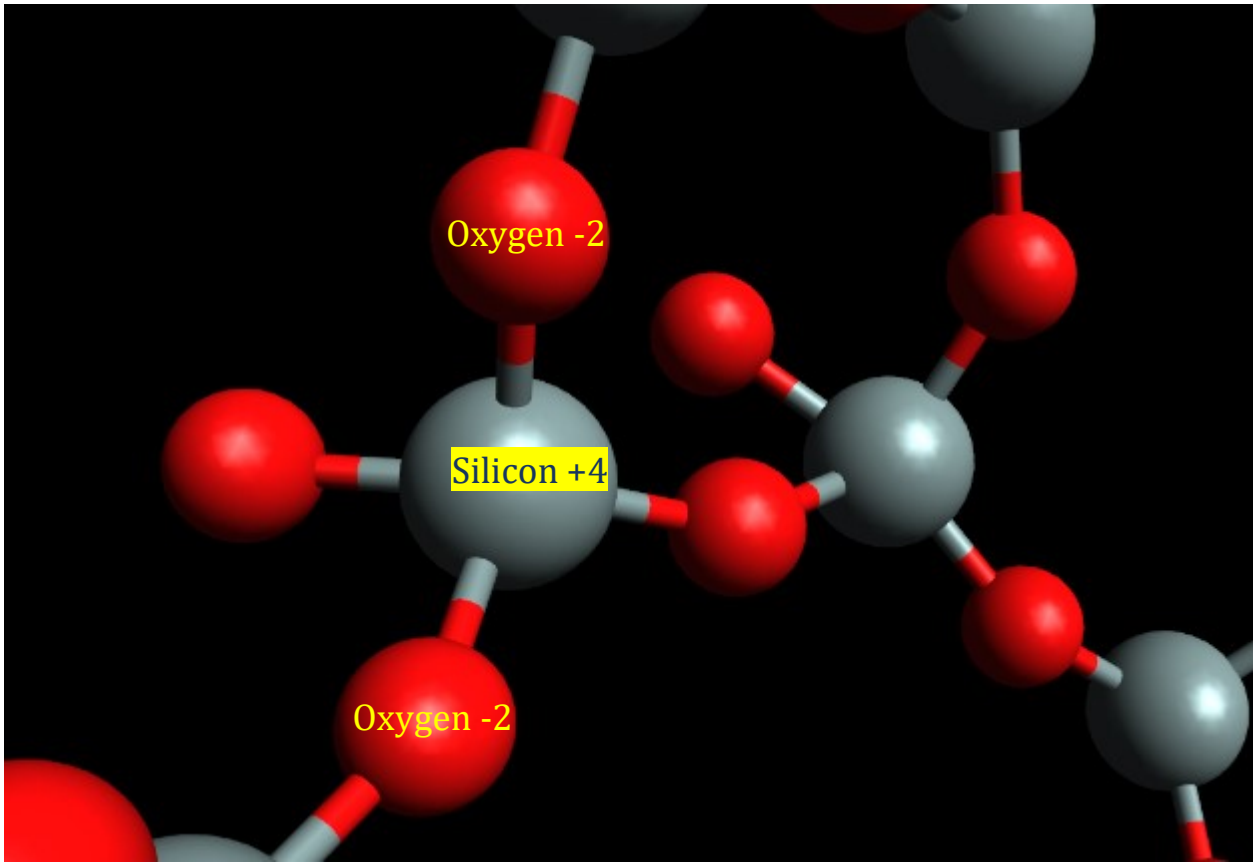

Figure 10 – A scheme showing the charge balances between silicon (+4) and oxygen (-2). Each oxygen has one negative charge to form a covalent bond with one positive charge from silicon. The bonds formed around silicon atom are covalent bonds.

2.4 LTA structure modification

Altering the silicon to cation ratio will directly alter some of key parameters that determine the properties of LTA, such as pore diameter, cavity volume, and energy of the LTA structure. The investigation of changing these parameters can help in designing zeolites that may be tuned to a specific application, whether it be separations or catalysis. These cations may determine the preference of a reaction site, and limit the size of particles or molecules that can be trapped within the zeolite.

2.4.1 Si/Al ratio and cation substitution

$$Si/Al\ Ratio = \frac{number\ of\ Silicon\ (Si) atoms\ in\ an\ unit\ cell}{number\ of\ Aluminum (Al) atoms\ in\ an\ unit\ cell} \qquad (1)$$

The silicon to aluminum ratio in equation 1 (Si/Al ratio) is a parameter used to determine the degree of cation substitution in a unit cell. During cation substitution, the silicon cation (Si^{4+}) can be substituted by cation pairs, such as Al^{3+}/M^{+} where M can be H^{+}, Na^{+}, as long as the substituted cation pair have the equivalent charge as Si^{4+}. Because a unit cell repeats in a crystal network, this ratio also applies to the overall ratio in a sheet and layers of zeolite structure. Without any aluminum substitution, the ratio is infinity because the number of silicon atoms in a unit cell is 24 but the denominator (number of aluminum atoms) is zero. For example, when 1 aluminum replaces 1 silicon atom in a silicate ring, the number of silicon atoms becomes 23 and aluminum becomes 1; thus the Si/Al ratio becomes 23/1 = 3. As more aluminum cations replace silicon to a maximum of 12, the Si/Al ratio decreases to a minimum of 1 (12 Si / 12 Al). Because Al^{3+} tend to repulse from adjacent Al^{3+}, the

substitution is unfavorable when more than half of the atoms in one unit cell (24 atoms) become substituted: as this will cause at least one Al^{3+} to be adjacent to another Al^{3+}. According to Lowenstein's rule, the linkages as Al-O-Al are forbidden in a zeolite framework ("Structure - Zeolites," 2017). Therefore, the minimum Si/Al ratio for aluminum cation substitution is 1. For an LTA unit cell with 24 silicon atoms in the unit cell, when there is no cation substitution, so the $Si/Al\ Ratio = \frac{Si}{Al} = \frac{24}{0} = \infty$.

2.4.2 Acidic site

When a pair of aluminum and cation substitutes into the LTA ring structure, an acidic surface site to be a Brønsted or Lewis acid based on the type of substitution. In Figure 11, a heteroatom in lower valency than Si, such as Al, is introduced, and only then after protonation the zeolite exhibits acidity("Methanol to Olefins," 2017). A Brønsted acid site is exhibited as the H^+ formed in Figure 11; for a Lewis acidic site is usually formed by metal cations such as the Na^+ or K^+ instead. These acidic sites will have different properties, which will affect the adsorption of molecules that come close to the pore structure. The study will investigate the effect of both types of acid sites in order to establish which site or ring type the extra-framework cations prefer to position themselves.

Figure 11 - The formation of acidic site when aluminum hydrogen pair is introduced in zeolite ("Methanol to Olefins," 2017)

2.4.3 Site distribution

In this study, each of the three rings is considered as a potential reaction site. In Figure 12, a cation in the 6-membered ring is defined as type 1; a cation in the 8-membered type 2; and a cation in the 4-membered ring type 3. When the Si/Al ratio is 23 (1 acidic site pair introduced), the acidic site can be located in each one of the ring types. However, for a Si/Al ratio of 3 (6 acidic sites introduced), the site distribution complicated, as a combination of sites must be taken into account. For Si/Al ratio of 1 (12 acidic sites), all the rings will be occupied by cations.

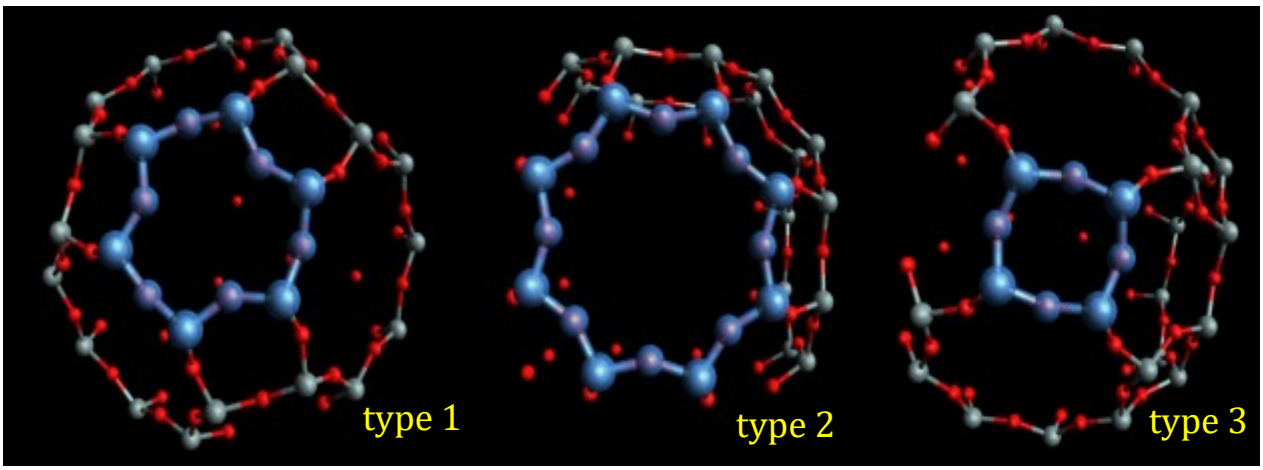

Figure 12 - From left to right, the highlighted ring is type 1, 6-membered ring; type 2, 8-membered ring; type 3, 4-membered ring.

2.5 Alkane and alcohol interaction to LTA surface and cavity

Due to the zeolite's microporous structure and ability in molecular cracking, this study will investigate LTA's adsorption properties of organic compounds. Because the linear chains of n-alkanes[2] exist primarily in crude oil in approximately 15% to 60% of the content ("Petroleum Composition," 2015), this study is concerned with LTA's interaction with some

[2] Also known as paraffin.

basic alkanes, such as methane or isobutane. Alcohols, because of its polarized –OH group, will be studied to determine the polarity effect within LTA.

2.6 Schrödinger's equation, wavefunctions, and the many-electron problem

Before understanding what density functional theory (DFT) is, we should look at some of the basic quantum mechanical concepts that are the basis of DFT. In quantum mechanics, a wavefunction, denoted as Ψ, describes all the information needed for a given system. The wavefunction describes the wave characteristics of a particle. It relates the possible configurations of a particle, and where it belongs in space at any time. Therefore, by solving for the wavefunction of a particle, we can understand the behavior of that particle at any certain space and time, and its relation with other particles. From Schrödinger's equation, a wavefunction for a single electron moving in a potential v(r) can be calculated by equation 2,

$$\left[-\frac{\hbar^2\nabla^2}{2m}+v(r)\right]\Psi(r)=\epsilon\Psi(r) \qquad (2)$$

In equation 2, the left side within the bracket contains the kinetic and potential energy term of the single electron. For the many electron problem, the Schrödinger's equation takes into account the electron-electron interactions. However, as more electrons are introduced, the many-electron problem becomes very difficult to solve for its total energy. Many powerful methods for solving the Schrödinger's equation were developed in the past, but the calculations became practically impossible for large and complex systems.

2.6.1 Density-functional Theory (DFT) and the Hohenberg-Kohn theorem

Density-functional theory (DFT) is a quantum mechanical modeling method used to investigate the electronic structure of atoms and molecules. The conceptual roots of DFT were supported theoretically after Hohenberg and Kohn established theorems (Hohenberg & Kohn, 1964). The theorem 1 states that "the external potential $v_{ext}(r)$, and hence the total energy, is a unique functional of the electron density n(r)." (S. J. Clark, 2003) Theorem 1 supports the fact that there is only one functional of the electron density that can represent the total energy of system of electrons. Finding that unique density functional therefore will yield the total energy of the electrons. Theorem 2 states that "[T]he groundstate energy can be obtained variationally: the density that minimizes the total energy is the exact groundstate density." (S. J. Clark, 2003) The theorems create a basis that shows a concrete detail of defining and seeking the total energy of the electrons. Despite providing powerful simplification of the many-electron problems, these two theorems do not provide the method of computing the ground-state density directly.

2.6.2 Kohn-Sham equations and potentials

Based on the Hohenberg-Kohn theorems, it was later by Kohn and Sham (Kohn & Sham, 1965) that devised a set of equations that be used to solve the Schrödinger's equation for complex systems. The advantage of the Kohn-Sham equations and potentials is their ability to simplify the solution as more particles are introduced. Instead of having to solve the complex wavefunctions, Kohn-Sham equations provide a ground-state wavefunction Ψ_{KS} that only requires the solution of a determinant of single-particle orbitals $\psi_i(r_i)$ (S. J. Clark, 2003):

$$\Psi_{KS} = \frac{1}{\sqrt{N!}} \det[\psi_1(r_1)\psi_2(r_2) \dots \psi_N(r_N)] \qquad (3)$$

In the equation 3, N is the number of electrons.

However, according to the Hohenberg-Kohn Theorems, only the minimum energy value is equivalent to the ground-state energy of the system of electrons. The wavefunction ψ_i has yet to be determined for the minimization. In the Kohn-Sham equations,

$$\left[-\frac{1}{2}\nabla^2 + v_{ks}(r)\right]\psi_i(r) = \varepsilon_i\psi_i(r) \qquad (4)$$

In equation 4, the ψ_i is the wavefunction of the electron state i, ε_i is the Kohn-Sham eigenvalue. The significance of the eigenvalues is that the highest total number of eigenvalues proved to be, by Perdew and Levy(Perdew & Levy, 1997), the minus ionization energy of the many-electron system. Therefore, the solving of the eigenvalues will give the total energy of the many-electron system. The Kohn-Sham equations simplifies the Schrödinger's equation by using the Kohn-Sham potential, which gives in part the average electrostatic effect of electrons interacting with electrons, rather than instantaneous interactions. However, the Kohn-Sham equations must be solved self-consistently, similarly to the Hartree-Fock approximation, by minimizing the energy with variation of the wavefunctions, i.e. orbitals. The self-consistent process, which is the same process that is used by CP2K("CP2K - About," 2016) to calculate the many-electron system's energy, starts with an initial guess of the wavefunctions. Then it takes iterating calculations of the energies with new wavefunctions until the self-consistent condition is reached(S. J. Clark, 2003). This self-consistent approach is needed because the Kohn-Sham potential depends on the wavefunctions, but the wavefunctions depend on the Kohn-Sham potential. Only a

self-consistent solution gives a wavefunction that is consistent with the corresponding Kohn-Sham potential.

2.6.3 Basis sets, periodic boundary condition and plane waves

A basis set is a set of functions that are used to represent the wavefunction in DFT in order for computers to solve the eigenvalue problem, as shown in the Kohn-Sham equations. A basis set can be composed of mathematical functions that mimic atomic orbitals. Plane-waves offer a complete basis set that is independent of the type of solid, and they treat all areas of space equally(S. J. Clark, 2003). With periodic boundary conditions (PBC), depicted for example in Figure 13, an infinite system can be modeled by only modeling a part of the system. PBC also lay the groundwork for modeling the unit cell in LTA, where each unit cell can be seen as having PBC. The cut-off energy E_{CUT} defines the number of plane-wavefunctions to be used and reduces the calculations needed by limiting the number of mathematical functions used.

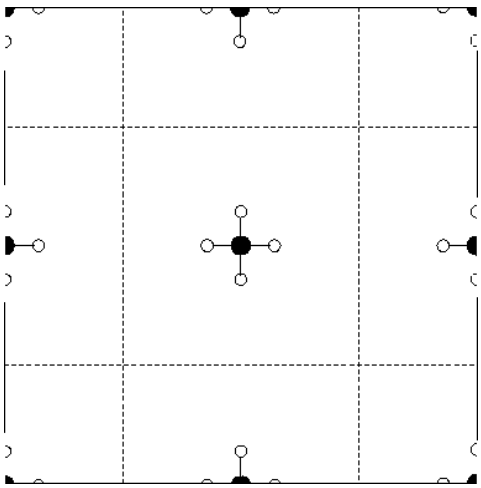

Figure 13 - An illustration of a supercell geometry for a molecule. The periodic boundary is shown as the dashed lines. (Segall, 1997)

2.6.4 Exchange-Correlation Potentials, Local Density Approximation (LDA), and Generalized Gradient Approximation (GGA)

The Kohn-Sham equation's potential energy term, as written in section 2.6.2,

$$\mathrm{v}_{KS}(r) = v(r) + \int \frac{\rho(r')}{|r - r'|} dr' + v_{xc}(r) \qquad (5)$$

relates directly to the eigenvalue calculations. In equation 5, the exchange-correlation potential, $\mathrm{v}_{xc}(r)$, modifies the potential energy term of the equation and is used to correct any approximations made when creating the Kohn-Sham potential. It is essentially a correction term. Much work had been done in seeking the accurate forms of the exchange-correlations. Firstly, Local Density Approximation (LDA) appeared to be the simplest form as LDA assumes the electron density can be treated as an uniform electron gas; at each point of the system, the exchange energy, $\mathrm{E}_{xc}^{LDA} = \int \rho(r)\, \epsilon_{xc}(\rho) dr$, is the same as a uniform electron gas's energy of the same density (S. J. Clark, 2003). The Generalized Gradient Approximation (GGA) improved upon LDA by introducing the gradient of the electron density, written as, $\mathrm{E}_{xc} = E_{xc}[\rho(r), \nabla\rho(r)]$. A popular GGA called PBE devised by Perdew, Burke, and Ernzerhof (Perdew et al., 1992), is primarily used in this study as the exchange-correlation potential in the calculations.

2.6.5 Pseudopotentials

To explain about pseudopotentials for electrons, firstly we have to look at the two types of electrons: core electrons that strongly bind in the inner atomic shells, and valence electrons that are outside of the core atomic region. A plane-wave basis set generally is suitable for describing wavefunctions of the valence atoms, but calculating all of the electrons (core and

valence) requires an exceptional amount of calculations, which make the calculations unpractical. Because core electrons generally remain unchanged (and in general, we focus on the behaviors of valence electrons), the pseudopotential approximation reduces the calculations by replacing the core electron's presence with a static electrostatic potential. The replacement still ensures that the core electron's effect on the atom occurs, so that the replacement does not affect the valence electron potential. A common pseudopotential approach was devised by Goedecker, Teter and Hutter (Goedecker, Teter, & Hutter, 1996) and is used in this study for the various elements.

2.6.6 Van der Waal's correction (vdW)

In the study of many-chemical systems, such as the interactions of alkanes and LTA, a shortcoming of all common GGA functionals is that they cannot describe long-range electron correlations that are responsible for dispersive van der Waals (vdW) forces very well(Grimme, 2006). The vdW interactions play a key role in electrostatic and exchange-repulsion, which cannot be neglected. In this study, organic compounds will interact with the LTA structure; therefore, a vdW correction is introduced to better describe interactions of zeolites with hydrocarbons.

3 Methodology

This section explains the method used in this work, which includes CP2K, input files, output files, coordinate selection for cation substitution, and organic compound placement within the zeolite. It will also explain the calculation for parameters such as pore opening size, accessible pore volume, adsorption energies, which will be compared and discussed in our work.

3.1 CP2K

CP2K is an open source quantum chemistry and solid-state physics software package that provides the framework, such as DFT, using the mixed Gaussian and plane waves approach (GPW). The program is written in FORTRAN 2003 and can be run efficiently in parallel using a combination of multi-threading and Message Passing Interface (MPI)("CP2K - About," 2016). Because the CP2K package is optimized for the mixed GPW method based on pseudopotentials, it is particularly suitable for this ab-initio LTA study. CP2K allows the user to calculate DFT energies and forces using norm-conserving, separable Goedecker-Teter-Hutter (GTH) pseudopotentials and gradient-corrected exchange functionals including Perdew-Burke-Ernzerhof (PBE) with non-local vdW corrections (PBE-vdW).

3.2 Input file and initial geometry setup

The input file contains the parameters for CP2K to calculate the energies of the chemical system through iteration. Figure 15 and 16 in the next two pages show a sample input file with various CP2K parameters and presets. The initial unit cell is created from the database of zeolite structures. With the help of molecular graphing software, Avogadro (Hanwell et al., 2012), I could visualize the unit cell and its atomic structure, as shown in Figure 16. Using Avogadro I could change the atomic structure of the zeolite. After replacing the silicon atom with an aluminum atom (blue) and placing the potassium atom (purple) at the center of the surface site, I could generate a coordinate file (with .xyz extension). I could then copy the generated coordinates into the CP2K input file such as under the COORD parameters in Figure 15. The other parameters related to the initial coordinates, such as KIND describe the basis set and pseudopotentials for corresponding elements in the initial geometries.

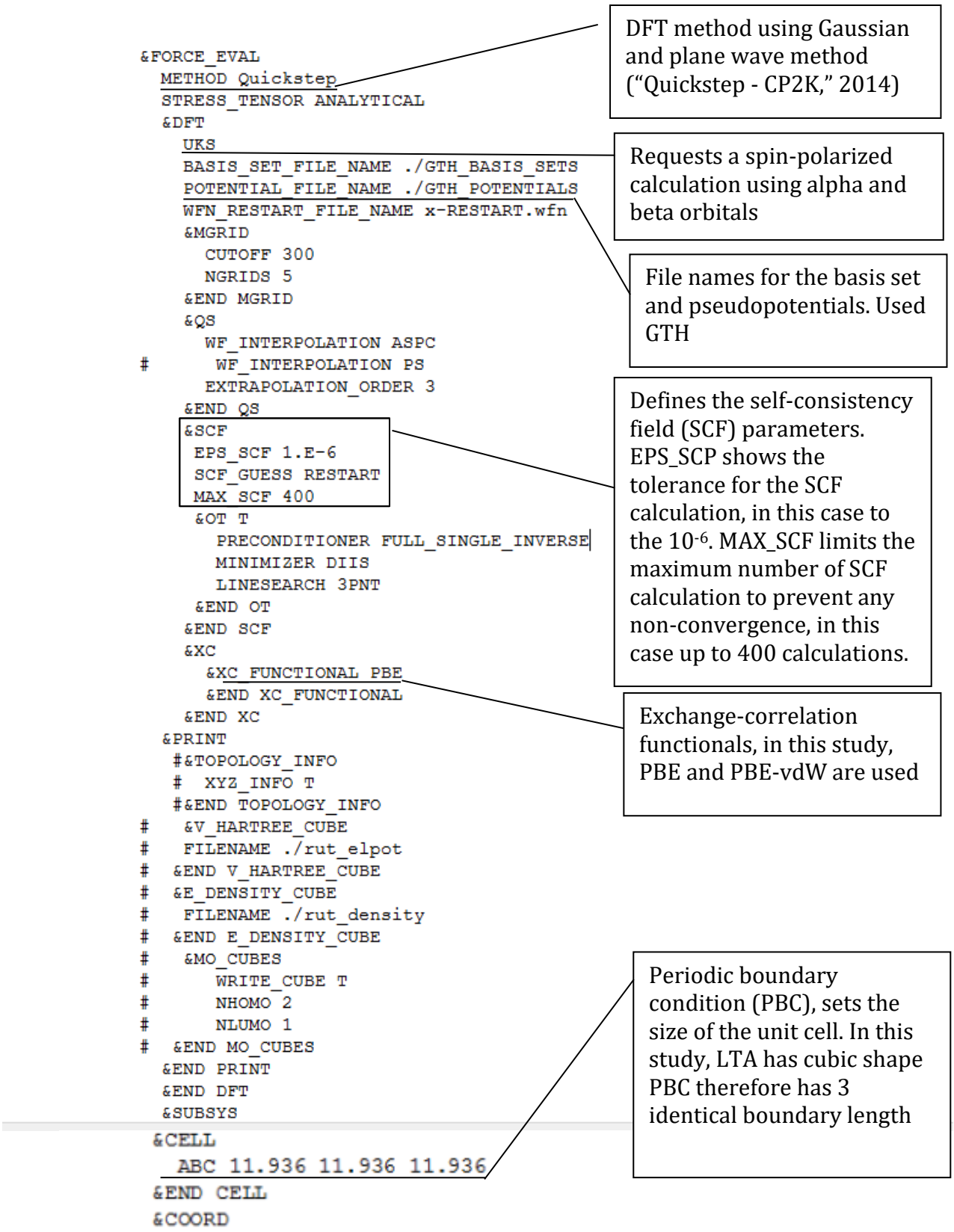

Figure 14 - A sample input file for CP2K to run a simulation in DFT. Some of the key parameters and settings are explained in the textboxes.

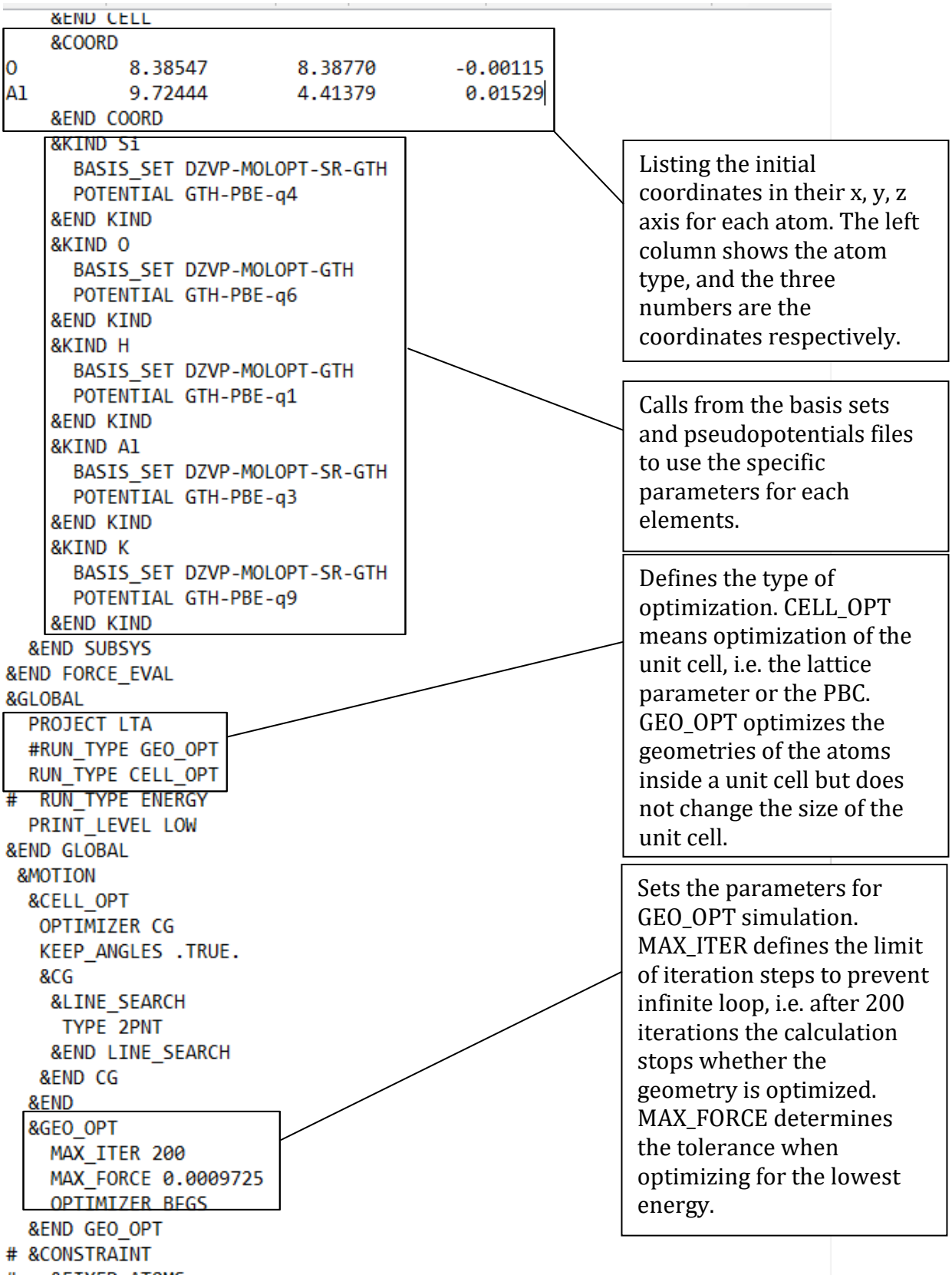

Figure 15 – Continued from the Figure 14 of the sample input file. Some key parameters and presets are explained in the textboxes.

Element	X	Y	Z
O	0.00061	8.30831	8.30400
O	0.00093	8.39313	3.53988
O	0.00055	3.61582	8.39718
O	3.54037	0.00563	3.53118
O	8.38643	-0.00150	8.38864
O	3.54317	-0.00126	8.39290
O	8.29857	-0.09536	3.62882
O	3.53408	3.52834	0.09534
O	8.38547	8.38770	-0.00115
O	8.31308	3.62238	0.07990
O	3.54893	8.38651	-0.00189
Al	-0.07111	2.20772	4.44867
Si	-0.00393	9.72805	7.51888
Si	-0.01344	9.76063	4.37978
Si	-0.01501	2.20033	7.61377
Si	4.44160	-0.05119	2.20164
Si	7.55720	0.00678	9.74778
Si	4.40587	-0.00521	9.73567
Si	7.57618	-0.01012	2.21041
Si	2.17991	4.42299	-0.01488
Si	9.75201	7.55602	-0.00520
Si	9.72444	4.41379	0.01529
Si	2.17451	7.56331	-0.00590
Si	2.15667	0.01359	7.57640
Si	9.72520	0.01915	4.39936
Si	9.76520	0.01549	7.55826
Si	2.18252	-0.02032	4.44614
Si	-0.01485	4.40898	9.77108
Si	-0.00266	7.56594	2.17806
Si	-0.02383	4.43208	2.20497
Si	-0.00211	7.56498	9.73141
Si	4.43770	2.18916	-0.03087
Si	7.55316	9.75199	0.00081
Si	4.40984	9.73787	-0.00920
Si	7.57206	2.19395	0.01576
K	2.43620	2.24736	2.42775

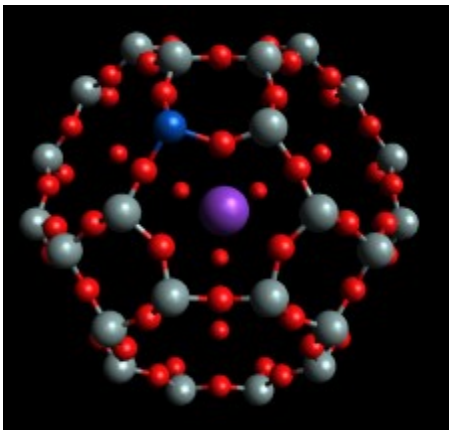

Coordinates for the K+/Al+

Figure 16 - A screenshot of LTA 1Ka-1Al S1 (1 potassium/aluminum substitution of type 1) in Avogadro as well as xyz coordinates. The blue sphere represents the potassium, the red spheres represent oxygen, and the grey spheres stand for silicon.

3.3 Output file interpretation

After CP2K starts a simulation from the input file, based on the type of optimization (CELL_OPT or GEO_OPT), an output file is generated. For cation substitutions, the calculations were performed by CELL_OPT, which optimizes the atom positions and cell size at the same time. In Figure 17, each cell was optimized based on the cell's three-dimensional size, vector a, b, c, as shown in optimization step 7 as 11.991, 12.028, 12.061 angstrom, respectively. The CELL_OPT calculations enable the cell parameters to change while looking for the local energy minima. At each step, CP2K also calculates the total energy of the unit cell based on the unit cell's optimized parameter a, b, c. The final geometry after CELL_OPT optimization is printed in an output .xyz file (similar as shown in Figure 19).

```
-------------------------
OPTIMIZATION STEP:      7
-------------------------

CELL| Volume [angstrom^3]:                                          1739.511
CELL| Vector a [angstrom]:      11.991     0.000     0.000    |a| =     11.991
CELL| Vector b [angstrom]:       0.000    12.028     0.000    |b| =     12.028
CELL| Vector c [angstrom]:       0.000     0.000    12.061    |c| =     12.061
CELL| Angle (b,c), alpha [degree]:                                     90.000
CELL| Angle (a,c), beta  [degree]:                                     90.000
CELL| Angle (a,b), gamma [degree]:                                     90.000

*******************************************************************************
***                         2PNT LINE SEARCH INFO                           ***
***                                                                         ***
***   DX (EVALUATED)=    0.000040          DX (THRESHOLD)=    0.250000      ***
***   DX (FITTED   )=    0.000358          DX (ACCEPTED )=    0.000358      ***
*******************************************************************************

--------  Informations at step =     7 ------------
 Optimization Method        =                  CG
 Total Energy               =      -913.1926092999
 Internal Pressure [bar]    =       106.6510315908
 Real energy change         =        -0.0000172274
 Decrease in energy         =                  YES
 Used time                  =            3947.188
```

Figure 17 - A partial output log shows a CELL_OPT calculation iteration step in CP2K.

For alkane-LTA/alcohol-LTA, Using GEO_OPT (geometry optimization), starting with the initial geometries, CP2K calculates the wavefunctions, and keeps changing the coordinates (geometry) of the system until the forces on the atoms are zero, indicating an equilibrium structure. In Figure 18, the initial iteration took 160 steps of changing or guessing the wavefunction in order to reach energy convergence (i.e. self-consistency) that met the EPS_SCF tolerance (1.E-6 hartree) set in the input file. CP2K records the wavefunction that leads to this specific convergence, which usually happens at the last step of each iteration. The geometry is then changed and a new wavefunction for this new geometry is then found through the iteration process. Once the lowest total energy is found after several geometry iteration steps, the wavefunctions are unique to the optimized geometries, and CP2K generates a new set of coordinates based on the geometries from that wavefunctions.

The output coordinate file (.xyz) contains a list of the geometries with the element coordinates below the different geometry steps; the output file also shows the energy E at the convergence. In Figure 19, the partial output file shows not only the coordinates of the final structure at geometry step 123, but it also calculates the energy in hartree after convergence. This means at step 123 the converged energy represents the lowest energy of the system of all the geometries, where each geometry also gives individual wavefunctions.

```
 *** SCF run converged in   160 steps ***


 Total electronic density (r-space):        -409.9999876885       0.0000123115
 Total core charge density (r-space):        409.9999999756      -0.0000000244
 Total charge density (r-space):                                  0.0000122871
 Total charge density (g-space):                                  0.0000122871

 Overlap energy of the core charge distribution:              0.00039935221286
 Self energy of the core charge distribution:             -2332.26478059758028
 Core Hamiltonian energy:                                   668.04736491397591
 Hartree energy:                                            974.14727723685337
 Exchange-correlation energy:                              -214.74657658024137
 Dispersion energy:                                          -0.17758528337445

 Total energy:                                             -904.99390095815420

 Integrated absolute spin density  :                              0.0000000304
 Ideal and single determinant S**2 :                   0.000000      -0.000000

ENERGY| Total FORCE_EVAL ( QS ) energy (a.u.):             -904.993901461693213


--------  Informations at step =     0 ------------
 Optimization Method        =                 BFGS
 Total Energy               =      -904.9939014617
 Used time                  =             1332.285
 -------------------------------------------------
```

Figure 18 – A partial output log shows a GEO_OPT calculation iteration step in CP2K.

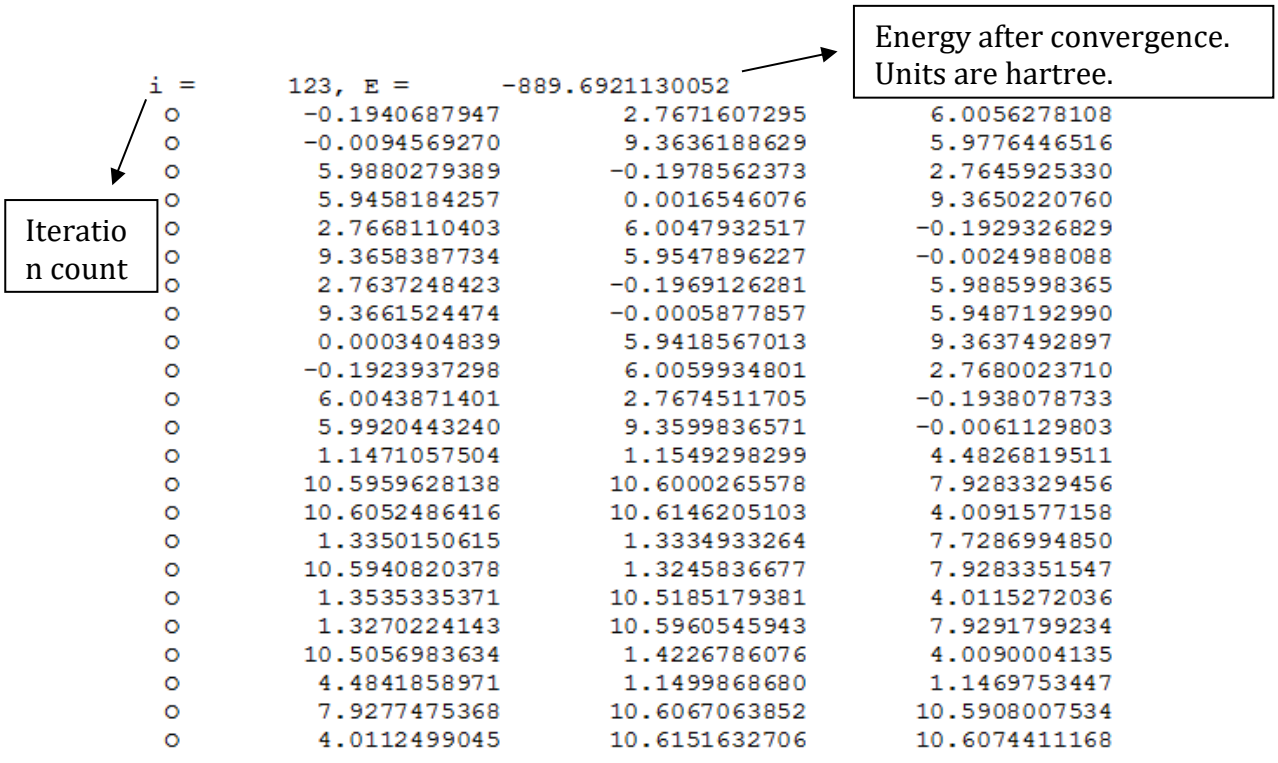

Figure 19 - A partial output file for LTA-propane-S1_vdw_surface (propane with vdW correction placed near the surface of LTA at site 1).

3.4 Site selection by varying the Si/Al ratio

As cation pairs are substituted into the LTA framework, the placement of the substituted atoms are critical to the stability of the zeolite structures. The Si/Al ratio, according to its definition, will decrease as more substituting cation pairs appear in LTA. When the Si/Al ratio is 23 (or 11 for Ca^{2+}), the substitution cation pair has the possibility of being placed near all the three types of rings. By comparing the energy at each ring type, I could determine the preferred cation location.

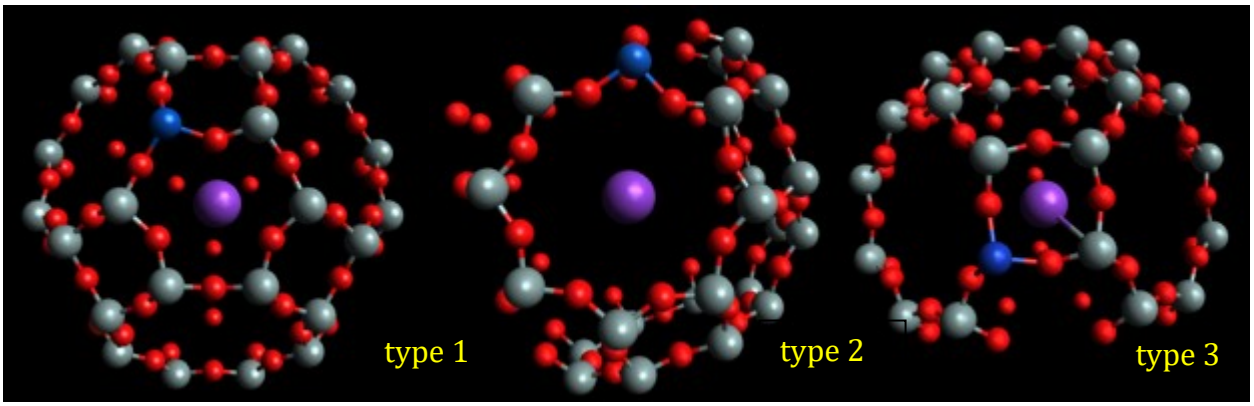

Figure 20 - From left to right, LTA in Si/Al = 23 (1 Na^+/Al^{3+} pair) with Na^+/Al^{3+} substituted in type 1, 2, and 3 rings respectively. The purple atom represents sodium, the blue aluminum, the red oxygen, and the grey silicon.

In order to decrease the silicon to cation ratio from infinity (no substitution) to a reasonable number, the cations were substituted in different numbers, with 1, 6 and 12 aluminums substituted in rings, varying among the three different membered rings (4-, 6-, or 8-member rings). In this study, hydrogen (H^+), sodium (Na^+), calcium (Ca^{2+}) and potassium (K^+) were substituted to balance the charges of when introducing aluminum into the pure LTA structure, where pure LTA has no aluminum presence. Aluminum in this study is called an in-framework cation, and substituted cations like (H^+, Na^+, K^+, Ca^{2+}) are

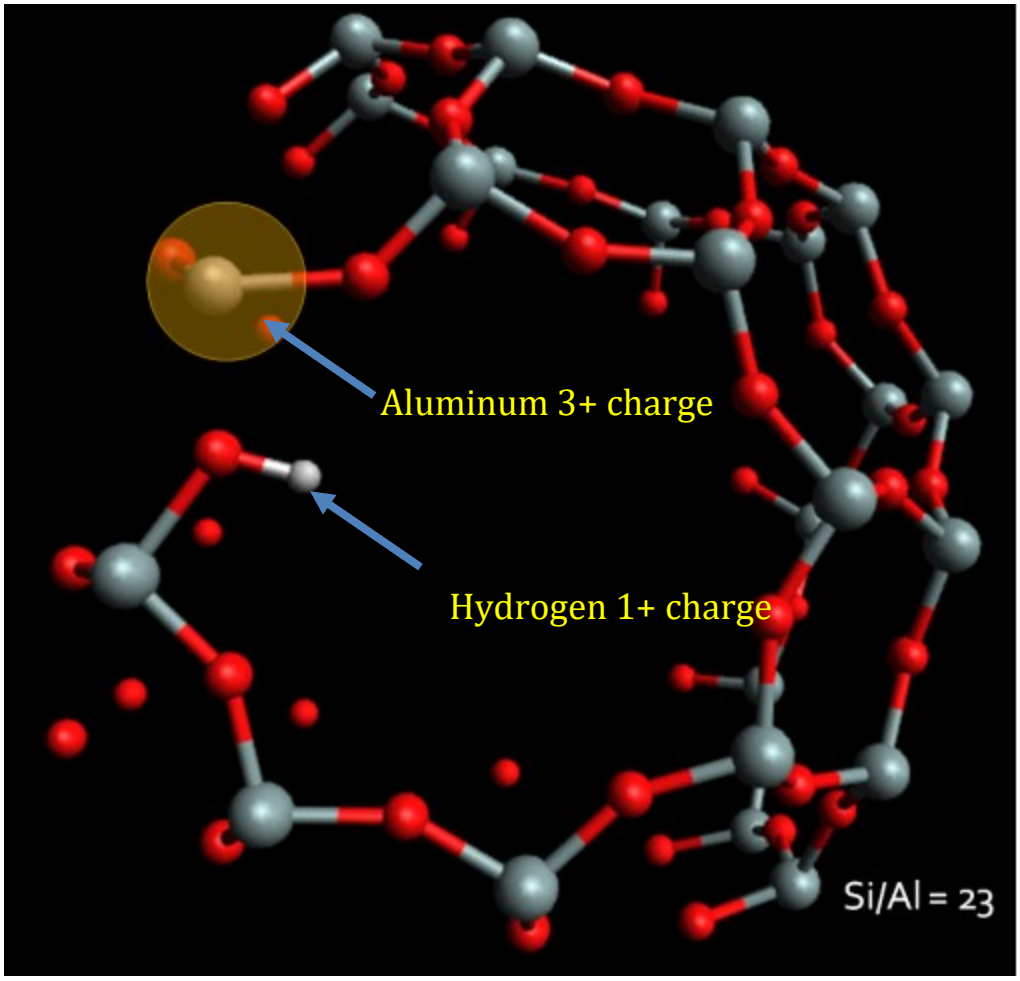

Figure 21 - LTA 8-membered ring, with 1 aluminum substitution and a hydrogen balancing charge. The Si/Al ratio is 23. The highlighted is the aluminum hydrogen pair. It also shows the introduced charge balancing atom is not a part of the framework.

called extra-framework cations. The extra-framework cations are not within the ring like the aluminum (Al^{3+}), which forms the covalent bond within the ring as in Figure 21.

Balancing charged elements with +2 charges, such as Ca^{2+}, requires 2 aluminum atoms per substitution in order to balance the charge. Therefore, the Si/Al ratio for 2 aluminums + 1 calcium is 11 instead of 23 as shown in Figure 22. The extra-framework cations were chosen so that they did not exceed a +2 charge.

For the Si/Al ratio of 3, 6 cation pairs (Al^{3+}/M^{+}, +1 charge) were introduced. With six extra-

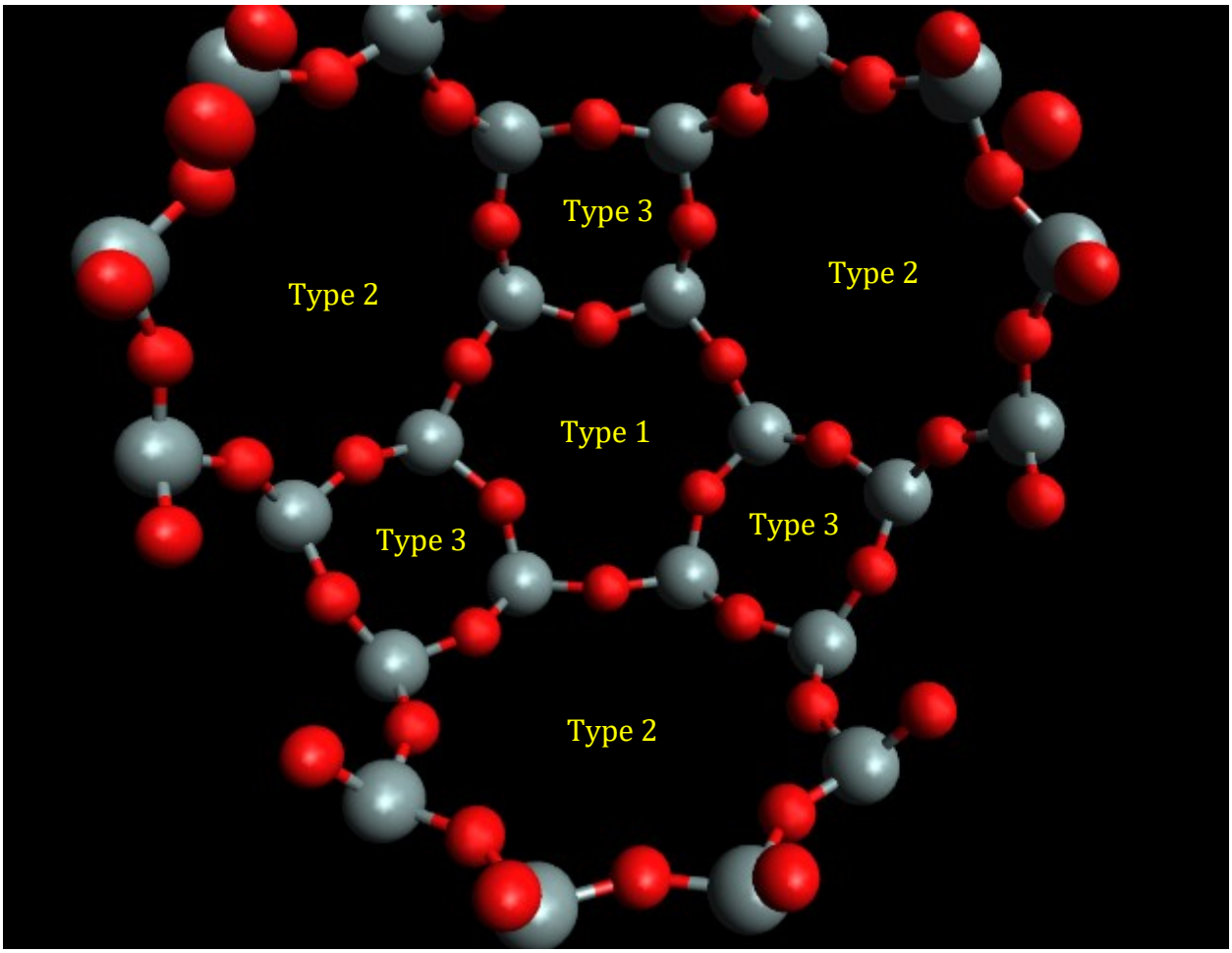

Figure 23 – A pure LTA unit cell framework illustrates the adjacent type of rings of each ring. In the center, it focuses to ring type 1, which its 6 adjacent ring types are type 2 and type 3, but none of type 1 itself.

framework cations (M^+), at least two types of rings must be filled in order to distribute the cation to avoid the repulsive forces between cations. For example in Figure 23, a type 1 ring (6-membered ring) has 6 adjacent rings with three that are type 2 (8-membered) and three that are type 3 (4-membered). In addition, because all three types of rings are adjacent, avoiding placing extra-framework cations such as type 2+2 will lead to a cation distribution where cations are far from each other to minimize the repulsions among the extra-framework cations. To determine whether a combination such as 2+2 is unstable, a test was run to determine the geometries change after initially placing two cations in the same ring type. In Figure 24, after initially placing K+ cations in the same type 2 rings for Al^{3+}/K^+ with 6 cation pairs, the final geometries optimized to distribute the K^+ to other ring types after calculations. Therefore, the distribution of the pairs in different ring types I considered were 1+2, 1+3 and 2+3, rather than putting cations within the same ring Out of the three possible combinations, I selected the optimal types based on their respective

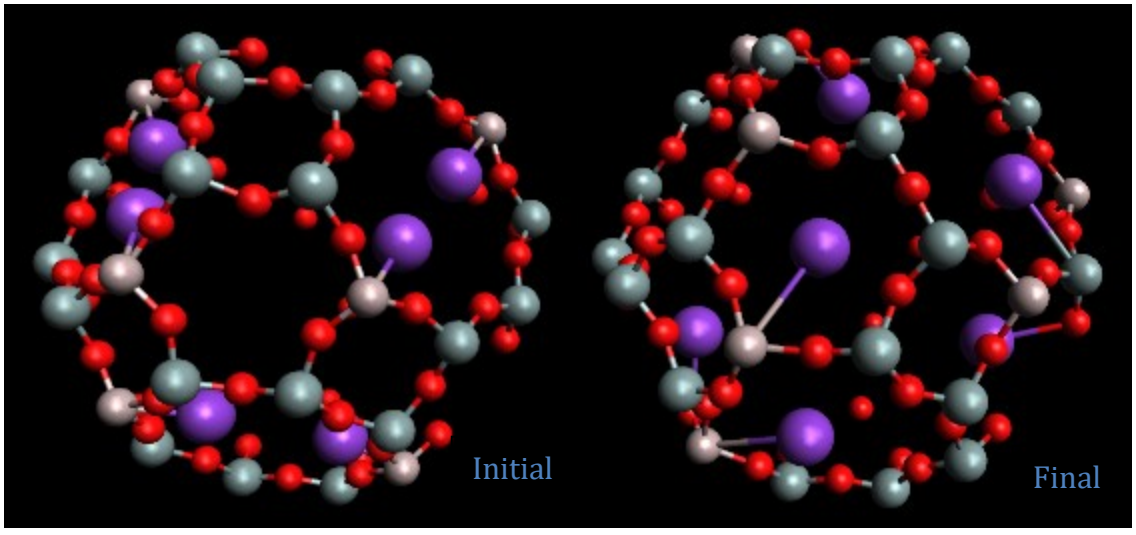

Figure 24 – A side-by-side geometry comparison for K^+ substitution at Si/Al = 6. On the left shows the initial geometries that have two potassium cations placed in the same ring type 2; on the right shows the final geometries after optimization.

energies after simulation.

For Si/Al =1, all ring types will be occupied by the extra-framework cations (M^+) because the 12 in-framework aluminum cations will be placed in the LTA with linkages Al-O-Si-O-Al. Therefore, there will be no preferred type of rings for extra-framework cations since all rings will be occupied. The exception will be for Al^{3+}/Ca^{2+} because there are 6 extra-framework calcium cations sharing 12 in-framework aluminum cations. Similar to the ring selection process of Si/Al = 3, calcium atoms will be placed based on 1+3, 2+3 and 1+2 types by comparing energies after geometry optimization.

3.5 Pore opening and accessible pore volume

Pore opening in LTA are important for determining the physical size of the interacting molecules and ions within the zeolite, and therefore determining the LTA's adsorbing selectivity and preference. The pore openings were measured from the coordinates from the output file. Because the largest pore opening is the 8-membered ring (type 2), the maximum pore diameter has to be located in type 2 rings. In a sample type 2 illustration in Figure 25, there are 4 possible pore diameters across from each oxygen atom (red) on the reaction site (T site). The measurement was taken in Avogadro using the measurement tool. In Figure 25, the dashed line indicates the distance between the two oxygen atoms

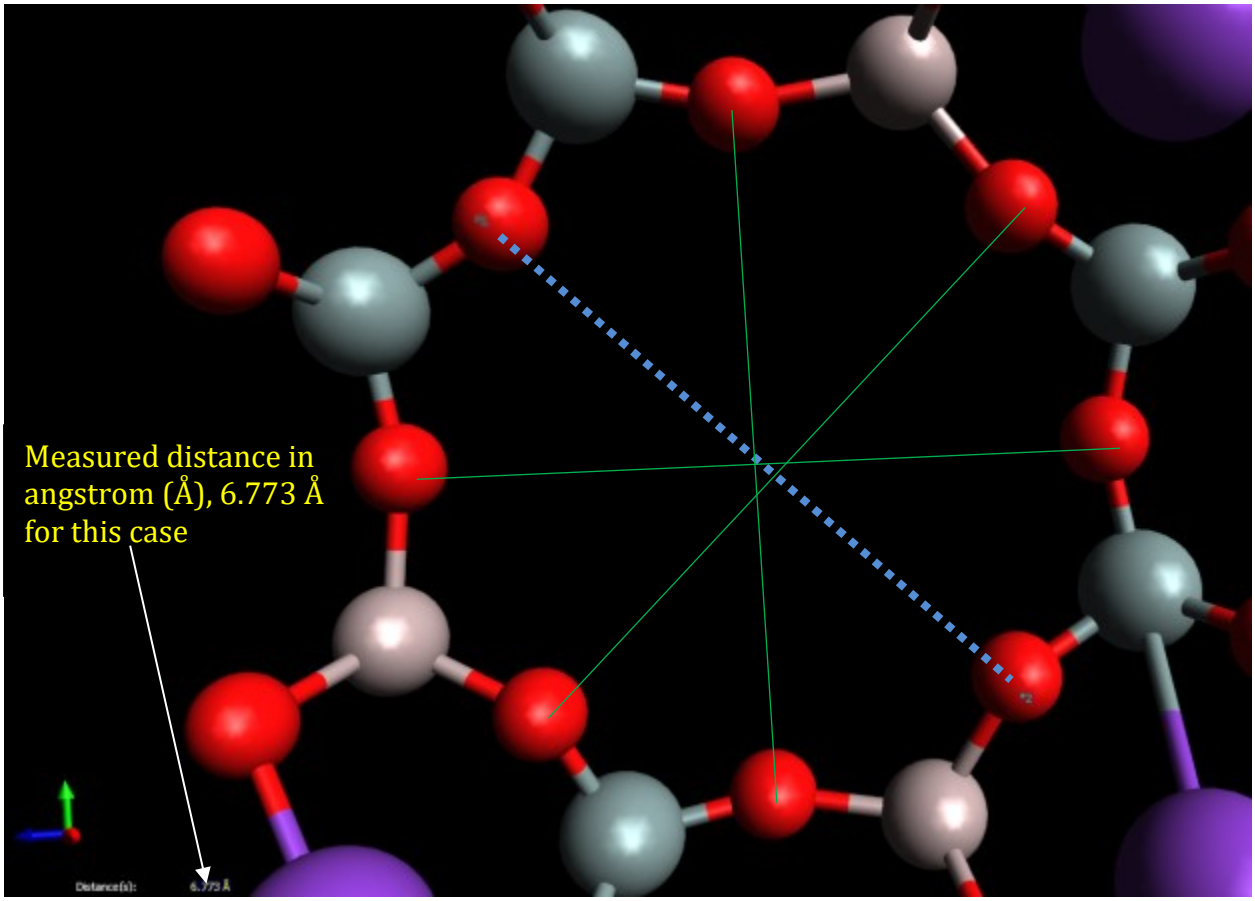

Figure 25 - The measurement for distance between two oxygen atoms in a surface site in LTA. The blue dashed line represents the distance for this measurement, and the green solid lines are the other 3 possible diameters in this site.

(6.773Å); the solid lines are the other three diameters in this ring. Because there are three 8-membered rings in each unit cell and each site has 4 possible diameters, each LTA unit cell had 12 diameters that determine the maximum pore opening area for molecules allowed to permeate through the pores. I could compare the minimum of the 12 diameters, and calculate the pore opening $A = \pi\left(\frac{D}{2}\right)^2$ with the minimum diameter for each simulation. This pore opening (in $Å^2$) will give us some insight on the effect of various cation substitutions on the structure of LTA.

The accessible pore volume was calculated with the output coordinates and an imaginary geometrical center of the unit cell. A distance measurement was taken from each atom to the center of the cell, similar to method as mentioned in the pore diameter above. The minimum distance becomes the radius for the maximum spherical volume that is accessible inside of the LTA cage. The closest atom to the center can be an oxygen atom, but it usually was an extra-framework cation as shown in simulations. The volume was calculated by $V_{accessible} = \frac{4}{3}\pi r^3$ where r is the minimum radius between atoms to the center of the cell. The pore accessible volume is another parameter that will indicate the changes of the LTA structure after the introduction of various types of cation pairs.

3.6 Alkane selection, alcohol selection, placement and adsorption energy calculations

For the interactions between alkane/LTA and alcohol/LTA, alkanes and alcohols range from C1 to C4 were studied. Figure 26 shows how alkanes can be placed near different ring types. Based on the size of the organic molecules, the energy of both organic compound and LTA were analyzed. The sum of both energies will be subtracted by the energy of the lone

organic compound and LTA. If the energy of adsorption is positive, then the interaction between the two molecules is endothermic, which means the adsorption will not occur; if negative, the reaction is considered exothermic, which means adsorption will likely to occur.

The energy of the molecule that was placed in the center of the unit cell was obtained for reference and comparison. And individual energy for LTA and the alkane/alcohol was also calculated. With the three energies, I could therefore calculate the adsorption energy with $\Delta E_{adsoprtion} = E_{LTA+organic\ compound} - (E_{LTA} + E_{organic\ compound})$. The energy of alkane near each of the three surfaces T-site was also obtained. The adsorption energy of alkanes near the surface site could therefore be calculated to determine their tendency of the alkane trapping or escaping from the ring.

The difference in approach for alcohols in regards to alkanes is how I treated the orientation of the alcohol relative to ring sites. Because alcohols have a hydroxyl group at the end of the hydrocarbon chain, either the –OH or the –3H side (a methyl group) could

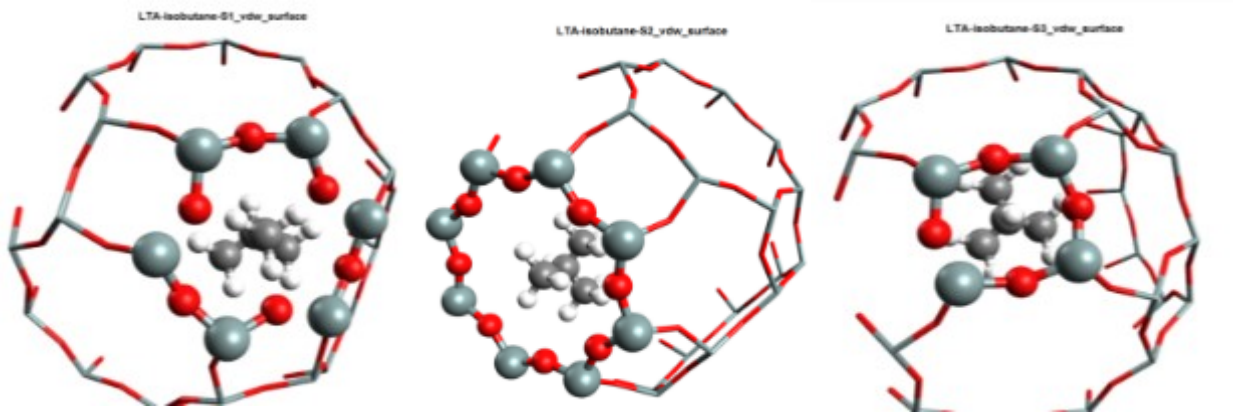

Figure 26 – From left to right, isobutane is placed near the surface of type 1, 2 and 3, respectively. The atoms in ball and stick represent the ring that forms the surface site, and the isobutane is placed inside of the LTA cage.

face towards the ring, which will change the energy of different orientation. As shown on the left of Figure 27, the isobutanol with the -3H was placed near the surface of ring type 1; where on the right of the same figure, 1-propanol had its –OH side placing near ring type 1. Comparing the adsorption energy of the two configurations could give us some indication of which orientation is preferred when the alcohol interacts near the surface site.

Also, we note that vdW corrections were taken into account in all the DFT simulations for alkane and alcohol calculations (the exchange functionals set to PBE-vdW).

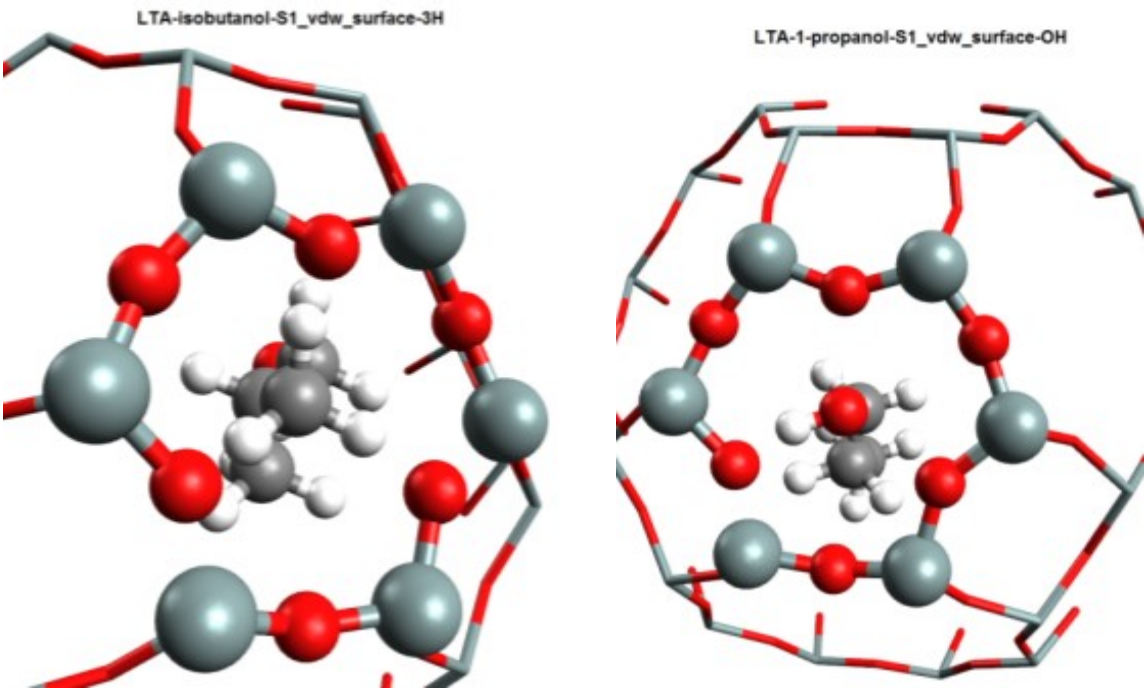

Figure 27 – On the left is isobutanol placed near the T-site 1 with its -3H oriented towards the site surface; on the right is 1-propanol with its –OH oriented towards the same site.

4 Results and Discussions

In this section, I will discuss the results obtained from CP2K in two parts. First, the effect of ion exchange and various cation substitutions on LTA will be determined by physical parameters ("Pore Opening Diameter" and "Accessible Pore Volume") and their ring type preference. Secondly, the effect of different alkane and alcohol at the surface of the pure LTA would be analyzed to study the adsorption tendency in LTA.

4.1 Effect of cation substitution in LTA

For the cation substitution calculations, four type of cation pairs (H^+/Al^{3+}, Na^+/Al^{3+}, K^+/Al^{3+} ,Ca^{2+}/Al^{3+}) were investigated in the LTA unit cell. In H^+/Al^{3+} substitution, the extra-framework hydrogen cations tended to stay close to the oxygen atom on the LTA framework due to the hydrogen's tendency of forming H-bond with oxygen on the LTA. As shown in Figure 28, a side-by-side comparison shows the geometries of the LTA after simulation. Hydrogen formed an H-bond and stayed near the perimeter of the ring structure. For the sodium atom (purple) as an example, different positions of the extra-framework cations were studied to compare the relative energies of their respective geometries. The most stable extra-cation positions might not be in the center, as shown in the lower part of Figure 28 that for the sodium cation's most stable position was near the two oxygen anions near Al^{3+}. This positioning is due to the attractive forces between the cation (sodium) and anions (oxygens). The relative positions of the extra-framework cations within the ring surface would be investigated for Na^+ and K^+. For all cation pair types, ring type preferences were taken into account to seek the most stable geometries.

For Na^+/Al^{3+} and K^+/Al^{3+} pairs, sodium and potassium had the same charge (+1) but different atomic size. Potassium's effective ionic radii was 138 pm (picometers), and sodium had an ionic radii of 102 pm (Shannon, 1976). For a Ca^{2+}/Al^{3+} pair, the effective ionic radii of Ca^{2+} was 100 pm, which was slightly less than sodium(Shannon, 1976). Due to calcium's +2 charge, when the Si/Al ratio was 1, only 6 (instead of 12) cation pairs could

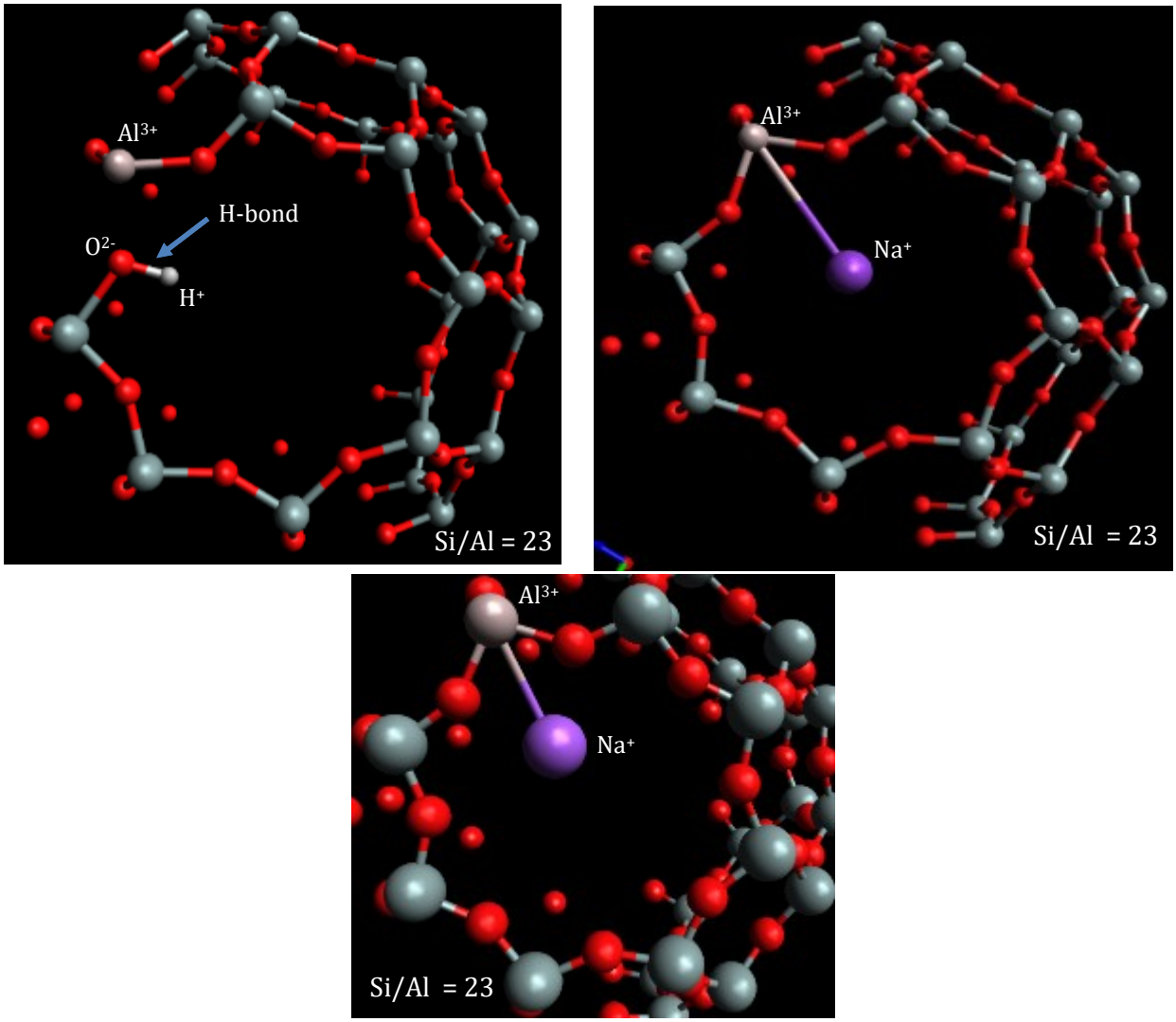

Figure 28 – A side-by-side comparison of H^+/Al^{3+} and Na^+/Al^{3+} substitution showing the positions of cations in a simulated geometry. On the upper left, the figure showed hydrogen cation forms a close H-bond close to the perimeter of the ring structure. On the upper right, it showed sodium atom (purple) stays in the center of the ring as one of the calculated geometries, but not the most stable. The lower figure represented to be the most stable geometries for the sodium cation, closer to the perimeter of the ring structure.

fill in the rings. Therefore, when the Si/Al ratio was 1, calcium only filled 6 out of 12 rings, but the other 3 cations (Na^+, K^+, H^+) occupied all 12 surface rings.

In the results, the energy values were converted from hartree to electron volt (eV), using the NIST's CODATA value of 1 hartree = 27.211386 eV ("NIST Reference," 2014). Detailed tables of the "Pore Opening Diameter" and "Accessible Pore Volume" can be found in Appendix A of this paper.

For initial calculations, the UKS setting (spin-polarized calculation using alpha and beta orbitals) was turned off to render faster calculation time. With UKS turned off, the DFT calculations used the same orbitals for paired alpha and beta electrons. With UKS switched on, both paired orbitals had individual wavefunctions, and thus would take more time for calculation. After determining the optimal site with UKS turned off, I performed the simulations with UKS on. This way, I could save more computer processing time and still obtain accurate results.

4.1.1 Results and discussion for Na^+/Al^{3+} Substitution

Table 1 - Effect of Na^+/Al^{3+} substitution on zeolite LTA geometry. UKS off. Red results are for most stable types.

Si/Al Ratio	Number of Al in Simulation Cell	Position of Cations in the Ring	Lattice Parameter (Å)	Accessible Pore Volume (Å^3)	Pore Opening Diameter (Å)	Relative Energy (eV)	Preferred Locations of Cations
∞	0	N/A	11.936	1338.71	6.861	0	N/A
23	1	Center	12.032	1007.77	6.680	0.106	Type 1
23	1	Edge	11.993	974.81	6.592	0.525	Type 1
23	1	Center	11.996	885.02	6.469	0.326	Type 2
23	1	Edge	11.993	951.53	6.559	0.000	Type 2
23	1	Center	11.997	599.23	6.543	0.666	Type 3
23	1	Edge	11.976	568.74	6.549	0.574	Type 3
3	6	Center	12.072	900.26	6.440	1.859	Type 1 + 3
3	6	Edge	12.275	663.99	6.655	3.232	Type 1 + 3
3	6	Center	12.211	857.23	6.368	0.000	Type 1 + 2
3	6	Edge	12.170	742.69	6.292	0.263	Type 1 + 2
3	6	Center	12.143	891.27	5.697	4.386	Type 2 + 3
3	6	Edge	12.221	653.61	5.697	4.464	Type 2 + 3
1	12	Center	12.428	693.11	6.143	0.000	All Types
1	12	Edge	12.492	696.74	6.143	1.216	All Types

Table 2 - Effect of Na^+/Al^{3+} substitution on zeolite LTA geometry. UKS on.

Si/Al Ratio	Number of Al in Simulation Cell	Lattice Parameter a (Å)	Accessible Pore Volume (Å^3)	Pore Opening Diameter (Å)	Preferred Locations of Cations
∞	0	11.936	1338.71	6.861	N/A
23	1	12.003	951.08	6.559	Type 2 - Edge
3	6	12.225	861.28	6.586	Type 1 + 2 - Center
1	12	12.428	682.56	6.515	All Types - Center

In Table 1, the numbers in red represent the optimal site based on the lowest energy achieved with UKS off. The energies of the DFT calculations showed that type 2 was the

preferred location for the extra-framework cation Na^+ to locate. The placement of the extra-framework Na^+ near the edge and the center was compared to investigate of the preferred spot for the extra-framework cation within the ring site itself. The energy with Na^+ near the edge of the LTA framework in ring type 2 indicated the most stable geometry based on the comparison of the relative energies of all six geometries at Si/Al = 23. In Figure 29, the position of the Na^+ (purple atom in the right image) was close to the two oxygen anions connecting to the in-framework Al^{3+} cation. In the geometry on the left of Figure 29 where Na^+ was positioned in the center of the ring type 2, the Na^+ was further from the LTA framework. Shown on the right of the Figure 29, the attraction from the oxygen anions to the Na^+ could be accounted for the lowest energy as the Al-Na distance was 2.888 angstrom compared to the Al-Na distance of 4.120 angstrom when the Na^+ that was at the center of the ring. As observed by both the calculated energies and geometries,

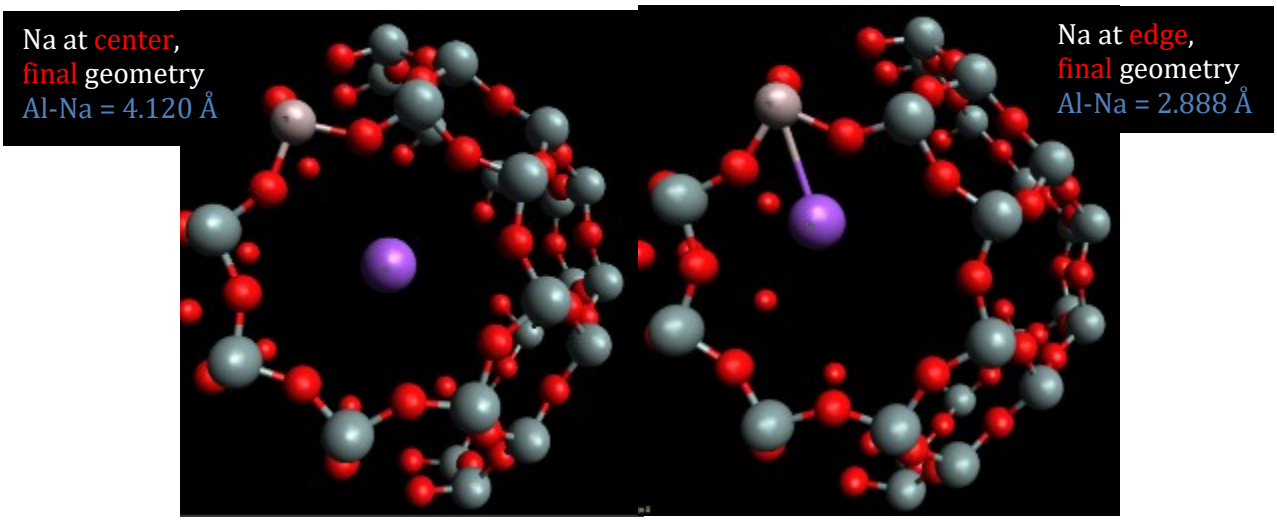

Figure 29 – The images of final geometries of the two different locations of extra-framework cation Na^+ in the 8-membered ring type 2, at Si/Al = 23. On the left was the geometry of an energy minimum in the center, and on the right was the geometry of an energy minimum near the edge of the LTA framework. The geometry on the right was more stable based on the energies. The distances between the in-framework cation (Al^{3+}, brown) and the extra-framework cation (Na^+, purple) were displayed at the top corners of the image.

Na^+ displayed the behavior of being attracted to the edge of the largest ring type, type 2. This behavior will be further discussed for Al^{3+}/K^+, in which potassium has the same charge (+1) but different size and atomic weight.

Table 3 - Comparison of Accessible Pore Volume and Pore Opening Diameter between UKS on and UKS off, for Na^+ at Si/Al = 11, 3, 1. The blue results indicate differences in values.

	UKS off	UKS on	UKS off	UKS on
Si/Al Ratio	Accessible Pore Volume ($Å^3$)	Accessible Pore Volume ($Å^3$)	Pore Opening Diameter (Å)	Pore Opening Diameter (Å)
∞	1338.71	1338.71	6.861	6.861
11	951.53	951.08	6.559	6.559
3	857.23	861.28	6.368	6.586
1	693.11	682.56	6.143	6.515

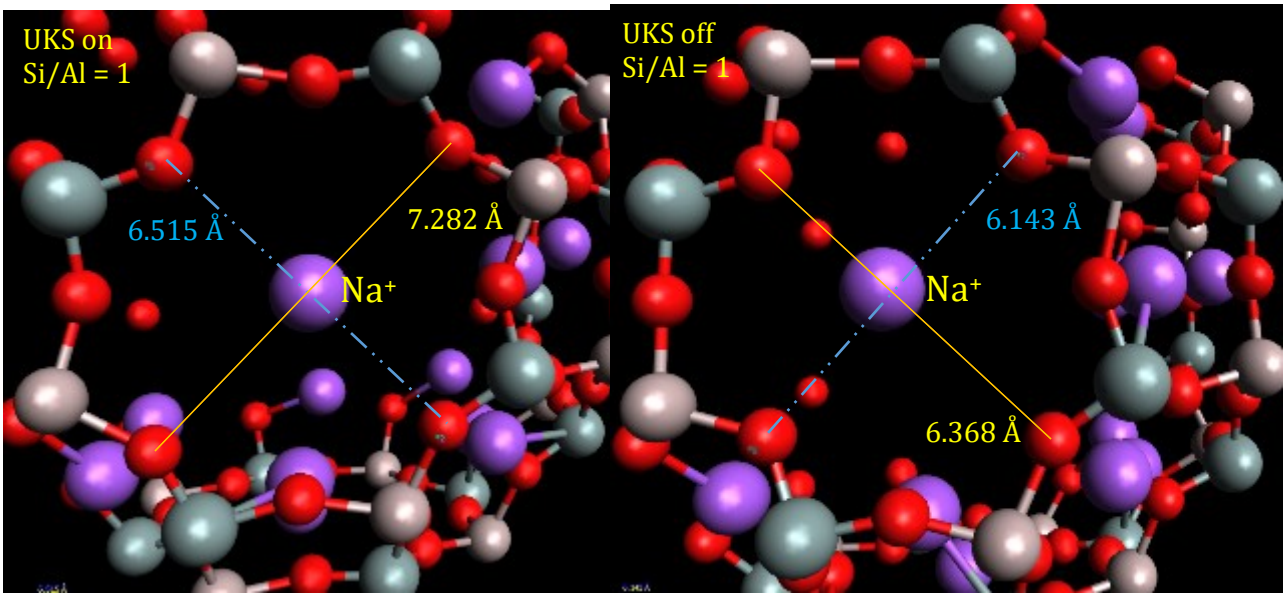

Figure 30 - – Images of the geometries for Na^+ at Si/Al = 1. UKS on shows on the left at ring type 2, UKS off showed on the right. The blue dashed lines represent the "Pore Opening Diameter" (the shortest diameter in ring type 2 between two opposite oxygen anions) with the blue text as the distances. The purple atoms represent Na^+, and the red atoms represent O^{2-}. The orange solid lines represent the diameters which are the on the same direction of the "Pore Opening Diameter" on the other image, with the yellow text as the distances. The orange solid line on the left of the figure is to be compared with the blue dashed line on the right, and vice versa.

In the column of "Relative Energies" in Table 1, for each of the same Si/Al ratio, the most negative value in the energies represents the most stable and thus preferred geometry among the positions of the extra-framework cation sodium, and is set to zero. In Table 2, based on the preferred site selections obtained in Table 1, the results show the simulated parameters with UKS on.

A difference in "Pore Opening Diameters" for UKS on and off was observed in Table 3. The "Accessible Pore Volume" between UKS on and off appeared to be consistent. I examined the images of the geometries between the two options in Figure 30 at Si/Al = 1, where the "Pore Opening Diameter" differed in value the most (6.515 Angstrom for UKS off versus 6.143 for UKS on). In Figure 30, the two values of "Pore Opening Diameter", illustrated as the two dashed lines, were in opposite directions. When comparing the "Pore Opening Diameter" from the same oxygen atoms in both images in Figure 30, the distance for UKS on was 7.282 Angstrom versus 6.143 Angstrom in UKS off, and 6.515 versus 6.368 from left to right image. The geometry with UKS off had shorter diameters than those in the same

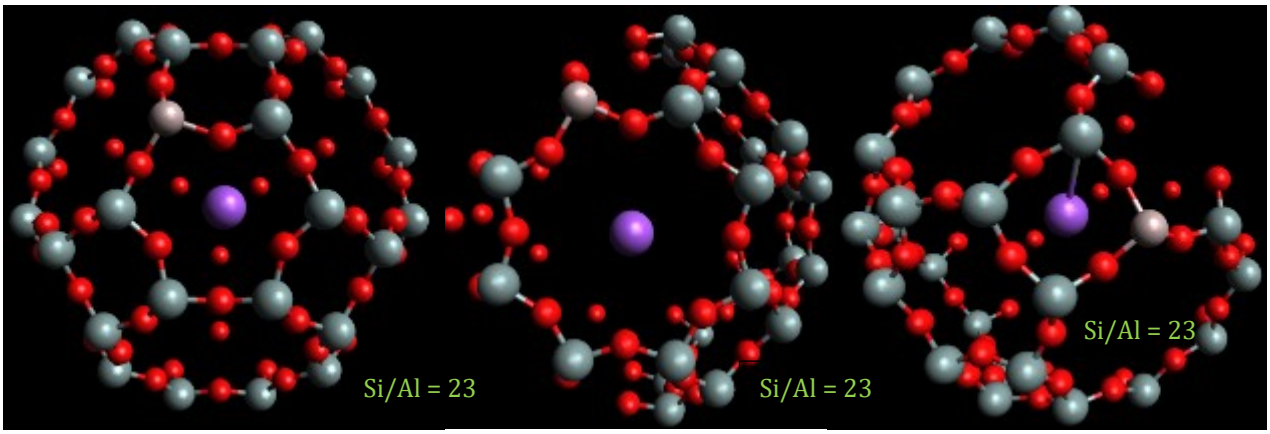

Figure 31 – From left to right, the illustration depicts Na^{+}/Al^{3+} substitution at Si/Al = 23 at the three ring type 1, 2, 3, respectively. The geometries were the simulated results with purple atoms Na^{+}, the red atom O, and the grey atom Si.

direction with UKS on. The UKS off option leads to a geometry that is different than UKS on, as observed in Figure 30. UKS on should be a more accurate method since every electron is modeled, as opposed to UKS off where symmetry lowers the number of unique electronic orbitals. A similar difference was also observed for Ca^{2+} (100 pm), which has a similar ionic radii to Na^{+} (102 pm). The UKS on and off option will further analyzed in the Ca^{2+} section.

From Table 1, the Si/Al ratio is proportional to the accessible pore volume. These results agreed intuitively with the notion that as more cations were introduced to the LTA, sodium cations occupied more physical space and shrunk the internal volume of the LTA. This could be explained by the increasing lattice parameter, which defined the volume of the cubic LTA unit cell ($V_{unit\ cell} = a^3$). As more cations substituted in the LTA (reflected by the increasing "Number of Al in Simulation Cell" and decreasing "Si/Al ratio"), the lattice parameter increased. The introduced cations caused the unit cell to expand because of the increased amount of aluminum cations substituted in the LTA framework and their extra-

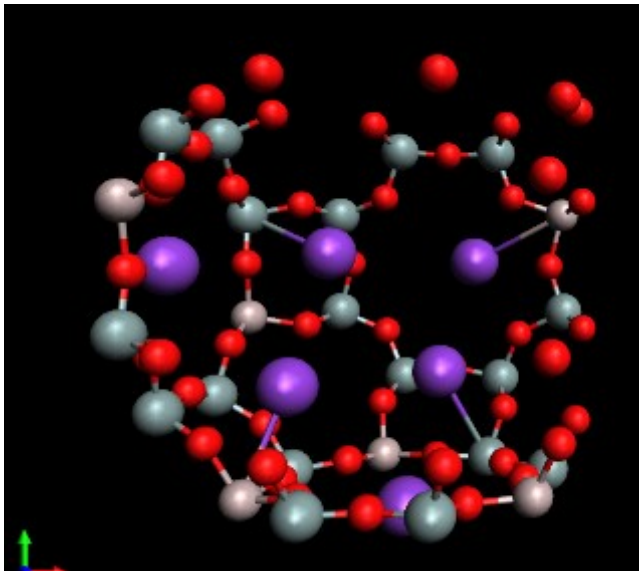

Figure 32 – A simulated geometry of LTA with Si/Al = 3, with sodium cation (purple) located near ring type 2 and 3. The illustration shows that sodium atoms were repulsed by the cations on the ring framework towards the center of the unit cell.

framework sodium cations, which could lead to more repulsion between the rings/atoms. An increase in lattice parameter would lessen this repulsion. However, the expansion of the simulation cell volume led to an increase of "Accessible Pore Volume". Based on the simulated geometries with sodium substitution, as shown in Figure 32, the extra-framework sodium cations were repulsed by the in-framework cations towards the center of the unit cell.

The "Pore Opening Diameter" became smaller in value with increased number of Al^{3+}/Na^{+} cation pairs. As depicted in Figure 33, the extra-framework sodium cations (purple) that were located in ring type 1 and 3 had strong repulsive forces in the rings. Because the 8-membered ring type 2 was adjacent to the other ring types, the repulsive potential

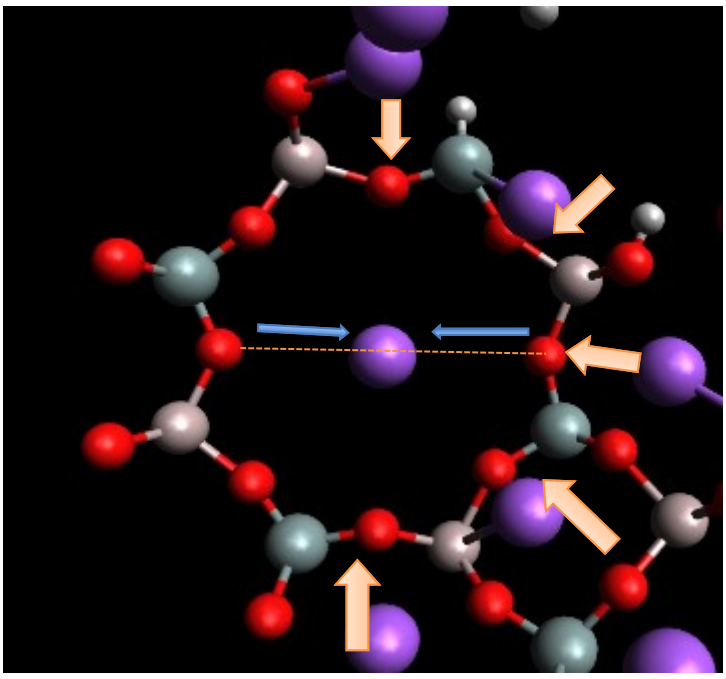

Figure 33 – A partial view of LTA with Si/Al = 1 that focused on the 8-membered ring. The purple atoms were sodium cations, the red were oxygen atoms. The yellow arrows represented the repulsive potentials caused by the sodium cations and indicated the direction of the forces that led to the bending of the Al-O-Si linkage. The bending of the bond linkage directly caused the Pore Opening Diameter to decrease. The blue arrows indicate attraction from the oxygen atoms to the sodium atom. The dashed orange line indicates the decrease in the Pore Opening Diameter.

therefore caused the oxygen cations to bend towards the center of the ring type 2. There could also be attractive forces between the O atoms and sodium cation in the pore center (as shown by blue arrows in Figure 33). The "Pore Opening Diameter" was measured in ring type 2 of the two oxygen atoms that had the shortest diameters of the four possible diameters; and therefore, due to the oxygen cation's bending towards the center, the "Pore Opening Diameter" decreased.

For Si/Al = 3, Na^+ cations had the lowest relative energy at the center of ring type 1+2. This notion was supported by the sizes of the 6-membered and 8-memebered rings, which were larger and thus more preferable than the type 3, the 4-membered ring. On the left of Figure 34, the geometry with sodium cation near the center of the ring type 2 was preferred than

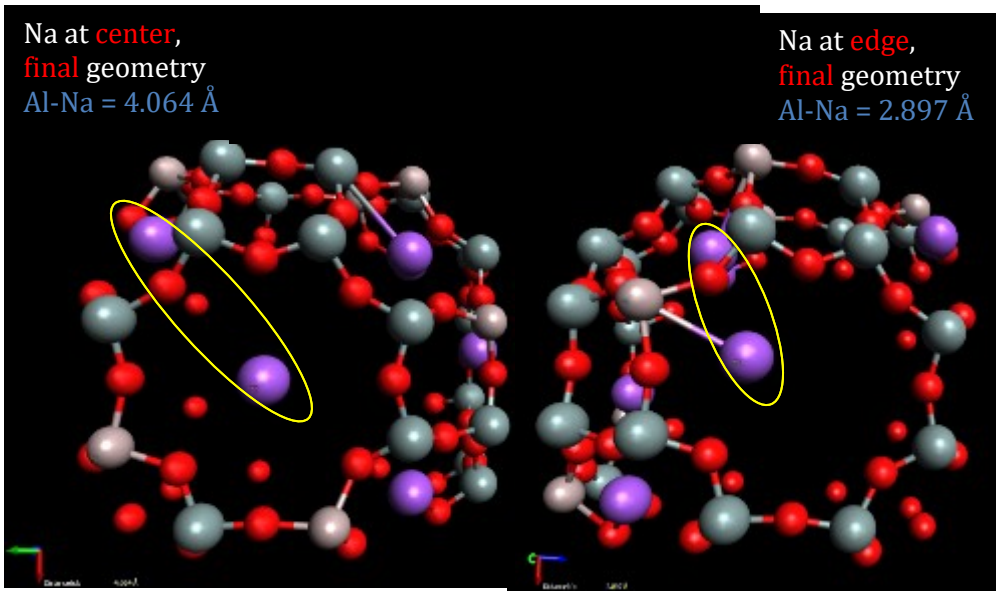

Figure 34 - The images of final geometries of the two different locations of extra-framework cation Na^+ in the 8-membered ring type 2, at Si/Al = 3. On the left was the geometry of an energy minimum in the center, and on the right was the geometry of an energy minimum near the edge of the LTA framework. The geometry on the left was more stable based on the energies. The distances between the in-framework cation (Al^{3+}, brown) and the extra-framework cation (Na^+, purple) were displayed at the top corners of the image. The yellow ovals depicted the distance between two adjacent sodium cations.

the cation near the edge of the LTA ring. In Si/Al = 3, the extra-framework sodium cation in type 2 was close to the extra-framework sodium cation in ring type 1, as highlighted in Figure 34. This repulsion between the extra-framework cations could therefore cause the geometry with the extra-framework cation in the center be more preferable, and therefore has the lower relative energy.

When comparing the geometries between the positions of extra-framework cation positions of center and edge for Na^+, in the lower two images of Figure 35, the final position of sodium was relatively more close to the edge of the LTA, reflected by the Al-Na distance of 2.888 Å. For K^+, in the lower two images of Figure 36, the final position of the potassium cation was relatively more close to the center of the ring, reflected by the Al-K distance of 3.588 Å. For Na^+, the position for sodium cation could be caused by the attracting forces by the two adjacent oxygen anions. The attractive forces could overcome the repulsive forces by the in-framework cations and led to a closer-to-edge position for Na^+ as shown in Figure 35. For K^+, the ionic radius of the extra-framework cations could contribute to the geometry difference, where K^+ has 138 pm and Na^+ has 102 pm. Due to the larger ionic radii, K^+ could have greater repulsive potential than Na^+ with the in-framework cations, such as Al^{3+} and Si^{4+}. The repulsive forces could overcome the attracting forces exerted by the oxygen anions, and therefore led to a closer-to-center extra-framework cation position.
When all sites were occupied by the cation pair (Si/Al = 1), the "Pore Opening Diameter" was the smallest among all other Si/Al ratios. The introduction of cation substitutions, supported by DFT results, decreased the values of two geometrical parameters: "Accessible Pore Volume" and "Pore Opening Diameter". These two parameters are important in determining the size of interacting molecules and ions that can move into or be trapped

inside the LTA structure; and these two physical parameters correlate to the amount of cation substitution (Si/Al ratio). These two parameters would play an important role in determining adsorption effectiveness.

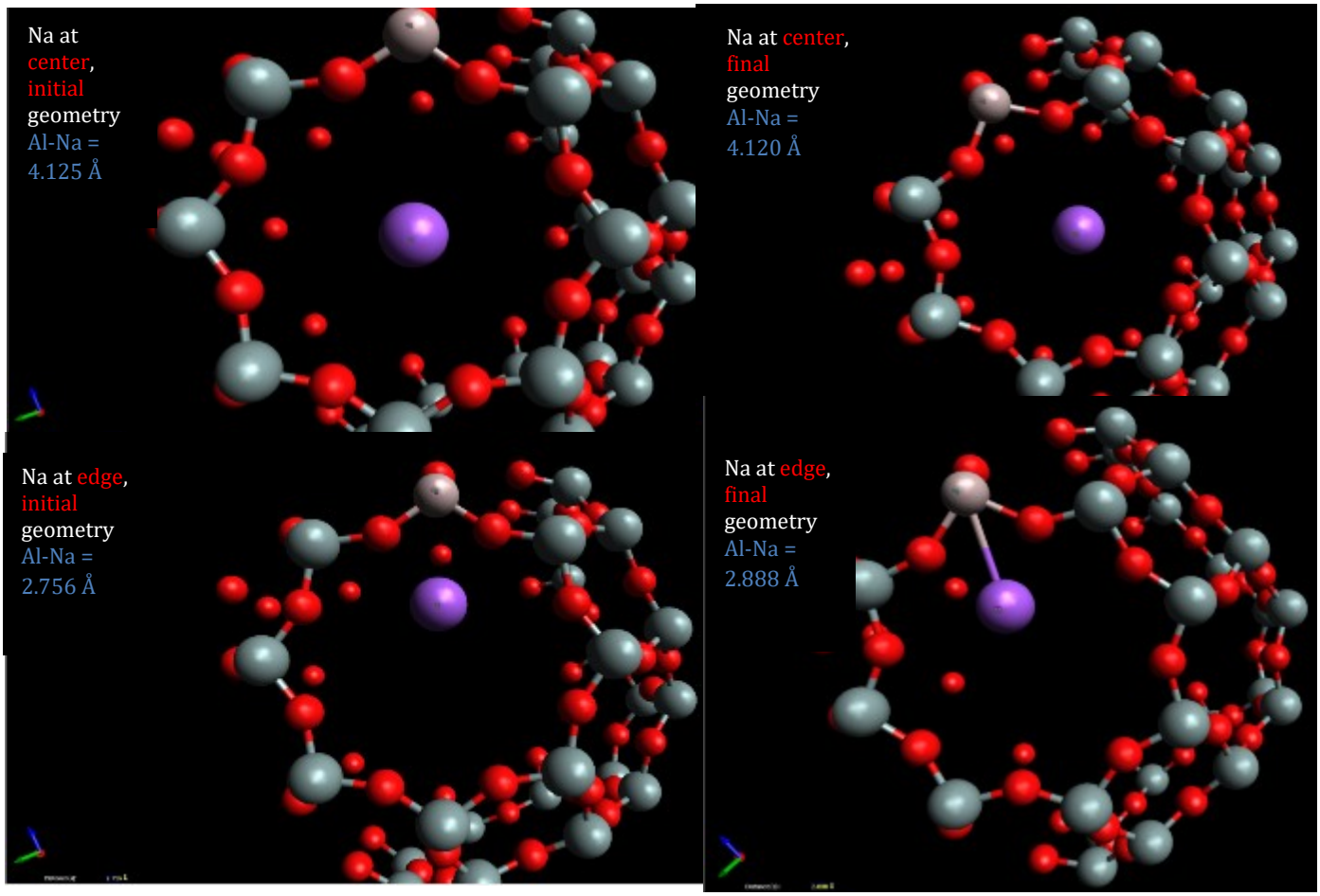

Figure 35 – Comparison of initial and final geometries of the two positions (center and edge) of the extra-framework cation Na^+ (purple) at Si/Al = 23. The upper left represented the relative position of the Na^+ near the center before geometry optimization; upper right represented its relative position after the optimization. The lower left represented the relative position of the Na^+ near the edge before geometry optimization; lower right represented its relative position after the optimization. The distance between the in-framework cation Al^{3+} and extra-framework Na^+ were showed in the figure.

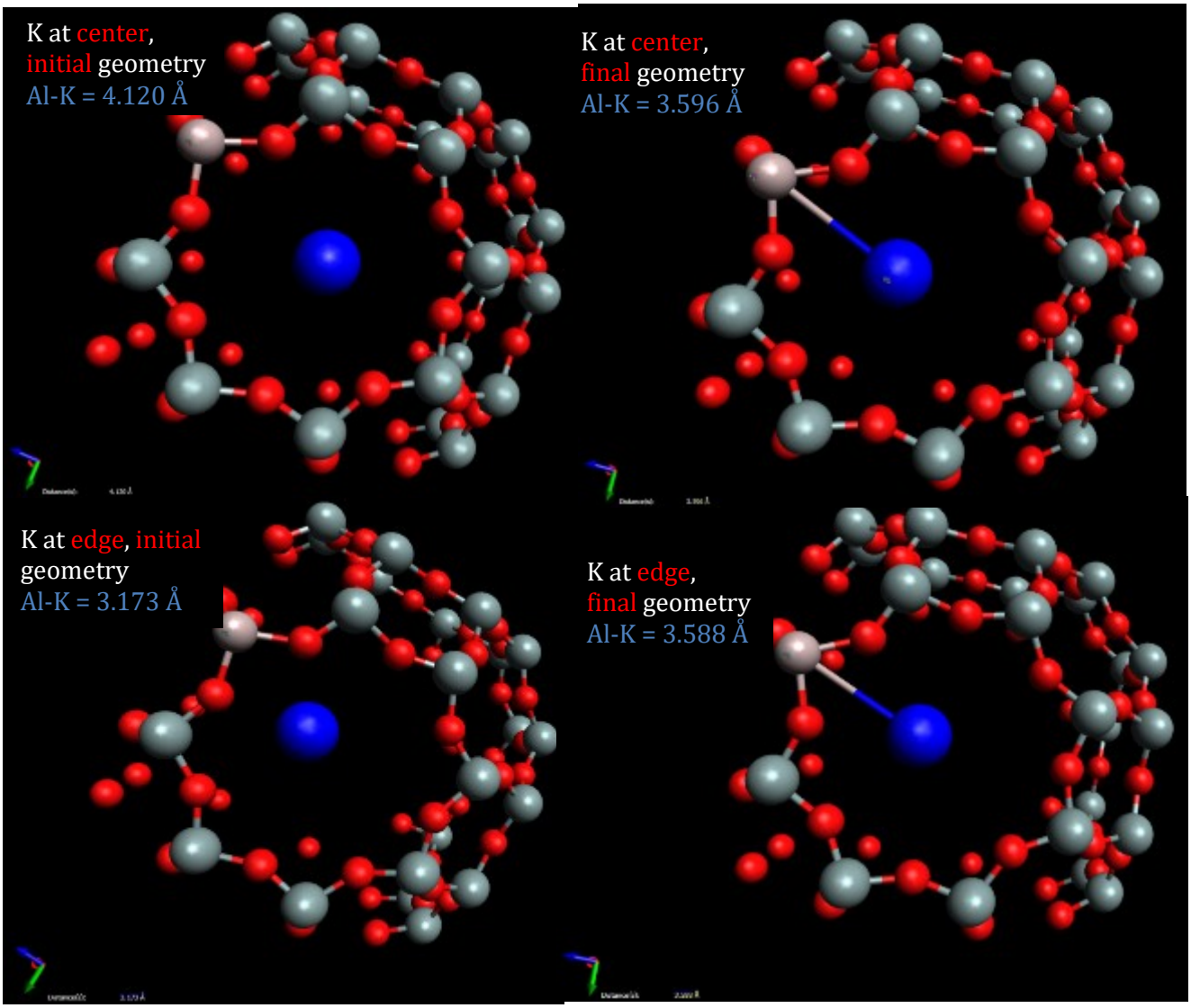

Figure 36 - Comparison of initial and final geometries of the two positions (center and edge) of the extra-framework cation K^+ (blue) at Si/Al = 23. The upper left represented the relative position of the K^+ near the center before geometry optimization; upper right represented its relative position after the optimization. The lower left represented the relative position of the K^+ near the edge before geometry optimization; lower right represented its relative position after the optimization. The distance between the in-framework cation Al^{3+} and extra-framework K^+ were showed in the figure.

4.1.2 Results and discussion for K^+/Al^{3+} Substitution

Table 4 - Effect of K^+/Al^{3+} substitution on zeolite LTA geometry. UKS off. Red results are for most stable types.

Si/Al Ratio	Number of Al in Simulation Cell	Lattice Parameter a (Å)	Relative Position of Cations in the Ring	Accessible Pore Volume ($Å^3$)	Pore Opening Diameter (Å)	Relative Energy (eV)	Preferred Locations of Cations
∞	0	11.936	N/A	1338.71	6.861	-867.7444	N/A
23	1	11.994	Center	494.99	6.613	0.395	Type 1
23	1	11.992	Edge	466.59	6.617	0.365	Type 1
23	1	11.989	Center	913.86	6.480	0.000	Type 2
23	1	11.993	Edge	890.19	6.531	0.001	Type 2
23	1	11.976	Center	334.90	6.540	0.441	Type 3
23	1	11.976	Edge	332.00	6.540	0.442	Type 3
3	6	12.073	Center	542.68	6.39	0.713	Type 1 + 3
3	6	12.011	Edge	570.80	6.277	0.136	Type 1 + 3
3	6	12.072	Center	520.15	6.402	0.040	Type 1 + 2
3	6	12.105	Edge	552.92	6.353	0.000	Type 1 + 2
3	6	12.098	Center	394.96	6.09	1.611	Type 2 + 3
3	6	12.078	Edge	400.95	6.136	1.374	Type 2 + 3
1	12	12.285	Center	432.68	6.209	1.839	All Types
1	12	12.327	Edge	479.49	6.209	0.000	All Types

Table 5 - Effect of K^+/Al^{3+} substitution on zeolite LTA geometry. UKS on.

Si/Al Ratio	Number of Al in Simulation Cell	Lattice Parameter a (Å)	Accessible Pore Volume ($Å^3$)	Pore Opening Diameter (Å)	Preferred Locations of Cations
∞	0	11.936	1338.71	6.861	N/A
23	1	11.990	914.77	6.529	Type 2 - Center
3	6	12.110	556.44	6.353	Type 1 + 2 - Edge
1	12	12.277	502.49	6.209	All Types - Edge

After determining in optimal ring locations for Al^{3+} as shown by the results in Table 4, for Si/Al = 23, ring type 2 is the most stable among the 3 types of rings. Although the "Relative Energy" for center and edge at ring type 2 were differed by 0.001 electron volt, type 2 ring was preferred comparing to the energies of the other ring types at Si/Al = 23. The

preferred ring location for K^+ agreed with the results in Na^+, where type 2 was also preferred. Both the calculated energies and geometries displayed the likelihood for 8-membered ring to interact with the extra-framework cations. For the lattice parameter and Si/Al ratio, the results indicated a correlation that is similar to that in Na^+/Al^{3+} substitution. The physical parameters of the most stable geometries in each Si/Al ratio were calculated with UKS on to compare with UKS off (red results in Table 4). The results with UKS on were consistent with the UKS off data, which also verified the accuracy of the calculated geometries.

Table 6 – Accessible Pore Volume and Pore Opening Diameter comparison between Na^+/Al^{3+} and K^+/Al^{3+} substitution at the most stable ring type.

	Accessible Pore Volume (Å^3)		Pore Opening Diameter (Å)	
Si/Al Ratio	Na^+/Al^{3+}	K^+/Al^{3+}	Na^+/Al^{3+}	K^+/Al^{3+}
∞	1338.71	1338.71	6.861	6.861
23	951.53	913.86	6.559	6.480
3	857.23	552.92	6.368	6.353
1	693.11	432.68	6.14	6.209

For Si/Al = 3, the relative energies in Table 4 showed that K^+ also tended to stay in ring type 1 and 2. By comparing the "Accessible Pore Volume" side-by-side between Na^+/Al^{3+} and K^+/Al^{3+} in Table 6, for the same Si/Al ratio, Na^+/Al^{3+} has greater "Accessible Pore Volume" and "Pore Opening Diameter" than K^+/Al^{3+}. Both the physical parameters showed agreement that as Si/Al ratio decreased, "Accessible Pore Volume" and "Pore Opening

Diameter" decreased. Because sodium and potassium cations have the same charge (+1), their difference in radii determines the change in physical structure of the LTA. In Figure 37, the "Accessible Pore Volume" for Na^+ was more than 500 $Å^3$ greater than that of K^+ at Si/Al = 3. As shown in the two 6-membered ring, the difference in the Accessible Pore Volume was observed by the extra-framework cation positioning towards the center of the LTA unit cell: Na^+ (blue) positioned above the surface ring when K^+ (purple) placed on the

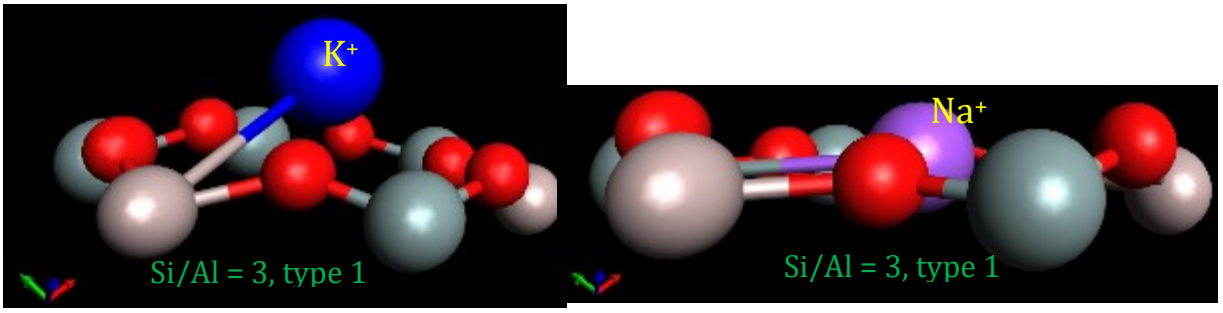

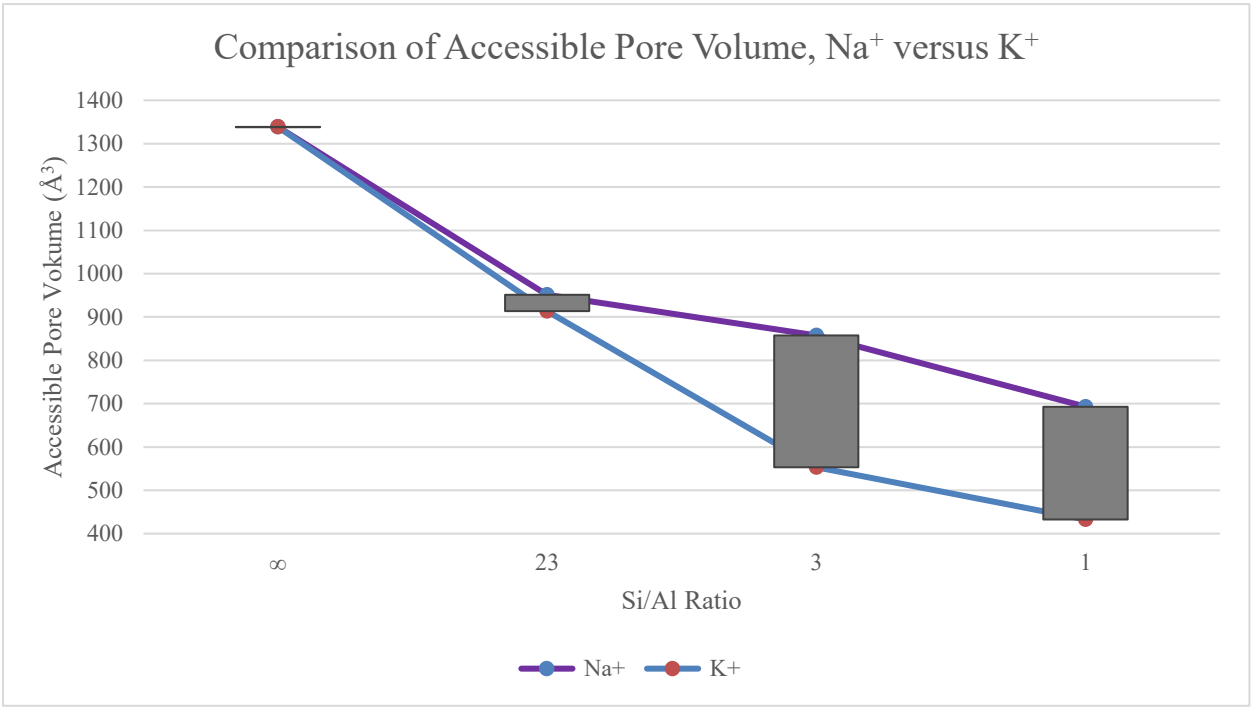

Figure 37 – Comparison of Accessible Pore Volume between Na^+ and K^+ at various Si/Al ratio. The purple line represents Na^+, the blue K^+. The grayed bars show as the difference in volume between Na^+ and K^+. Both at Si/Al = 3 ring type 2, the upper left image depicted sodium cation's position (blue) relative to the surface ring; the upper right image depicted potassium cation (purple).

surface ring. K^+ cations showed repulsion from the surface ring, and this could be caused by its greater ionic radii than Na^+ cation's effective ionic radii. The repulsive forces between the in-framework cations (Al^{3+} and Si^{4+}) and the extra-framework cations led to this change in LTA's physical parameter. Even though both cation pairs have the same +1 charge, K^+ apparently could allow adsorption molecules and ions that were smaller than could be allowed in Na^+. The results showed that potassium cation substitution could be useful in trapping smaller molecules compared to sodium. This trait defined by the two physical parameters could be useful in a molecule selection process.

4.1.3 Results and discussion for H^+/Al^{3+} Substitution

Table 7 - Effect of H^+/Al^{3+} substitution on zeolite LTA geometry. UKS off.

Si/Al Ratio	Number of Al in Simulation Cell	Lattice Parameter a (Å)	Accessible Pore Volume ($Å^3$)	Pore Opening Diameter (Å)	Preferred Locations of Cations
∞	0	11.936	1338.71	6.861	N/A
23	1	12.00	1096.44	6.586	All Types
3	6	12.118	1000.72	6.086	All Types
1	12	12.390	802.01	6.215	All Types

Table 8 - Effect of H^+/Al^{3+} substitution on zeolite LTA geometry. UKS on.

Si/Al Ratio	Number of Al in Simulation Cell	Lattice Parameter a (Å)	Accessible Pore Volume ($Å^3$)	Pore Opening Diameter (Å)	Preferred Locations of Cations
∞	0	11.936	1338.71	6.861	N/A
23	1	12.013	1096.52	6.664	All Types
3	6	12.118	1000.72	6.365	All Types
1	12	12.390	858.54	6.702	All Types

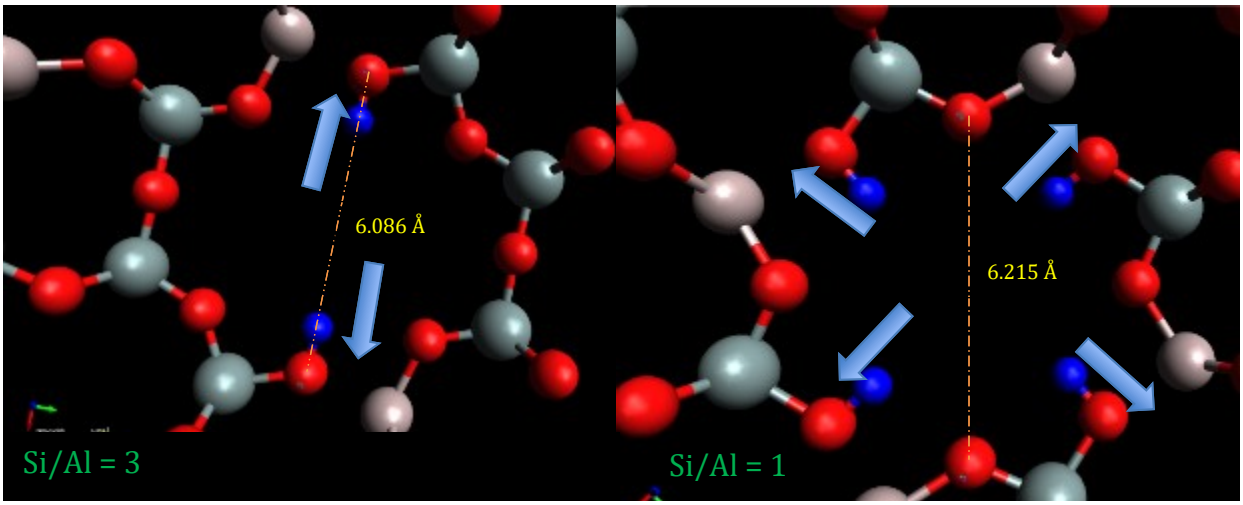

Figure 38 – Comparison of Al^{3+}/H^+ Pore Opening Diameter between Si/Al = 3 and Si/Al = 1. The blue atoms represent H^+, red represent O^{2-}. The dashed orange line represent the Pore Opening Diameter (the shortest diameter in ring type 2 between two opposite oxygen anions). The blue filled arrows signify the direction of forces caused by repulsion from other H^+.

The results for hydrogen cation pair were more straightforward because the hydrogen ion stays close to the ring structure where the Al^{3+} is. Due to the short length and strong strength of H-bond, hydrogen bonded closely to nearby oxygen atoms that were on the LTA structure. Unlike sodium and potassium that tended to stay to the center of a ring, hydrogen cations formed a close affinity to oxygen atoms in the ring. The lattice parameter, in agreement with the previous two substitutions, increased as the Si/Al ratio increased. The "Accessible Pore Volume" for H^+/Al^{3+} substitution appeared to be larger than the other two cation substitutions, where the cation (Na^+ or K^+) located in the center of the ring. Hydrogen cations have the shortest ionic radii compared to the other two extra-framework cations. As hydrogen cations were attracted to the oxygen anions, depicted in Figure 38, the extra-framework cations were not close to the center of the unit cell. This physical change could mean that the hydrogen substitution can allow larger molecules to move into or be trapped within the LTA cage.

At Si/Al = 1 the "Pore Opening Diameter" increased with decreased Si/Al ratio. The smallest "Pore Opening Diameter" occurred when Si/Al ratio = 3. In Figure 38, I took a closer examination at the geometries of the type 2 rings at the Si/Al = 3 and Si/Al = 1. At Si/Al = 3, the "Pore Opening Diameter" was observed between the two oxygen anions with the hydrogen cations forming H-bonds. The strong repulsion between the hydrogen cations could be exerting forces to keep the two oxygen anions further apart, as shown on the left of the Figure 38. At Si/Al = 1, the "Pore Opening Diameter" was measured between two oxygen anions without the H-bonds. There were four repulsive forces being exerted onto the LTA framework, depicted as the filled blue arrows in Figure 37. Because of the circle-type geometry of the ring, the repulsive forces might stretch the ring in the way shown on the right of Figure 38. Because there were four repulsive forces at Si/Al = 1 than two forces at Si/Al = 3, the "Pore Opening Diameter" was

6.215 Å than 6.086 Å, respectively. This showed that for hydrogen substitution, a smaller Pore Opening Diameter might not occur by introducing more cation substitutions. By finding and controlling the Pore Opening Diameter, it can be beneficial to select the type of molecules that we wish to adsorb based on the pore opening. The smaller the pore opening on the surface, the more selective it is for larger molecules to be adsorbed.

4.1.4 Results and discussion for Ca^{2+}/Al^{3+} Substitution

Table 9 - Effect of Ca^{2+}/Al^{3+} substitution on zeolite LTA geometry. UKS off. Red results indicate the most stable geometries.

Si/Al Ratio	Number of Al in Simulation Cell	Relative Position of Cations in the Ring	Lattice Parameter (Å)	Accessible Pore Volume (Å^3)	Pore Opening Diameter (Å)	Relative Simulation Energy (eV)	Preferred Locations of Cations
∞	0	N/A	11.936	1338.71	6.861	0.000	N/A
11	2	Center	12.009	769.22	6.61	0.000	Type 1
11	2	Edge	12.009	831.42	6.61	0.083	Type 1
11	2	Center	11.994	968.18	6.464	0.057	Type 2
11	2	Edge	11.984	970.48	6.464	0.684	Type 2
11	2	Center	11.999	575.18	6.474	2.076	Type 3
11	2	Edge	12.003	576.52	6.474	1.756	Type 3
3	6	Center	12.053	890.38	6.272	0.000	Type 1 + 2
3	6	Edge	12.029	846.32	6.272	0.083	Type 1 + 2
3	6	Center	12.002	703.39	6.195	0.057	Type 1 + 2 + 3
3	6	Edge	12.083	582.24	6.195	0.684	Type 1 + 2 +3
3	6	Center	12.029	601.98	6.024	2.076	Type 2 + 3
3	6	Edge	12.061	598.71	6.024	1.756	Type 2 + 3
1	12	Center	12.227	930.93	6.177	0.000	Type 1 + 2
1	12	Edge	12.235	873.11	6.177	0.102	Type 1 + 2
1	12	Center	12.199	665.09	6.021	6.060	Type 2 + 3
1	12	Edge	12.173	614.63	6.021	5.821	Type 2 + 3

Table 10 - Effect of Ca^{2+}/Al^{3+} substitution on zeolite LTA geometry. UKS on.

Si/Al Ratio	Number of Al in Simulation Cell	Lattice Parameter (Å)	Accessible Pore Volume (Å^3)	Pore Opening Diameter (Å)	Preferred Locations of Cations
∞	0	11.936	1338.71	6.861	N/A
11	2	12.009	768.41	6.667	Type 1 - center
3	6	12.138	947.04	6.491	Type 1 + 2 – center
1	12	12.227	930.97	6.483	Type 1 + 2 - center

The relative energies showed that type 1 and 2 rings were more preferable than type 3 rings in Table 9. For Si/Al = 11, the center of ring type 1 was the most stable form for Ca^{2+}, as shown in Table 9. The attracting forces from the 6 oxygen anions on the left of Figure 39 could contribute to the stability as shown by the lowest relative energy, where on the middle Figure 39 there were only 4 oxygen anions near Ca^{2+}. When observed physically for Ca^{2+} at Si/Al = 11 in Figure 38, the Ca-Al distances in ring type 3 were the shortest among the three ring types. The Ca atom was close to four other cations in the ring, so could have strong repulsive forces, which would lower the total energy compared to the Ca atom in the other ring structures.

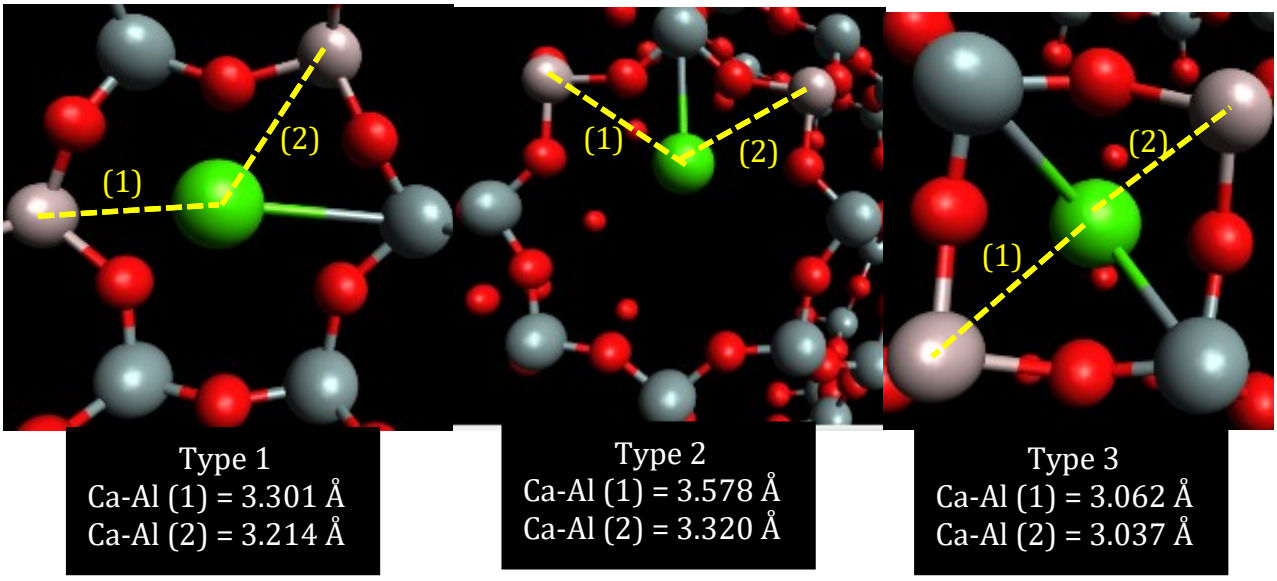

Figure 39 – From left to right, the figure shows the simulated geometries at Si/Al = 11 with calcium cation (green) near the center of ring type 1, 2, 3, respectively. The yellow dashed lines represent the distance between the center of the extra-framework Ca^{2+} and the centers of the two in-framework Al^{3+}. Each Ca-Al distance was labeled as (1) or (2) to compare the distances across the three images.

In Table 9, as the Si/Al ratio decreased, the Accessible Pore Volume increased. The Accessible Pore Volume for calcium was counterintuitive to the trend I discussed for the other three types of extra-framework cations. I took a closer look at the geometries for Si/Al =3. I chose this specific Si/Al ratio because this was a ratio common to all three cation types. In Figure 40, the extra-framework cation's position for Ca^{2+} is similar to Na^{+}, which gave them a similar Accessible Pore Volume. A possible explanation of the behavior of Ca^{2+} as shown in Figure 40 could be based on its ionic radius. The ionic radii for K^{+} was 138 pm,

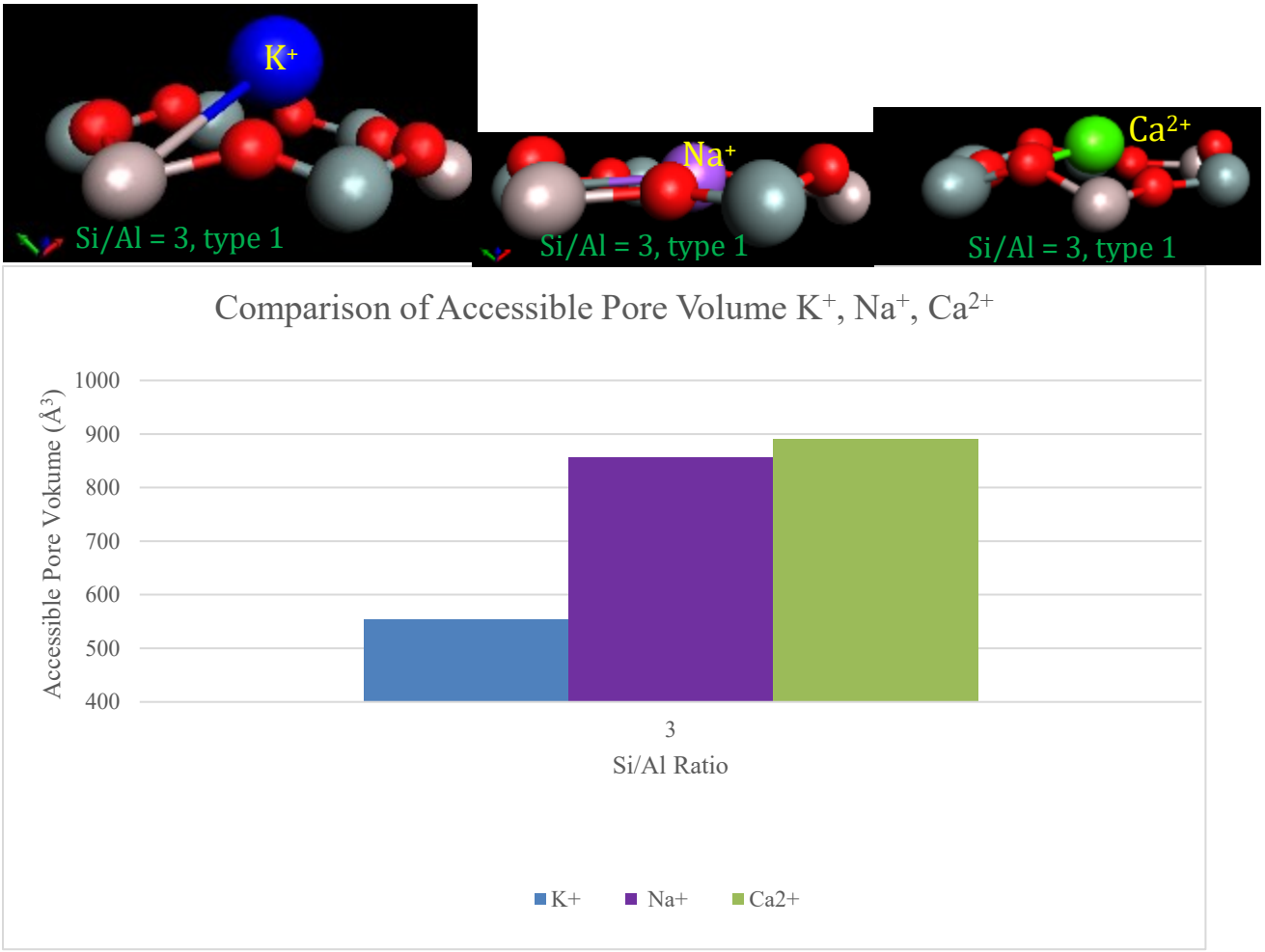

Figure 40 – Comparison of Accessible Pore Volume for K+, Na^{+} and Ca^{2+} at Si/Al ratio = 3. The blue bar represents K^{+}, the purple Na^{+}, and the green Ca^{2+}. The upper left image depicted potassium cation's (blue) position relative to the surface ring; the upper middle image depicted sodium cation (purple), and the upper right calcium cation (green).

which made the repulsion between the in-framework cations and the extra-framework cation greater than those of smaller ionic radii of Na^+ (102 pm) and Ca^{2+} (100 pm). As Figure 40 shows, the K atom was out of the ring, while Na and Ca were closer to the ring. When I measured the Accessible Pore Volume I began at the middle of the zeolite cell and measured to the closest cation, which was often the extra-framework cation. Since the K atom was farthest from the ring center (and closest to the cell center), the distance used to calculate Accessible Pore Volume is smallest for K^+.

Table 11 – Comparison of Accessible Pore Volume and Pore Opening Diameter between UKS on and UKS off, for Ca^{2+} at Si/Al = 11, 3, 1. The blue results indicate differences in values.

	UKS off	UKS on	UKS off	UKS on
Si/Al Ratio	Accessible Pore Volume ($Å^3$)	Accessible Pore Volume ($Å^3$)	Pore Opening Diameter (Å)	Pore Opening Diameter (Å)
∞	1338.71	1338.71	6.861	6.861
11	769.22	768.41	6.61	6.667
3	890.38	947.04	6.272	6.491
1	930.93	930.97	6.177	6.483

A difference in "Pore Opening Diameters" for UKS on and off was observed in Table 11. The "Accessible Pore Volume" between UKS on and off appeared to be consistent. I took a close look at the images of the geometries between the two options in Figure 41 at Si/Al = 1, where the "Pore Opening Diameter" differed in value the most (6.272 Angstrom for UKS off versus 6.483 for UKS on). On the left of Figure 41, Ca^{2+} appeared to be attracted to the left of ring type 2; on the right of Figure 41, Ca^{2+} appeared to be at the top of ring type 2. The difference in the relative position of the extra-framework cation appeared to affect the location of the "Pore Opening Diameter", as shown in Figure 41, where the two dashed lines

were in opposite directions. The results for Na^+ cations between UKS on and off options had a similar behavior in the physical parameters, which could be explained by their similar ionic radius.

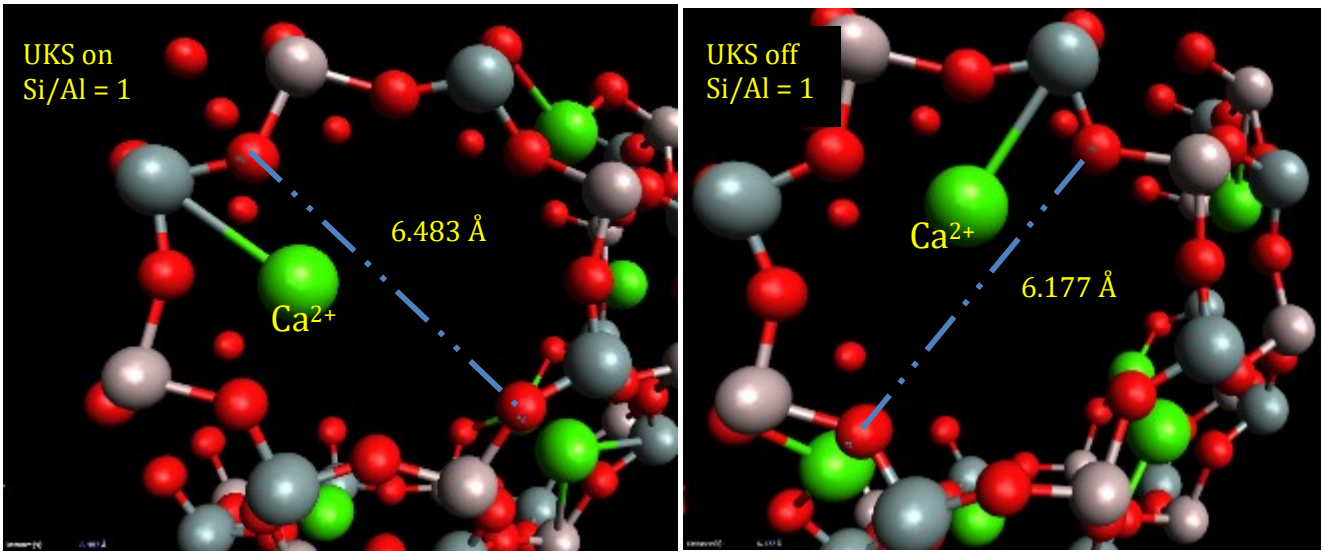

Figure 41 – Images of the geometries for Ca^{2+} at Si/Al = 1. UKS on showed on the left at ring type 2, UKS off showed on the right. The blue dashed line represented the "Pore Opening Diameter" (the shortest diameter in ring type 2 between two opposite oxygen anions). The green atoms represent Ca^{2+}, and the red atoms represent O^{2-}.

Table 12 – A comparison of physical parameters between Ca^{2+}/Al^{3+} and Na^+/Al^{3+} substitution at Si/Al ratio = 3, at most stable geometries

Substitution Element	Si/Al Ratio	Number of Al in Simulation Cell	Lattice Parameter a (Å)	Accessible Pore Volume ($Å^3$)	Pore Opening Diameter (Å)	Preferred Locations of Cations
Ca^{2+}/Al^{3+}	3	6	12.053	890.38	6.272	Type 1 + 2
Na^+/Al^{3+}	3	6	12.211	857.23	6.368	Type 1 + 2

A common ionic exchange occurs in a water softening process, where sodium cations exchange with calcium cations in water. This LTA study determined the physical

parameters for both present elements and their effect on the LTA structure. As shown in Table 12, the effects of calcium and sodium cations were compared at a Si/Al ratio = 3. This Si/Al was chosen to make a similar comparison between all cation types. The results could also be discussed at Si/Al =1, but the geometries for Na^+ due to the repulsion among the 12 extra-framework cations made the geometries complicated, therefore I chose more clear geometries for the same Si/Al ratio comparison. At Si/Al = 3, The LTA structure all had 6 aluminums in the rings. In a water softening process[3], if LTA with sodium cations were emerged into water with calcium, the ionic exchange would make the pore less accessible as the "Pore Opening Diameter" shrunk (6.368 Angstrom to 6.272 Angstrom). This could be an indication of when the calcium had substituted with the sodium, which completed the water softening process.

[3] For an explanation of the water softening process, refer to background section 2.2.1 in this paper for an explanation and illustration.

4.2 Adsorption of alkanes and alcohols in LTA

The effect of alkane and alcohol interactions with LTA structures was studied by comparing the energies of adsorption. The adsorption energies of alkane and alcohol in the center of the unit cell is compared as a reference to when the molecules were placed near the rings. In the results, the energy values are converted from hartree to electron volt (eV), using the NIST's CODATA value of 1 hartree = 27.211386 eV ("NIST Reference," 2014). Detailed tables of all energies for modeled molecules and zeolites can be found in Appendix B of this paper. The tables for the adsorption energies are also located in Appendix B in this study; the images of simulated geometries are located in Appendix C.

4.2.1 Results and discussion for alkane interacting with LTA

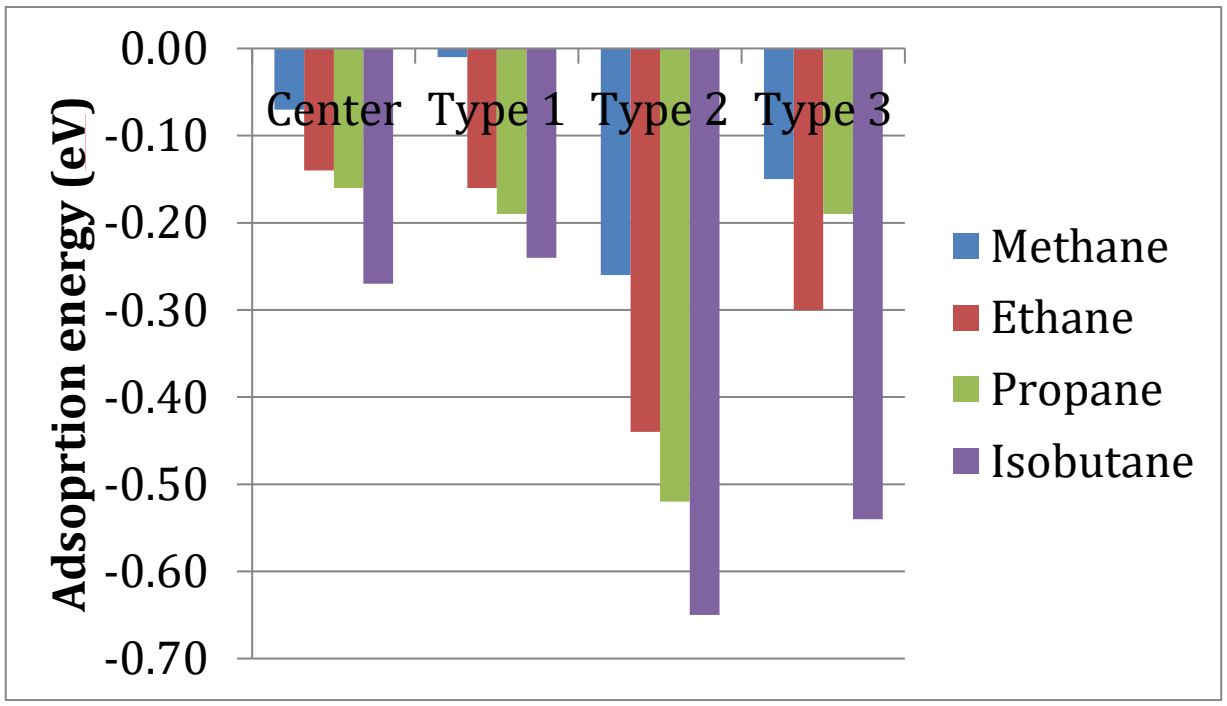

Figure 42 - Comparison of adsorption energies for alkanes at each ring type. Center means the alkane is placed in the center of the unit cell.

In Figure 42, the adsorption energies for alkanes in the center of the unit cell were calculated as a reference value. Comparing to the adsorption energies in the center, the adsorption energies for alkanes near ring type 2 were more negative. This could be explained by the distances between the molecule the ring, and the number of atoms in ring type 2. Ring type 2 has eight oxygen anions, more than the other two ring types. These in-framework anions could account for the greater attracting forces, which stabilized the geometries. But the distances between the alkanes and Si^{4+} cations in type 2 are further than the other two ring types, therefore less of repulsion between the Si^{4+} and alkane as shown on the right of Figure 43. In ring type 1 and 3, the distances between alkanes and Si^{4+} are closer, therefore imposing greater repulsion than attraction. The balance in

repulsion and attraction indicated that type 2 had the most stable interaction between the alkane molecule and LTA framework.

By comparing the adsorption energies side-by-side for different sizes of alkanes, it was clear that isobutane (depicted as the purple bars) had the largest adsorption energy in absolute value. Isobutane (C_4H_{10}) had the largest molecular size among the four studied alkanes so would be expected to interact more with the zeolite This phenomenon could be useful for understanding the cracking process in crude oil, where the majority of its content consists of long, large chains of alkanes. LTA showed, from this DFT result, that it would perform well as it could be highly select and adsorb larger alkane products due to the difference in adsorption energies.

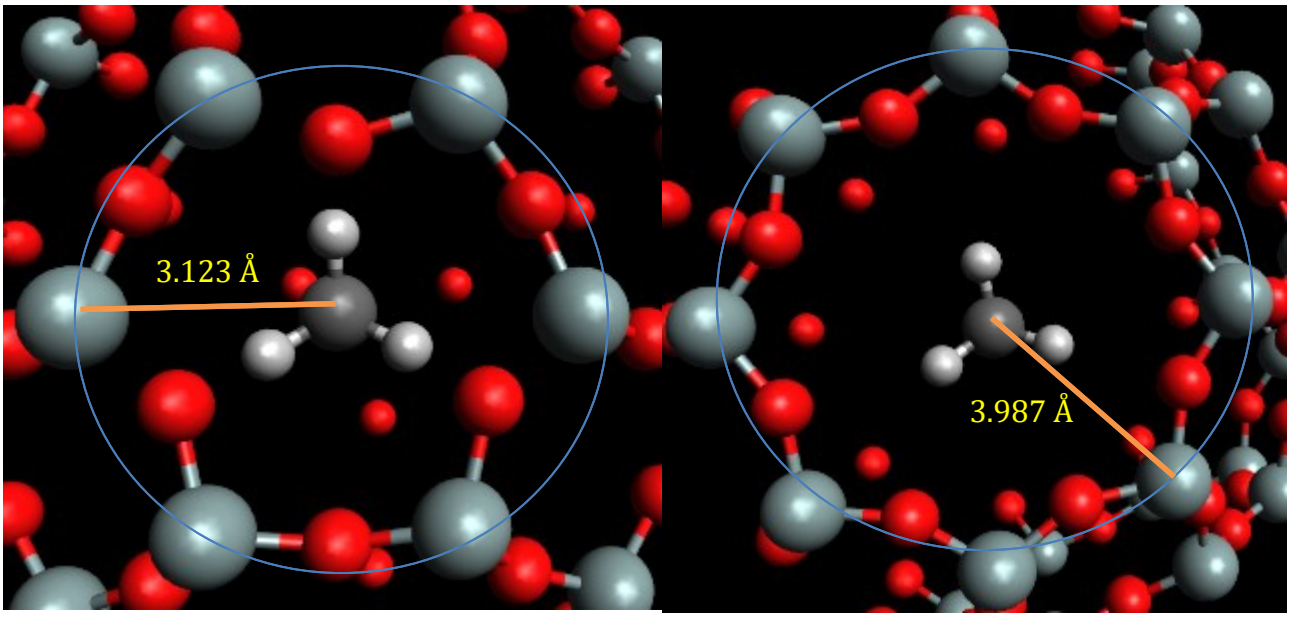

Figure 43 – The image on the left showed methane interacted with pure LTA at the surface of ring type 1, on the right showed methane at ring type 2. The comparison of the two geometries was intended to show the intermolecular distance between the alkane and LTA surface which physically hindered the adsorption based on repulsion between silicon atoms (light grey) and the carbon atoms (dark grey). The numbers in yellow represented the shortest distance from the center of carbon atom to the in-framework silicon atoms.

In Figure 42, an increase in absolute value of adsorption energies from methane to isobutane was observed in LTA's ring type 2 (8-membered ring). This could be due to the increase of carbon atoms in alkanes as its length increases. Type 2 also had overall lowest (most exothermic) adsorption energies compared to type 1 and 3. The pore opening of type 2 ring is larger than the other two types. In Figure 43, the comparison of methane near the ring type 1 and type 2 showed that the smaller ring type 1 had a closer distance to the methane and therefore stronger repulsion forces between the LTA and methane. The repulsion could contribute to the lower adsorption energies in type 1. For ring type 2, the larger pore size incurred less repulsions between the LTA and methane; therefore, the adsorption energies were greater in value for alkanes at the ring type 2. Knowing the locations of adsorption for the pure zeolite could be helpful when cation substitution happened.

4.2.2 Results and discussion for alcohol interactions with LTA

In Figure 44, the adsorption energies for alcohols at the center of the unit cell showed similar trend for types 2 and 3. The adsorption energies increased in absolute values from methanol (blue bar) to isobutanol (purple bar); this was comparable to the trend observed in the LTA/alkane interactions: the larger alcohols also had more carbon atoms, which contributed to more repulsions between the carbon atoms and the in-framework silicon

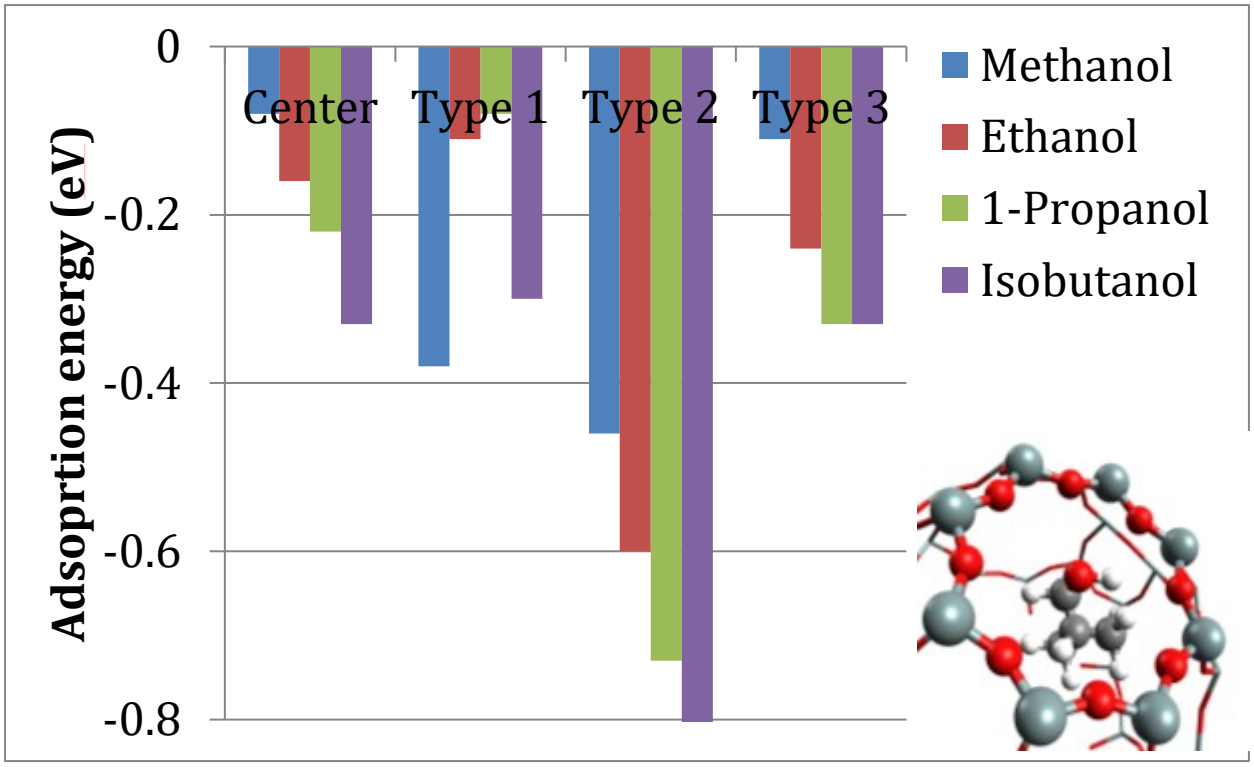

Figure 44 - Comparison of adsorption energies for alcohols with –OH facing each ring. "Center" means the alkane is placed in the center of the unit cell. The picture in lower right depicts the alcohol with –OH facing a ring.

atoms. Type 2 ring also showed as the preferred surface site for alcohols with –OH facing the zeolite rings. Similar to the explanation for LTA's interaction with alkanes, the repulsions between the LTA and alcohols when the alcohols are too close could contribute to the larger ring preference, ring type 2. Isobutanol at type 2 (purple bar) had the greatest in absolute value compared to other alcohols. Pure LTA, as supported by the adsorption

energies in DFT simulations, could selectively adsorb alcohols; and therefore, for example, in a mixture of alcohols ranging from C1-C4, the results indicated that isobutanol would tend to be strongly adsorbed to the LTA structure at ring type 2, whereas other alcohols would most likely not be trapped. In Figure 45, similar to the results of alcohols with –OH facing zeolite rings, are shown results where the methyl group faces the ring (-3H). The figure shows consistency between our results in that the two orientations (-OH, -3H) share various trends. Ring type 2 is the most preferred surface site for alcohols to be adsorbed.

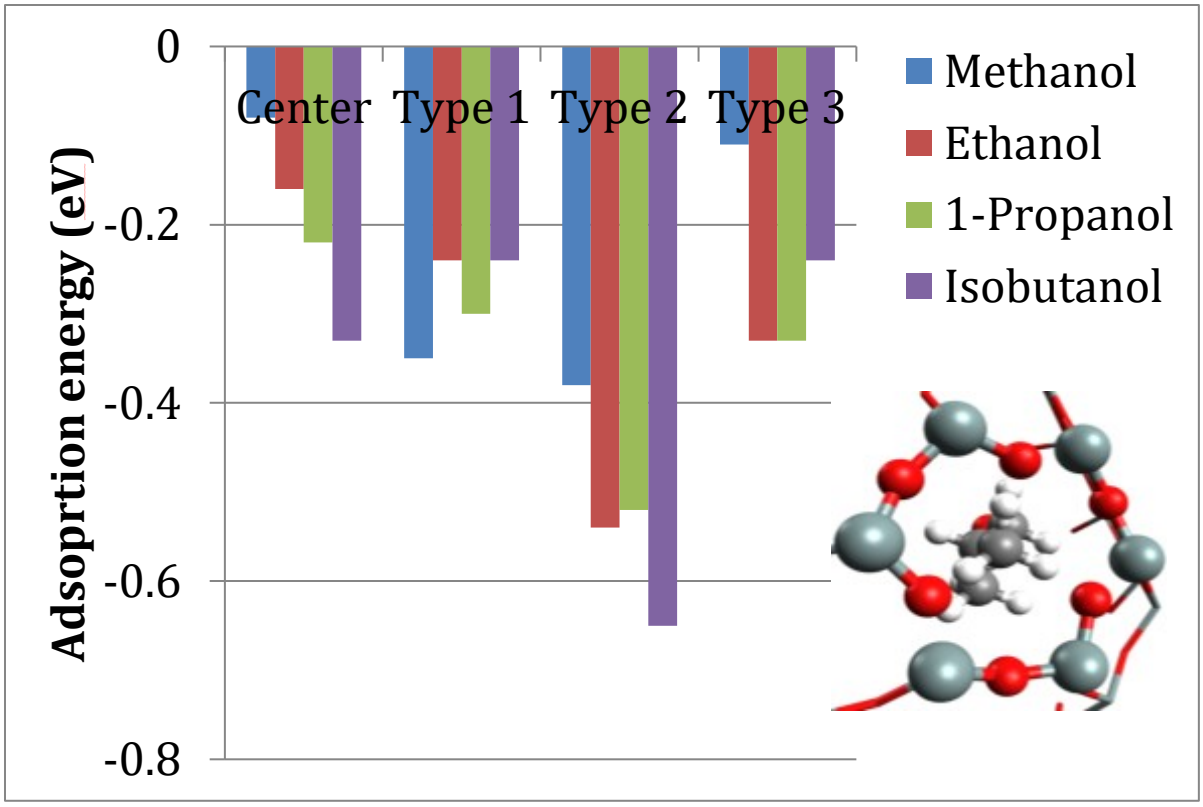

Figure 45 - Comparison of adsorption energies for alcohol with –3H facing each ring type. Center means the alkane is placed in the center of the unit cell. The scheme on lower right depicts the alcohol with –3H facing a ring.

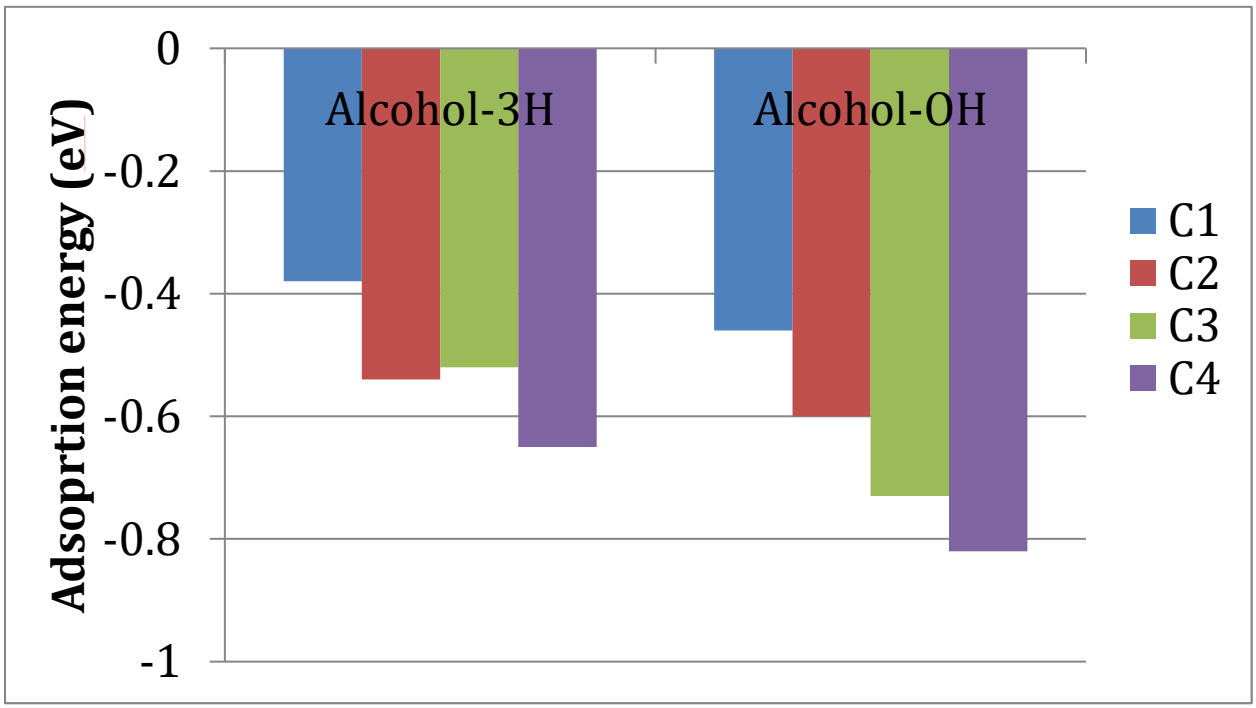

Figure 46 - Comparison of adsorption energies for the orientations 3H and OH of the alcohols from C1 to C4 for the molecules at ring type 2 (8-membered ring). Bars on the left are the adsorption energies for the -3H orientation, on the right for the –OH orientation.

The purpose of studying both orientations for alcohols was to explore whether orientation of the –OH group or the -3H group will affect the adsorbing behavior in LTA. Because both –OH and -3H preferred ring type 2 as the adsorption location, the adsorption energies of the alcohols in the two opposite orientations are compared, as shown in Figure 46.

The results show that the pure LTA preferred to adsorb alcohols with the –OH orientation facing the zeolite ring. This could be explained by the polarity of the alcohol itself, where the hydroxyl group intuitively tended to interact more actively with the surface rings of the LTA due to the O-H bond. In addition, the length of the alcohol chain increased (from C1 to C4), the adsorption energies became greater in absolute value. This indicated a possible correlation between the sizes of the alcohols, as observed in LTA-alkane interactions.

In Figure 47, adsorption energies for alkanes and alcohols were compared. The adsorption energies of alcohols were greater in absolute value than the alkanes. The main difference in

the molecular compositions between the alkanes and alcohols was the hydroxyl group on alcohols which has a net negative charge because of the O atom. Because the pure LTA was loaded with Si^{4+} cations, the interactions between the hydroxyl group on alcohols and the LTA framework were therefore greater than both the alkane and the –H side for alcohols, which were practically the same with alkane in this scenario. In a mixture of both alkanes and alcohols, based on the adsorption energy difference, the pure LTA would prefer adsorption with alcohols on its ring sites. The results indicated that a molecule selection process could occur due to the adsorption energy difference. The adsorption energies could provide some information on LTA's application for instance in biofuel production (which may have higher hydroxyl content than pure petroleum), where the pure LTA is able to select alcohols preferably base on their adsorption energy differences in the LTA-compound interactions, also possibly based on the sizes of the organic compounds.

5 Conclusions

In this LTA zeolite surface study, with theoretical support from density functional theory, the changes of the zeolite LTA during various cation substitutions were investigated. By varying the Si/Al ratio, the preferred ring type for extra-framework cation substitution was observed by comparing their energies. After determining the site preference, LTA's pore accessible volumes and its pore diameters were calculated and analyzed to study the effect of cation substitution on the physical properties of the LTA framework. Adding the cation pairs changed the geometries of LTA as we observed a decrease in their Pore Opening Diameter and Accessible Pore Volume. The magnitude of alkane and alcohol interactions with pure LTA framework was also studied for C1 to C4. The preferred adsorption sites for alkanes and alcohols were also determined by calculating and comparing their adsorption energies. This LTA zeolite study hopes to provide some theoretical support for future research on the LTA structure, and its application in catalytic cracking, biofuel production, and water purification process. These results shed some light on the understanding of pure LTA's interactions with C1-C4 alkanes, in the hope to provide some information on how larger alkanes and alcohols could be simulated with pure LTA and LTA with cation substitution.

6 Recommendations for future studies

This LTA study can be further expanded by modeling longer and larger alkanes and alcohols interacting with the LTA framework. Beyond the short length alkanes we modeled, longer chain alkanes such as octane are the primary content in gasoline. The effect of cation substitutions on the adsorption of alkanes and alcohols can help in the understanding of more realistic LTA zeolites. LTA has also recently been studied for its adsorption ability to selectively remove radioactive cesium (Ce) from nuclear waste(Lee et al., 2017). LTA has also been studied for cation substitution, such as copper (Cu^{2+}), as catalysts in diesel engines to reduce emitted pollutants nitrogen oxides (NO_x) (Ryu et al., 2017). Besides LTA, a variety of other zeolite microporous structures are of interest for their abilities in adsorption, such as Faujasite (FAU). Furthermore, other exchange functionals and basis sets can be used, in order to explore where increased accuracy can be obtained for these types of simulations.

7 Acknowledgements

I would like to thank specially to my advisor Professor N. Aaron Deskins for his support and guidance to this DFT study in LTA surface. Thanks to the WPI's department of chemical engineering for the high performance computer (HPC) clusters for the processors to run the simulations in CP2K. Also thanks to Juan Garcia, a Ph.D. graduated from WPI, who provided many insights in programming that relate to the scope of this project.

8 Bibliography

Brita Natural Water Filtration Process. (2017, March 28). Retrieved March 28, 2017, from https://brita.ca/water-filtration-process/

Clark, J. (2002). Catalysts in the petrochemical industry.

Clark, S. J. (2003, May 4). The Hohenberg-Kohn Theorems. Retrieved April 26, 2017, from http://cmt.dur.ac.uk/sjc/thesis_ppr/node12.html

CP2K - About. (2016). Retrieved from https://www.cp2k.org/about

Cundy, C. S., & Cox, P. A. (2003). The Hydrothermal Synthesis of Zeolites: History and Development from the Earliest Days to the Present Time. *Chemical Reviews*, *103*(3), 663–702. https://doi.org/10.1021/cr020060i

Database of Zeolite Structures. (2017, March 28). Retrieved from http://america.iza-structure.org/IZA-SC/ftc_table.php

Fawer, M., Postlethwaite, D., & Klüppel, H.-J. (1998). Life cycle inventory for the production of zeolite a for detergents. *The International Journal of Life Cycle Assessment*, *3*(2), 71–74. https://doi.org/10.1007/BF02978490

Goedecker, S., Teter, M., & Hutter, J. (1996). Separable dual-space Gaussian pseudopotentials. *Physical Review B*, *54*(3), 1703–1710.

Grimme, S. (2006). Semiempirical GGA-type density functional constructed with a long-range dispersion correction. *Journal of Computational Chemistry*, *27*(15), 1787–1799. https://doi.org/10.1002/jcc.20495

Hanwell, M. D., Curtis, D. E., Lonie, D. C., Vandermeersch, T., Zurek, E., & Hutchison, G. R. (2012). Avogadro: an advanced semantic chemical editor, visualization, and analysis

platform. *Journal of Cheminformatics*, *4*(1), 17. https://doi.org/10.1186/1758-2946-4-17

Hohenberg, P., & Kohn, W. (1964). Inhomogeneous Electron Gas. *Physical Review*, *136*(3B), B864–B871.

Kohn, W., & Sham, L. J. (1965). Self-Consistent Equations Including Exchange and Correlation Effects. *Physical Review*, *140*(4A), A1133–A1138.

Lee, H. Y., Kim, H. S., Jeong, H.-K., Park, M., Chung, D.-Y., Lee, K.-Y., … Lim, W. T. (2017). Selective Removal of Radioactive Cesium from Nuclear Waste by Zeolites: On the Origin of Cesium Selectivity Revaealed by Systematic Crystallographic Studies. *The Journal of Physical Chemistry C*. https://doi.org/10.1021/acs.jpcc.7b02432

Methanol to Olefins. (2017, March 30). Retrieved March 30, 2017, from http://www.cchem.berkeley.edu/molsim/teaching/fall2009/mto/cat.html

NIST Reference. (2014). Retrieved from http://physics.nist.gov/cgi-bin/cuu/Value?threv

Perdew, J. P., Chevary, J. A., Vosko, S. H., Jackson, K. A., Pederson, M. R., Singh, D. J., & Fiolhais, C. (1992). Atoms, molecules, solids, and surfaces: Applications of the generalized gradient approximation for exchange and correlation. *Physical Review B*, *46*(11), 6671–6687.

Perdew, J. P., & Levy, M. (1997). Comment on ``Significance of the highest occupied Kohn-Sham eigenvalue''. *Physical Review B*, *56*(24), 16021–16028.

Petroleum Composition. (2015). Retrieved from http://www.petroleum.co.uk/composition

Ryu, T., Ahn, N. H., Seo, S., Cho, J., Kim, H., Jo, D., … Hong, S. B. (2017). Fully Copper-Exchanged High-Silica LTA Zeolites as Unrivaled Hydrothermally Stable NH3-SCR

Catalysts. *Angewandte Chemie*, *129*(12), 3304–3308. https://doi.org/10.1002/ange.201610547

Shannon, R. D. (1976). Revised effective ionic radii and systematic studies of interatomic distances in halides and chalcogenides. *Acta Crystallographica Section A*, *32*(5), 751–767. https://doi.org/10.1107/S0567739476001551

Structure - Zeolites. (2017, March 29). Retrieved March 29, 2017, from http://www.ch.ic.ac.uk/vchemlib/course/zeolite/structure.html

True, W. R. (2012, July 2). Global ethylene capacity continues advance in 2011. Retrieved April 10, 2017, from http://ezproxy.wpi.edu/login?url=http://search.proquest.com.ezproxy.wpi.edu/docview/1037992852?accountid=29120

9 Appendices

A. Ring size calculations for cation exchanges

LTA-al1-na1-s2							
	Diameter 1	Diameter 2	Diameter 3	Diameter 4	Min. Radius	Pore area Å^2	Min. distance from center
Ring 1	6.771	6.469	6.588	6.675	3.2345	32.86731171	5.956
Ring 2	6.847	6.774	6.847	6.779	3.387	36.03962521	Internal Volume Å^3
Ring 3	6.732	6.83	6.731	6.795	3.3655	35.58353272	885.0191673

LTA-al1-na1-s3							
	Diameter 1	Diameter 2	Diameter 3	Diameter 4	Min. Radius	Pore area Å^2	Min. distance from center
Ring 1	6.744	6.786	6.742	6.785	3.371	35.69993108	5.23
Ring 2	6.671	6.876	6.613	6.859	3.3065	34.34685105	Internal Volume Å^3
Ring 3	6.543	6.903	6.748	6.872	3.2715	33.62356218	599.2301767

LTA-al6-na6-s1s2							
	Diameter 1	Diameter 2	Diameter 3	Diameter 4	Min. Radius	Pore area Å^2	Min. distance from center
Ring 1	6.697	6.781	6.368	6.881	3.184	31.84901393	5.893
Ring 2	6.773	6.984	6.771	7.117	3.3855	36.00771056	Internal Volume Å^3
Ring 3	6.633	6.785	6.414	6.603	3.207	32.31080606	857.2311274

LTA-al1-k1-s1							
	Diameter 1	Diameter 2	Diameter 3	Diameter 4	Min. Radius	Pore area Å^2	Min. distance from center
Ring 1	6.804	6.871	6.665	6.78	3.3325	34.88913393	4.806
Ring 2	6.733	6.79	6.662	6.773	3.331	34.85773293	Internal Volume Å^3
Ring 3	6.613	6.776	6.859	6.72	3.3065	34.34685105	464.9860338

LTA-al1-k1-s3							
	Diameter 1	Diameter 2	Diameter 3	Diameter 4	Min. Radius	Pore area Å^2	Min. distance from center
Ring 1	6.61	6.859	6.665	6.865	3.305	34.31569509	4.308
Ring 2	6.737	6.869	6.54	6.884	3.27	33.59273609	Internal Volume Å^3
Ring 3	6.733	6.789	6.738	6.775	3.3665	35.60468192	334.9004208

LTA-al6-k6-s1s2							
	Diameter 1	Diameter 2	Diameter 3	Diameter 4	Min. Radius	Pore area Å^2	Min. distance from center
Ring 1	6.798	6.81	6.879	6.829	3.399	36.29545139	4.989
Ring 2	6.402	6.517	6.884	6.596	3.201	32.19001811	Internal Volume Å^3
Ring 3	6.885	6.603	6.483	6.682	3.2415	33.00972639	520.1506208

LTA-al2-ca1-s2							
	Diameter 1	Diameter 2	Diameter 3	Diameter 4	Min. Radius	Pore area Å^2	Min. distance from center
Ring 1	6.73	6.851	6.733	6.796	3.365	35.57296047	6.137
Ring 2	6.464	6.693	6.529	6.499	3.232	32.81652394	Internal Volume Å^3
Ring 3	6.61	6.785	6.727	6.79	3.305	34.31569509	968.1819442

LTA-al2-ca1-s3							
	Diameter 1	Diameter 2	Diameter 3	Diameter 4	Min. Radius	Pore area Å^2	Min. distance from center
Ring 1	6.682	6.877	6.474	6.869	3.237	32.91813875	5.159
Ring 2	6.736	6.877	6.479	6.878	3.2395	32.96900507	Internal Volume Å^3
Ring 3	6.734	6.794	6.732	6.777	3.366	35.59410654	575.1553885

LTA-al6-ca3-s1s2s3							
	Diameter 1	Diameter 2	Diameter 3	Diameter 4	Min. Radius	Pore area Å^2	Min. distance from center
Ring 1	6.556	7.333	6.548	7.059	3.274	33.67497041	5.517
Ring 2	6.338	7.068	6.569	7.337	3.169	31.54963586	Internal Volume
Ring 3	6.343	7.42	6.195	6.966	3.0975	30.14203035	703.3922212

LTA-al6-ca3-s2s3							
	Diameter 1	Diameter 2	Diameter 3	Diameter 4	Min. Radius	Pore area Å^2	Min. distance from center
Ring 1	6.024	7.067	6.426	6.715	3.012	28.50098094	5.238
Ring 2	6.212	6.96	6.342	6.212	3.106	30.30768575	Internal Volume Å^3
Ring 3	6.614	6.992	6.475	6.965	3.2375	32.92830887	601.9841985

LTA-al12-ca6-s2s3							
	Diameter 1	Diameter 2	Diameter 3	Diameter 4	Min. Radius	Pore area Å^2	Min. distance from center
Ring 1	6.17	6.973	6.127	7.085	3.0635	29.48394837	5.415
Ring 2	6.089	7.088	6.125	6.978	3.0445	29.11936026	Internal Volume Å^3
Ring 3	6.237	6.963	6.021	7.179	3.0105	28.47260058	665.0954736

LTA-al1-na1-s1-uks							
	Diameter 1	Diameter 2	Diameter 3	Diameter 4	Min. Radius	Pore area Å^2	Min. distance from center
Ring 1	6.896	6.961	6.768	6.843	3.384	35.97581004	6.225
Ring 2	6.937	6.932	6.809	6.831	3.4045	36.41300743	Internal Volume Å^3
Ring 3	6.922	6.844	6.931	6.831	3.4155	36.64868971	1010.431034

LTA-al6-na6-s1s3-uks							
	Diameter 1	Diameter 2	Diameter 3	Diameter 4	Min. Radius	Pore area Å^2	Min. distance from center
Ring 1	6.958	6.77	6.894	6.889	3.385	35.99707548	6.051
Ring 2	6.966	7.154	6.974	7.226	3.487	38.199156	Internal Volume Å^3
Ring 3	6.828	6.974	6.834	6.755	3.3775	35.83773783	928.0472071

LTA-al12-na12-uks							
	Diameter 1	Diameter 2	Diameter 3	Diameter 4	Min. Radius	Pore area Å^2	Min. distance from center
Ring 1	7.282	7.284	6.515	7.039	3.2575	33.33640176	5.462
Ring 2	6.823	7.179	7.053	7.204	3.4115	36.5628991	Internal Volume Å^3
Ring 3	7	7.045	6.781	7.199	3.3905	36.11414772	682.5644996

LTA-al6-k6-s2s3							
	Diameter 1	Diameter 2	Diameter 3	Diameter 4	Min. Radius	Pore area Å^2	Min. distance from center
Ring 1	6.56	6.878	6.09	6.882	3.045	29.12892562	4.563
Ring 2	6.339	7.067	6.612	6.782	3.306	34.33646416	Internal Volume Å^3
Ring 3	6.432	7.142	6.205	6.686	3.1025	30.23941972	397.9605438

LTA-al6-na6-s2s3							
	Diameter 1	Diameter 2	Diameter 3	Diameter 4	Min. Radius	Pore area Å^2	Min. distance from center
Ring 1	6.894	6.969	5.697	7.19	2.8485	25.49073278	5.97
Ring 2	6.174	7.287	6.683	6.872	3.087	29.93802396	Internal Volume Å^3
Ring 3	6.707	7.175	5.959	6.866	2.9795	27.88923824	891.2747493

LTA-al1-k1-s2-uks							
	Diameter 1	Diameter 2	Diameter 3	Diameter 4	Min. Radius	Pore area Å^2	Min. distance from center
Ring 1	6.782	6.884	6.783	6.847	3.391	36.12480007	6.022
Ring 2	6.73	6.823	6.529	6.705	3.2645	33.47982803	Internal Volume Å^3
Ring 3	6.787	6.831	6.904	6.821	3.3935	36.17808541	914.7677871

LTA-al6-k6-s1s3-uks							
	Diameter 1	Diameter 2	Diameter 3	Diameter 4	Min. Radius	Pore area Å^2	Min. distance from center
Ring 1	6.838	6.765	6.95	6.451	3.2255	32.68465951	5.061
Ring 2	6.71	6.838	6.969	6.554	3.277	33.73671214	Internal Volume Å^3
Ring 3	6.84	6.952	6.777	6.881	3.3885	36.07155401	542.9972389

LTA-al12-k12-uks							
	Diameter 1	Diameter 2	Diameter 3	Diameter 4	Min. Radius	Pore area Å^2	Min. distance from center
Ring 1	7.207	6.76	6.888	6.952	3.38	35.89081111	4.691
Ring 2	6.581	7.001	7.43	6.651	3.2905	34.01524967	Internal Volume Å^3
Ring 3	7.169	6.792	6.822	6.796	3.398	36.27409798	432.3992263

LTA-al1-h1-uks							
	Diameter 1	Diameter 2	Diameter 3	Diameter 4	Min. Radius	Pore area Å^2	Min. distance from center
Ring 1	6.79	6.896	6.791	6.82	3.395	36.21007547	6.397
Ring 2	6.869	6.836	6.724	6.664	3.332	34.87866536	Internal Volume Å^3
Ring 3	6.924	6.835	6.922	6.867	3.4175	36.69162271	1096.522788

LTA-al6-h6-uks							
	Diameter 1	Diameter 2	Diameter 3	Diameter 4	Min. Radius	Pore area Å^2	Min. distance from center
Ring 1	6.696	7.005	6.365	7.255	3.1825	31.81901251	6.205
Ring 2	6.518	6.906	6.804	7.191	3.259	33.36711004	Internal Volume Å^3
Ring 3	6.423	6.669	7.068	7.285	3.2115	32.40154547	1000.723197

LTA-al12-h12-uks							
	Diameter 1	Diameter 2	Diameter 3	Diameter 4	Min. Radius	Pore area Å^2	Min. distance from center
Ring 1	6.702	7.037	6.846	6.949	3.351	35.27757537	5.896
Ring 2	6.727	6.778	6.943	7.023	3.3635	35.54125317	Internal Volume Å^3
Ring 3	6.744	6.754	6.838	6.95	3.372	35.72111484	858.540988

LTA-al2-ca1-s1-uks							
	Diameter 1	Diameter 2	Diameter 3	Diameter 4	Min. Radius	Pore area Å^2	Min. distance from center
Ring 1	6.748	6.942	6.801	6.958	3.374	35.76350121	5.682
Ring 2	6.667	6.926	6.739	6.914	3.3335	34.91007579	Internal Volume Å^3
Ring 3	6.807	6.949	6.76	6.913	3.38	35.89081111	768.4087427

LTA-al6-ca3-s1s2-uks							
	Diameter 1	Diameter 2	Diameter 3	Diameter 4	Min. Radius	Pore area Å^2	Min. distance from center
Ring 1	6.922	7.102	6.765	6.744	3.372	35.72111484	6.092
Ring 2	7.052	7.032	6.872	6.72	3.36	35.46732442	Internal Volume Å^3
Ring 3	6.841	7.066	6.86	6.491	3.2455	33.09124444	947.039936

LTA-al12-ca6-s1s2-uks							
	Diameter 1	Diameter 2	Diameter 3	Diameter 4	Min. Radius	Pore area Å^2	Min. distance from center
Ring 1	6.856	6.672	6.483	7.384	3.2415	33.00972639	6.057
Ring 2	6.589	6.727	6.632	7.011	3.2945	34.09799922	Internal Volume Å^3
Ring 3	6.856	7.237	6.864	6.868	3.428	36.91743333	930.8106213

LTA-al2-ca1-s1							
	Diameter 1	Diameter 2	Diameter 3	Diameter 4	Min. Radius	Pore area Å^2	Min. distance from center
Ring 1	6.61	6.87	6.619	6.865	3.305	34.31569509	5.684
Ring 2	6.694	6.878	6.741	6.867	3.347	35.19340582	Internal Volume Å^3
Ring 3	6.669	6.88	6.731	6.884	3.3345	34.93102393	769.220442

LTA-al6-k6-s1s2-edge-uks							
	Diameter 1	Diameter 2	Diameter 3	Diameter 4	Min. Radius	Pore area Å^2	Min. distance from center
Ring 1	6.632	6.69	6.534	6.787	3.267	33.53112631	5.102417951
Ring 2	6.353	6.694	6.608	6.554	3.1765	31.69914818	Internal Volume Å^3
Ring 3	6.816	6.887	6.624	6.9	3.312	34.46121053	556.4378948

LTA-al6-ca3-s1s2							
	Diameter 1	Diameter 2	Diameter 3	Diameter 4	Min. Radius	Pore area Å^2	Min. distance from center
Ring 1	6.877	6.53	6.496	6.508	3.248	33.14224427	5.968
Ring 2	6.594	6.272	6.979	6.495	3.136	30.89598039	Internal Volume Å^3
Ring 3	6.365	6.899	6.75	6.794	3.1825	31.81901251	890.3792958

LTA-al12-ca6-s1s2							
	Diameter 1	Diameter 2	Diameter 3	Diameter 4	Min. Radius	Pore area Å^2	Min. distance from center
Ring 1	6.463	6.703	6.242	6.703	3.121	30.60112621	6.057265344
Ring 2	6.417	6.927	6.177	7.055	3.0885	29.96712532	Internal Volume Å^3
Ring 3	6.871	6.485	6.973	6.228	3.114	30.4640114	930.9329572

LTA-al3-na6-s1s3-edge							
	Diameter 1	Diameter 2	Diameter 3	Diameter 4	Min. Radius	Pore area Å^2	Min. distance from center
Ring 1	7.583	6.989	7.038	7.013	3.4945	38.36365372	5.411993629
Ring 2	7.116	7.359	6.995	7.758	3.4975	38.42955177	Internal Volume Å^3
Ring 3	7.241	6.834	6.655	7.087	3.3275	34.78451889	663.988319

LTA-al3-na6-s1s2-edge							
	Diameter 1	Diameter 2	Diameter 3	Diameter 4	Min. Radius	Pore area Å^2	Min. distance from center
Ring 1	6.689	6.292	7.06	6.75	3.146	31.09333524	5.61789275
Ring 2	6.648	7.17	6.932	6.696	3.324	34.71138183	Internal Volume Å^3
Ring 3	7.174	6.353	6.529	6.765	3.1765	31.69914818	742.6923338

LTA-al3-na6-s2s3-edge							
	Diameter 1	Diameter 2	Diameter 3	Diameter 4	Min. Radius	Pore area Å^2	Min. distance from center
Ring 1	6.707	6.866	5.959	7.175	2.9795	27.88923824	5.383645916
Ring 2	5.697	6.969	6.894	7.19	2.8485	25.49073278	Internal Volume Å^3
Ring 3	6.872	6.683	7.287	6.174	3.087	29.93802396	653.609077

LTA-al12-na12-edge							
	Diameter 1	Diameter 2	Diameter 3	Diameter 4	Min. Radius	Pore area Å^2	Min. distance from center
Ring 1	6.441	7.075	6.262	7.084	3.131	30.79753858	5.499543389
Ring 2	6.428	7.363	6.171	7.206	3.0855	29.90893674	Internal Volume Å^3
Ring 3	6.143	7.099	6.368	7.37	3.0715	29.63813774	696.7364121

LTA-al12-k12-edge							
	Diameter 1	Diameter 2	Diameter 3	Diameter 4	Min. Radius	Pore area Å^2	Min. distance from center
Ring 1	6.758	6.514	6.707	6.553	3.257	33.32616881	4.855474819
Ring 2	6.772	7.088	6.354	6.827	3.177	31.70912824	Internal Volume Å^3
Ring 3	6.209	6.815	6.771	6.977	3.1045	30.27841945	479.494608

LTA-al2-ca1-s1-edge							
	Diameter 1	Diameter 2	Diameter 3	Diameter 4	Min. Radius	Pore area Å^2	Min. distance from center
Ring 1	6.731	6.884	6.669	6.88	3.3345	34.93102393	5.833242165
Ring 2	6.619	6.685	6.61	6.87	3.305	34.31569509	Internal Volume Å^3
Ring 3	6.694	6.878	6.741	6.867	3.347	35.19340582	831.4164795

LTA-al2-ca1-s2-edge							
	Diameter 1	Diameter 2	Diameter 3	Diameter 4	Min. Radius	Pore area Å^2	Min. distance from center
Ring 1	6.499	6.529	6.693	6.464	3.232	32.81652394	6.141841625
Ring 2	6.61	6.79	6.727	6.785	3.305	34.31569509	Internal Volume Å^3
Ring 3	6.733	6.851	6.73	6.796	3.365	35.57296047	970.4752175

LTA-al2-ca1-s3-edge							
	Diameter 1	Diameter 2	Diameter 3	Diameter 4	Min. Radius	Pore area Å^2	Min. distance from center
Ring 1	6.682	6.869	6.474	6.877	3.237	32.91813875	5.163068689
Ring 2	6.732	6.794	6.734	6.777	3.366	35.59410654	Internal Volume Å^3
Ring 3	6.479	6.877	6.736	6.878	3.2395	32.96900507	576.5172655

LTA-al6-ca3-s1s2-edge							
	Diameter 1	Diameter 2	Diameter 3	Diameter 4	Min. Radius	Pore area Å^2	Min. distance from center
Ring 1	6.877	6.53	6.496	6.508	3.248	33.14224427	5.867885642
Ring 2	6.75	6.794	6.365	6.899	3.1825	31.81901251	Internal Volume Å^3
Ring 3	6.495	6.594	6.272	6.979	3.136	30.89598039	846.3179135

LTA-al6-ca3-s1s2s3-edge							
	Diameter 1	Diameter 2	Diameter 3	Diameter 4	Min. Radius	Pore area Å^2	Min. distance from center
Ring 1	7.42	6.343	6.966	6.195	3.0975	30.14203035	5.180109014
Ring 2	6.338	7.337	6.569	7.068	3.169	31.54963586	Internal Volume Å^3
Ring 3	6.548	7.333	6.556	7.059	3.274	33.67497041	582.2443833

LTA-al6-ca3-s2s3-edge							
	Diameter 1	Diameter 2	Diameter 3	Diameter 4	Min. Radius	Pore area Å^2	Min. distance from center
Ring 1	6.865	6.342	6.96	6.212	3.106	30.30768575	5.228493614
Ring 2	6.715	6.426	7.067	6.024	3.012	28.50098094	Internal Volume Å^3
Ring 3	6.475	6.992	6.614	6.965	3.2375	32.92830887	598.7125409

LTA-al12-ca6-s1s2-edge							
	Diameter 1	Diameter 2	Diameter 3	Diameter 4	Min. Radius	Pore area Å^2	Min. distance from center
Ring 1	6.463	6.703	6.242	6.703	3.121	30.60112621	5.929170412
Ring 2	6.228	6.871	6.485	6.973	3.114	30.4640114	Internal Volume Å^3
Ring 3	7.055	6.417	6.927	6.177	3.0885	29.96712532	873.112905

LTA-al12-ca6-s2s3-edge							
	Diameter 1	Diameter 2	Diameter 3	Diameter 4	Min. Radius	Pore area Å^2	Min. distance from center
Ring 1	6.125	7.088	6.089	6.978	3.0445	29.11936026	5.274421101
Ring 2	6.127	6.973	6.17	7.085	3.0635	29.48394837	Internal Volume Å^3
Ring 3	6.237	7.179	6.021	6.963	3.0105	28.47260058	614.6289466

LTA-al12-k12-edge-uks							
	Diameter 1	Diameter 2	Diameter 3	Diameter 4	Min. Radius	Pore area Å^2	Min. distance from center
Ring 1	6.514	6.707	6.553	6.758	3.257	33.32616881	4.931891262
Ring 2	6.209	6.815	6.771	6.977	3.1045	30.27841945	Internal Volume Å^3
Ring 3	6.772	7.088	6.354	6.827	3.177	31.70912824	502.4919255

LTA-al6-na6-s1s2-uks							
	Diameter 1	Diameter 2	Diameter 3	Diameter 4	Min. Radius	Pore area Å^2	Min. distance from center
Ring 1	7.068	6.846	6.665	6.887	3.3325	34.88913393	5.902255268
Ring 2	6.586	6.754	7.107	6.872	3.293	34.06695636	Internal Volume Å^3
Ring 3	7.144	7.348	7.145	7.038	3.519	38.90347594	861.2764545

B. Adsorption energies for molecules inside of LTA

LTA+Alkane (center of unit cell)			
LTA+methane	LTA	Methane	**Adsorption**
-23832.87	-23613.10	-219.76	**0.00**
LTA+ethane	LTA	Ethane	**Adsorption**
-24020.09	-23613.10	-406.98	**0.00**
LTA+propane	LTA	Propane	**Adsorption**
-24207.39	-23613.10	-594.26	**-0.03**
LTA+isobutane	LTA	Isobutane	**Adsorption**
-24394.74	-23613.10	-781.58	**-0.05**

LTA+Alkane with **vdW** (center of unit cell)			
LTA+methane	LTA	Methane	**Adsorption**
-23837.47	-23617.62	-219.76	**-0.08**
LTA+ethane	LTA	Ethane	**Adsorption**
-24024.79	-23617.62	-406.98	**-0.19**
LTA+propane	LTA	Propane	**Adsorption**
-24212.20	-23617.62	-594.26	**-0.33**
LTA+isobutane	LTA	Isobutane	**Adsorption**
-24399.72	-23617.62	-781.58	**-0.52**

LTA+Alkane with **vdw** (surface of **site 1**)			
LTA+methane	LTA	Methane	**Adsorption**
-23837.41	-23613.10	-219.76	**-4.54**
LTA+ethane	LTA	Ethane	**Adsorption**
-24023.30	-23613.10	-406.98	**-3.21**
LTA+propane	LTA	Propane	**Adsorption**
-24210.30	-23613.10	-594.26	**-2.94**
LTA+isobutane	LTA	Isobutane	**Adsorption**
-24399.69	-23613.10	-781.58	**-5.01**

LTA+Alkane with **vdw** (surface of **site 2**)			
LTA+methane	LTA	Methane	**Adsorption**
-23837.66	-23613.10	-219.76	**-4.79**
LTA+ethane	LTA	Ethane	**Adsorption**
-24025.09	-23613.10	-406.98	**-5.01**
LTA+propane	LTA	Propane	**Adsorption**
-24212.56	-23613.10	-594.26	**-5.20**
LTA+isobutane	LTA	Isobutane	**Adsorption**
-24400.10	-23613.10	-781.58	**-5.42**

LTA+Alkane with **vdw** (surface of **site 3**)			
LTA+methane	LTA	Methane	**Adsorption**
-23837.55	-23613.10	-219.76	**-4.68**
LTA+ethane	LTA	Ethane	**Adsorption**
-24024.96	-23613.10	-406.98	**-4.87**
LTA+propane	LTA	Propane	**Adsorption**
-24212.23	-23613.10	-594.26	**-4.87**
LTA+isobutane	LTA	Isobutane	**Adsorption**
-24399.99	-23613.10	-781.58	**-5.31**

LTA+Alcohol (center of unit cell)			
LTA+methanol	LTA	Methanol	**Adsorption**
-24268.48	-23613.10	-655.35	**-0.02**
LTA+ethanol	LTA	Ethanol	**Adsorption**
-24455.91	-23613.10	-842.78	**-0.03**
LTA+1-propanol	LTA	1-Propanol	**Adsorption**
-24643.19	-23613.10	-1030.06	**-0.03**
LTA+isobutanol	LTA	Isobutanol	**Adsorption**
-24830.54	-23613.10	-1217.36	**-0.08**

LTA+Alcohol with **vdW** (center of unit cell)			
LTA+methanol	LTA	Methanol	**Adsorption**
-24273.10	-23617.62	-655.35	**-0.13**
LTA+ethanol	LTA	Ethanol	**Adsorption**
-24460.65	-23617.62	-842.78	**-0.24**
LTA+1-propanol	LTA	1-Propanol	**Adsorption**
-24648.06	-23617.62	-1030.06	**-0.38**
LTA+isobutanol	LTA	Isobutanol	**Adsorption**
-24835.60	-23617.62	-1217.36	**-0.63**

LTA+Alcohol with **vdW** (surface of **site 1, OH-surface**)			
LTA+methanol	LTA	Methanol	**Adsorption**
-24273.40	-23617.62	-655.35	-0.43
LTA+ethanol	LTA	Ethanol	**Adsorption**
-24460.59	-23617.62	-842.78	-0.19
LTA+1-propanol	LTA	1-Propanol	**Adsorption**
-24647.92	-23617.62	-1030.06	**-0.24**
LTA+isobutanol	LTA	Isobutanol	**Adsorption**
-24835.58	-23617.62	-1217.36	**-0.60**

LTA+Alcohol with **vdW** (surface of **site 2, OH-surface**)			
LTA+methanol	LTA	Methanol	**Adsorption**
-24273.43	-23617.62	-655.35	**-0.46**
LTA+ethanol	LTA	Ethane	**Adsorption**
-24461.00	-23617.62	-842.78	**-0.60**
LTA+1-propanol	LTA	1-Propanol	**Adsorption**
-24648.41	-23617.62	-1030.06	**-0.73**
LTA+isobutanol	LTA	Isobutanol	**Adsorption**
-24835.79	-23617.62	-1217.36	**-0.82**

LTA+Alcohol with **vdW** (surface of **site 3, OH-surface**)			
LTA+methanol	LTA	Methanol	**Adsorption**
-24273.13	-23617.62	-655.35	**-0.16**
LTA+ethanol	LTA	Ethanol	**Adsorption**
-24460.73	-23617.62	-842.78	**-0.33**
LTA+1-propanol	LTA	1-Propanol	**Adsorption**
-24648.17	-23617.62	-1030.06	**-0.49**
LTA+isobutanol	LTA	Isobutanol	**System**
-24835.60	-23617.62	-1217.36	**-0.63**

LTA+Alcohol with **vdW** (surface of **site 1, 3H-Surface**)			
LTA+methanol	LTA	Methanol	**System**
-24273.38	-23617.62	-655.35	**-0.40**
LTA+ethanol	LTA	Ethanol	**System**
-24460.73	-23617.62	-842.78	-0.33
LTA+1-propanol	LTA	1-Propanol	**System**
-24648.14	-23617.62	-1030.06	-0.46
LTA+isobutanol	LTA	Isobutanol	**System**
-24835.52	-23617.62	-1217.36	**-0.54**

LTA+Alcohol with **vdW** (surface of **site 2, 3H-Surface**)			
LTA+methanol	LTA	Methanol	**System**
-24273.40	-23617.62	-655.35	**-0.43**
LTA+ethanol	LTA	Ethanol	**System**
-24461.03	-23617.62	-842.78	**-0.63**
LTA+1-propanol	LTA	1-Propanol	**System**
-24648.36	-23617.62	-1030.06	**-0.68**
LTA+isobutanol	LTA	Isobutanol	**System**
-24835.93	-23617.62	-1217.36	**-0.95**

LTA+Alcohol with **vdW** (surface of **site 3, 3H-Surface**)			
LTA+methanol	LTA	Methanol	**System**
-24273.13	-23617.62	-655.35	**-0.16**
LTA+ethanol	LTA	Ethanol	**System**
-24460.81	-23617.62	-842.78	**-0.41**
LTA+1-propanol	LTA	1-Propanol	**System**
-24648.17	-23617.62	-1030.06	**-0.49**
LTA+isobutanol	LTA	Isobutanol	**System**
-24835.52	-23617.62	-1217.36	**-0.54**

C. Geometry visualization of alkanes and alcohols in LTA

I. Alkane geometries

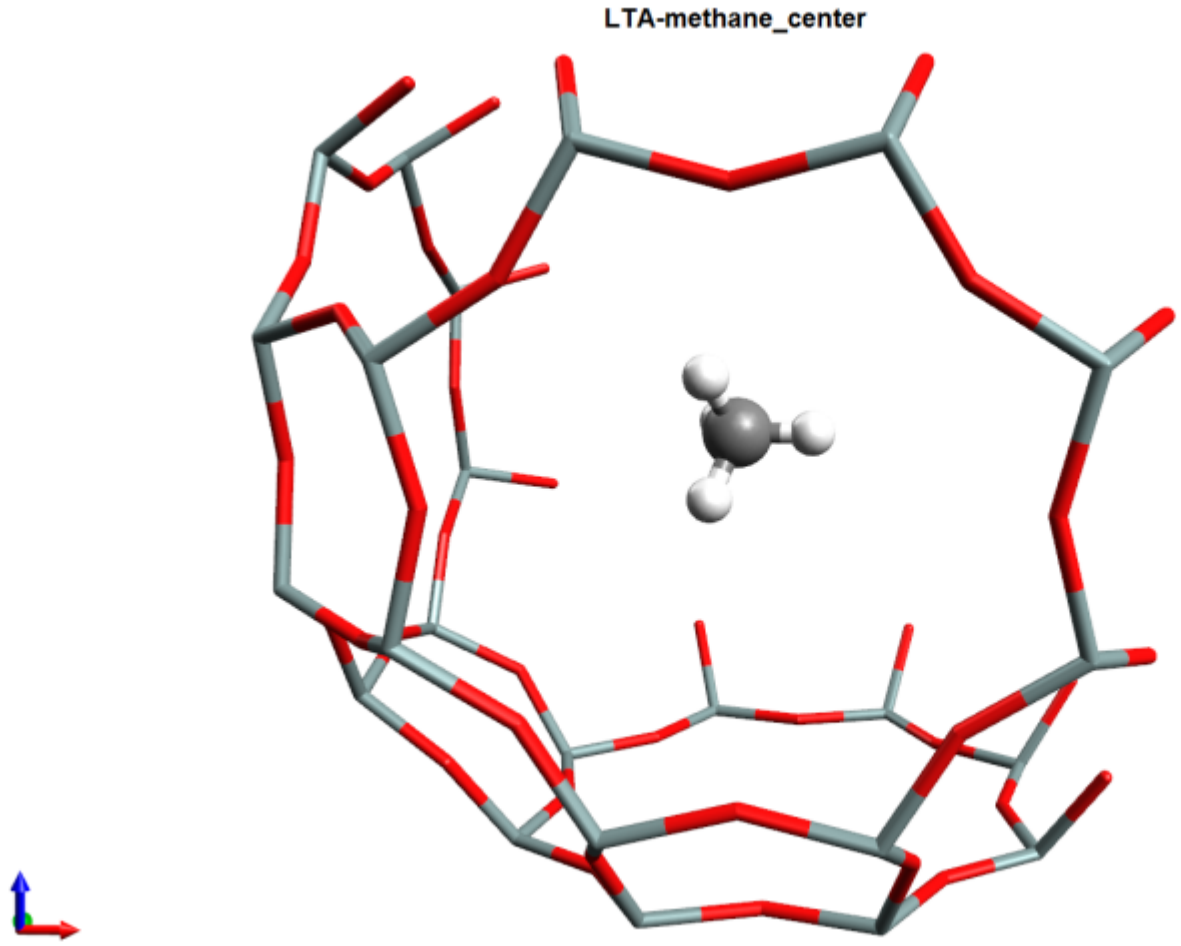

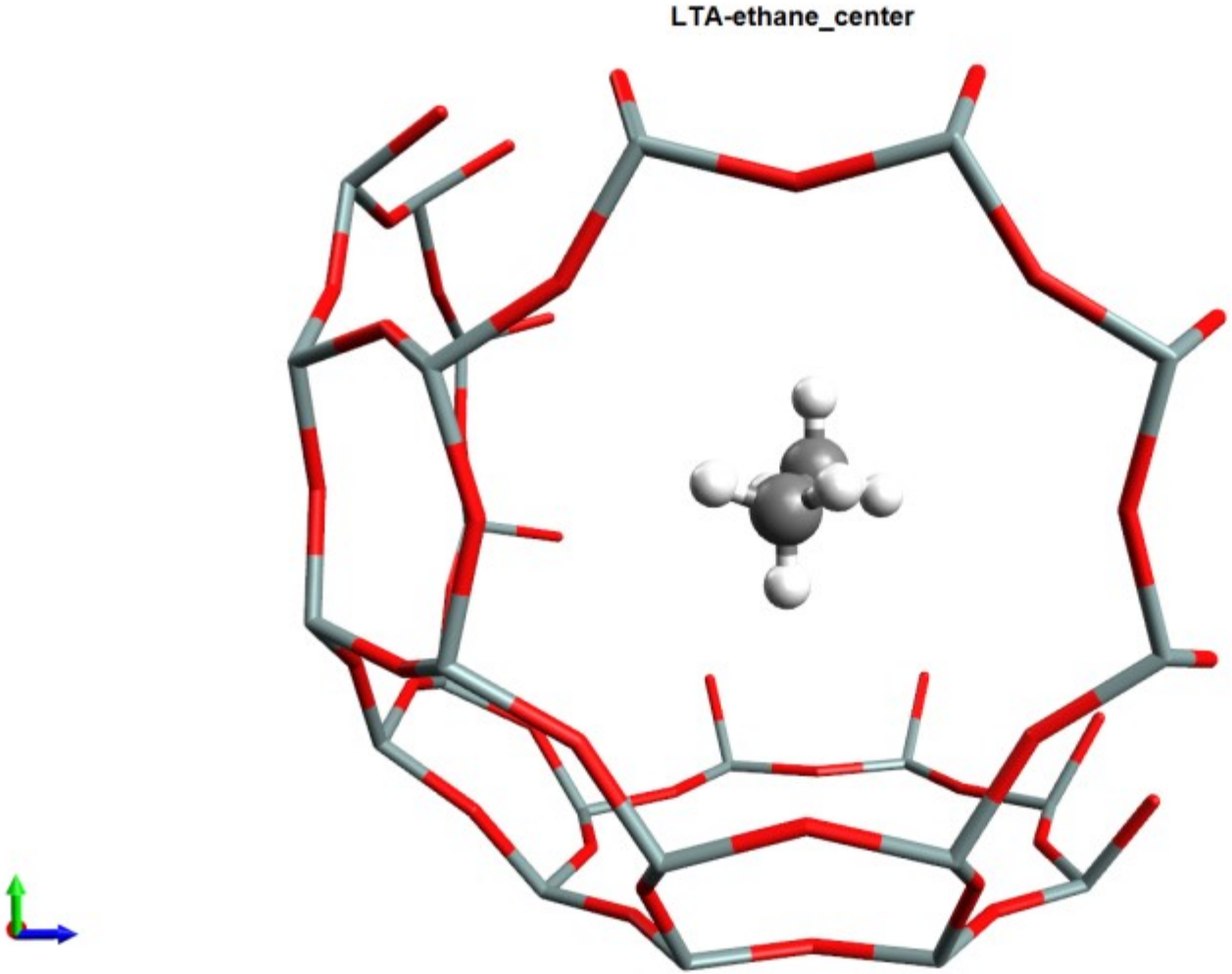
LTA-ethane_center

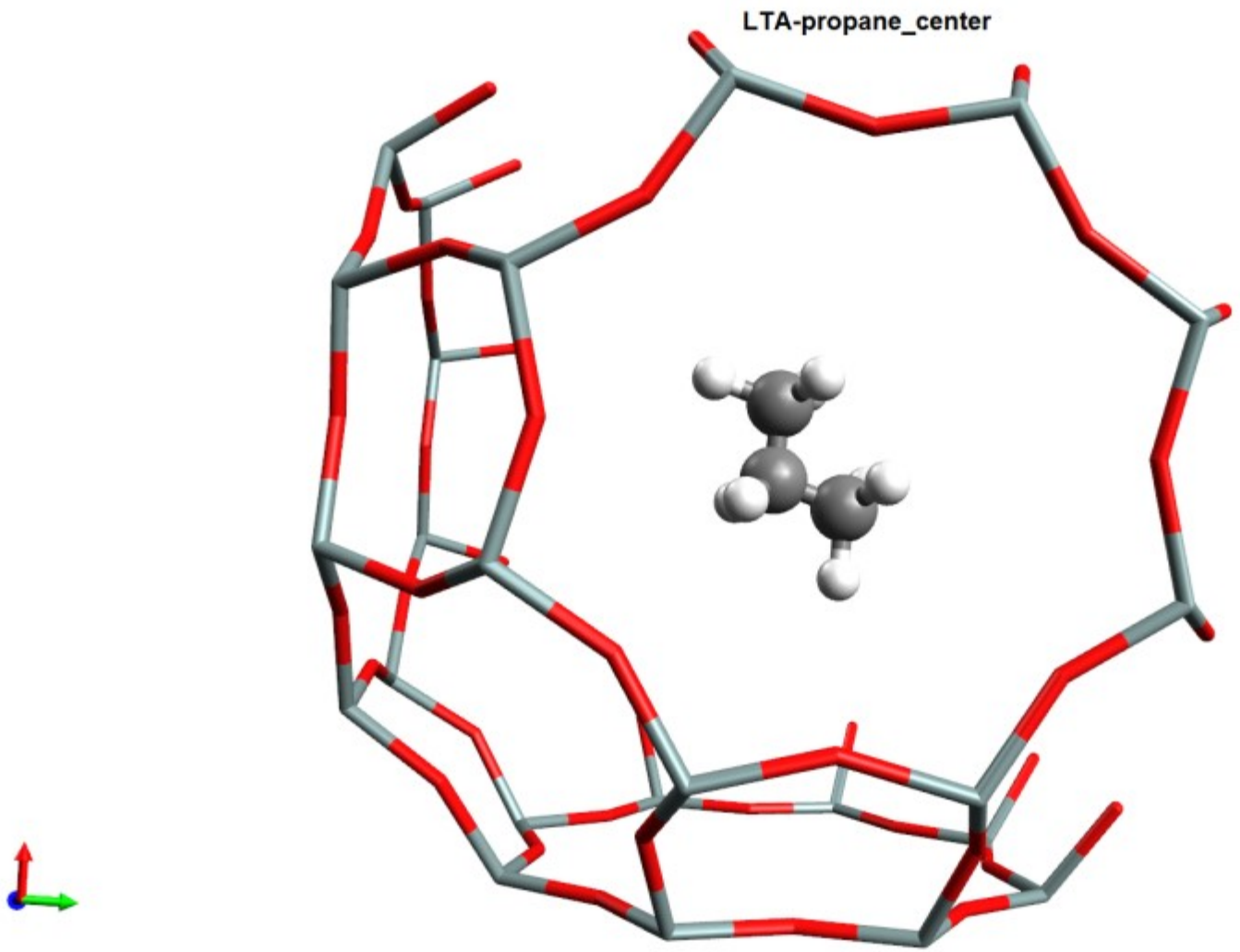
LTA-propane_center

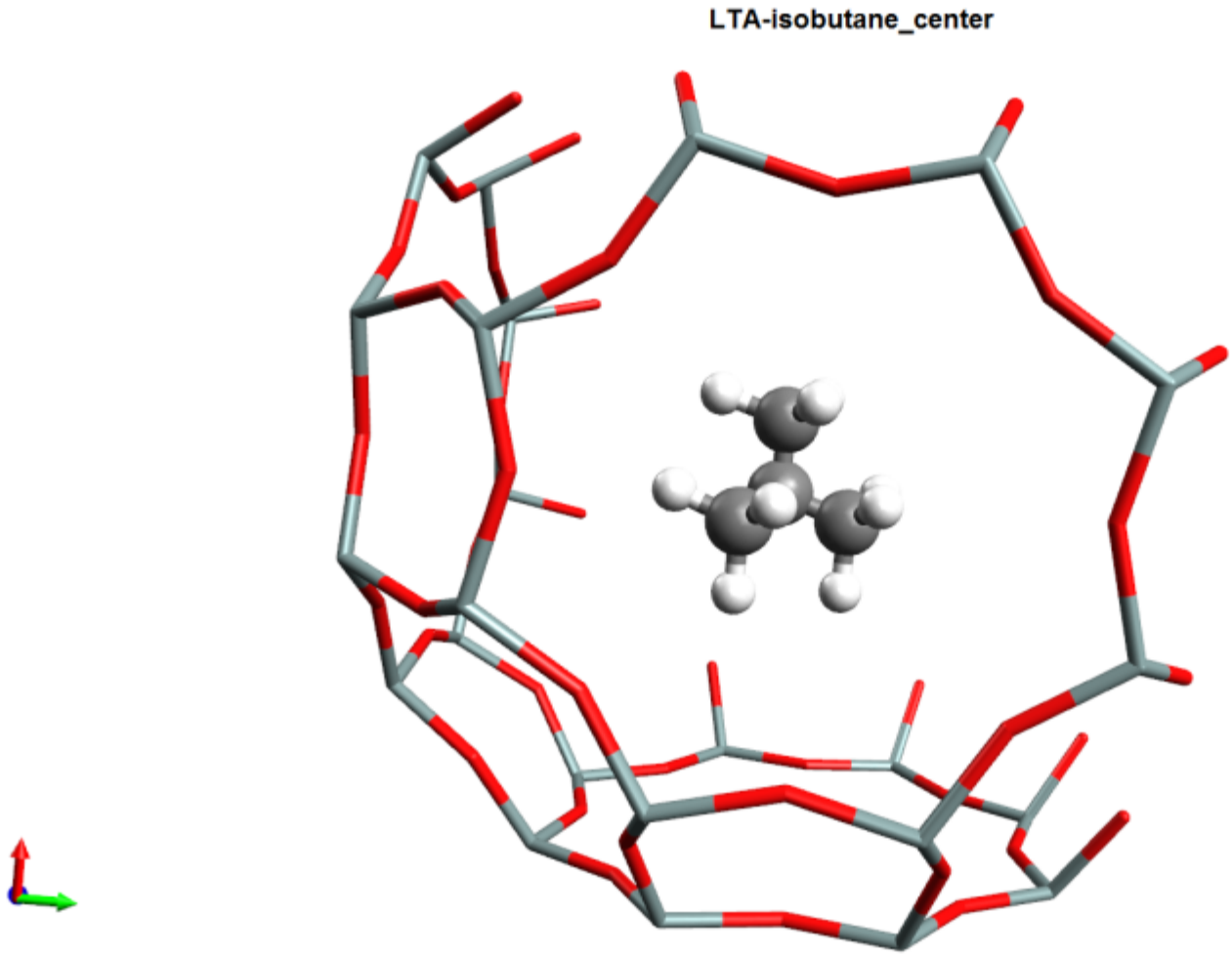
LTA-isobutane_center

LTA-methane-S1_vdw_surface

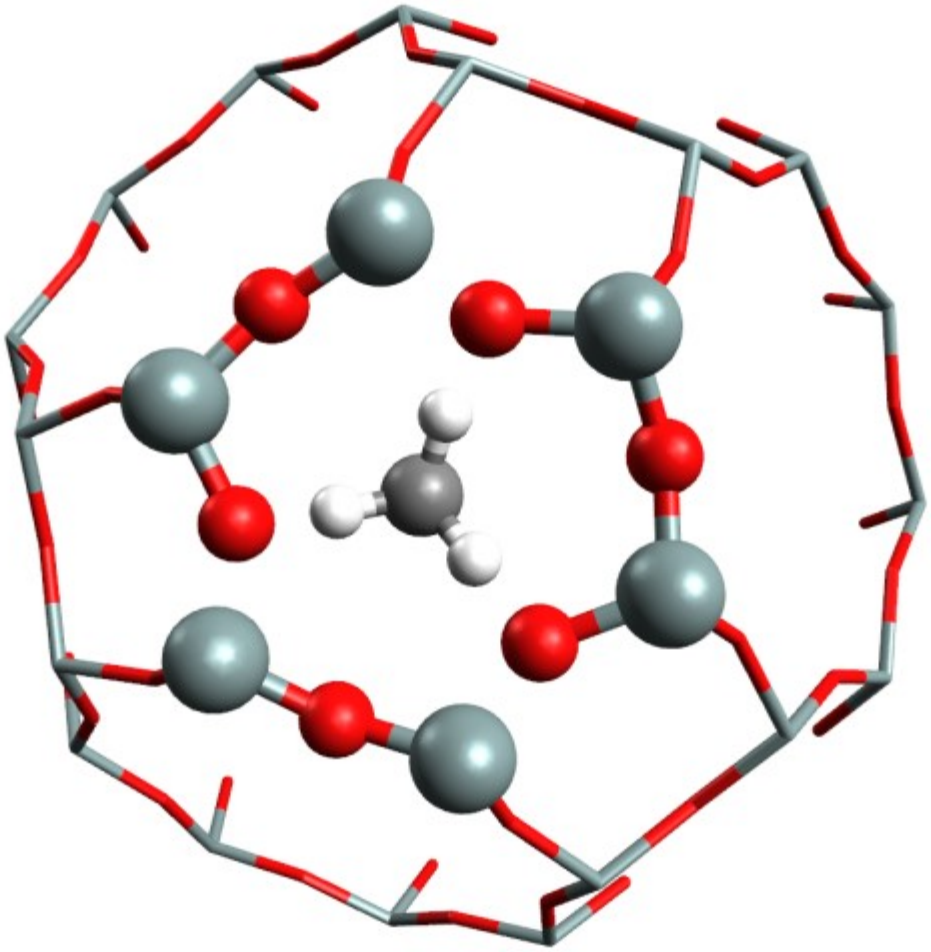

LTA-ethane-S1_vdw_surface

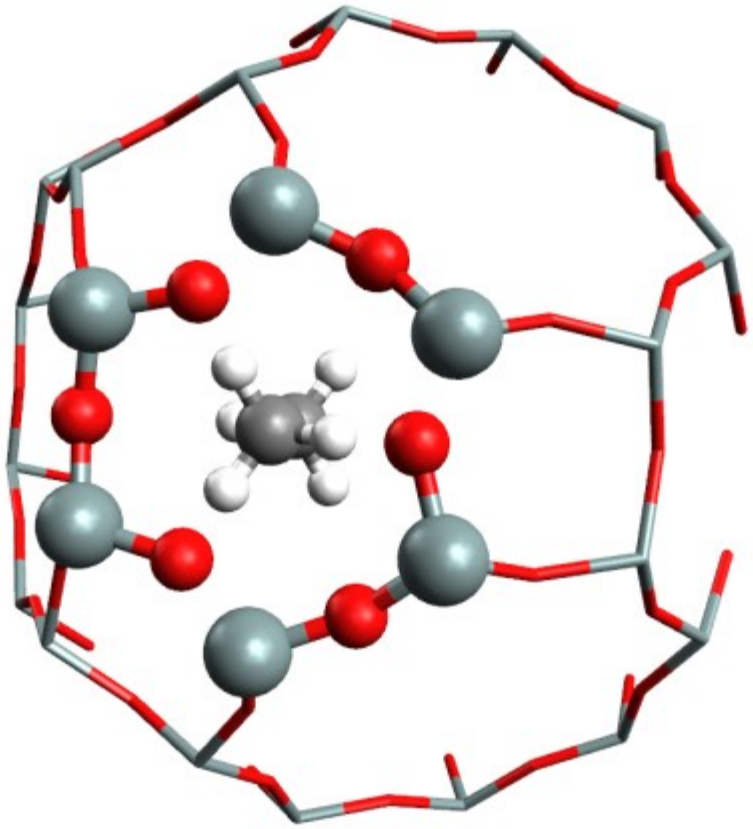

LTA-propane-S1_vdw_surface

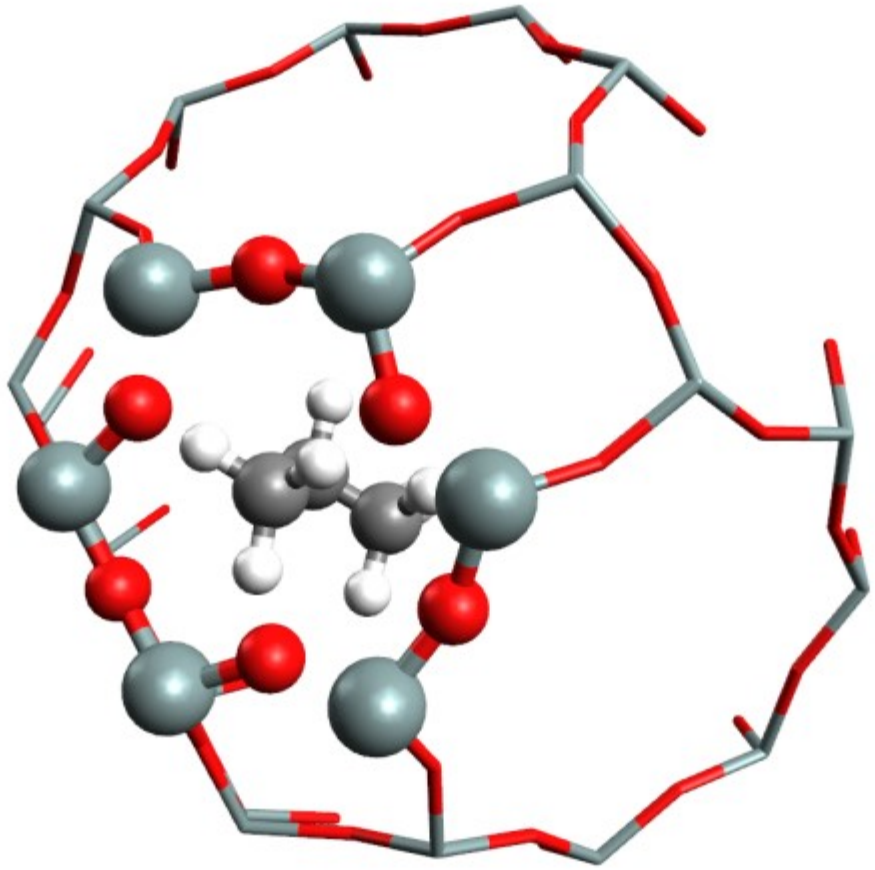

5.

LTA-isobutane-S1_vdw_surface

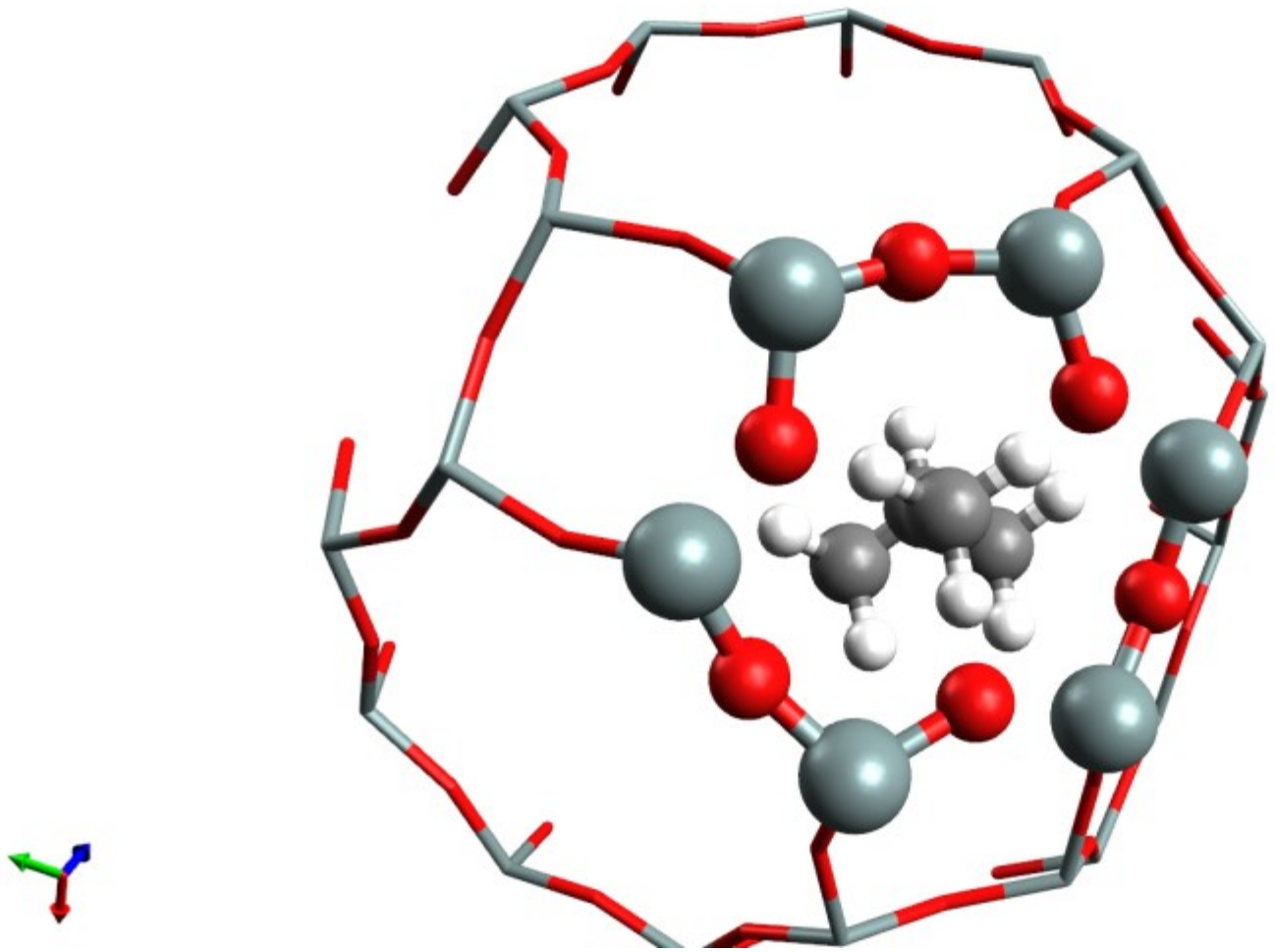

LTA-methane-S2_vdw_surface

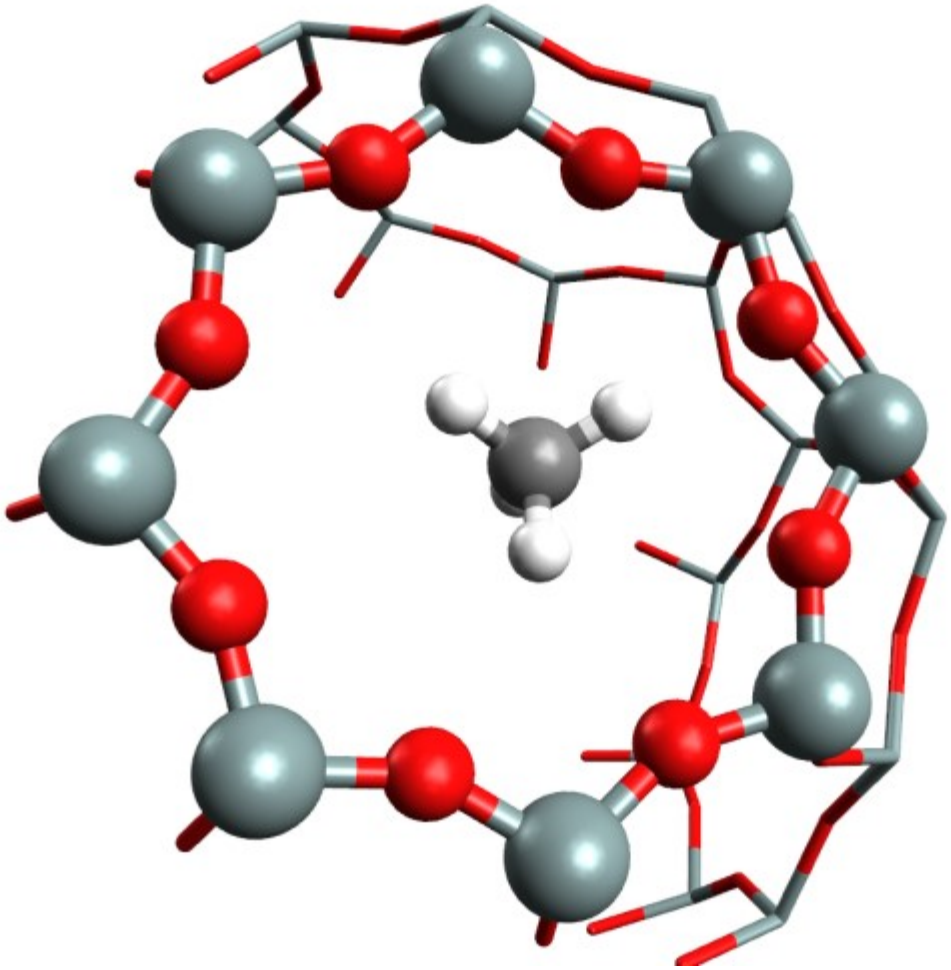

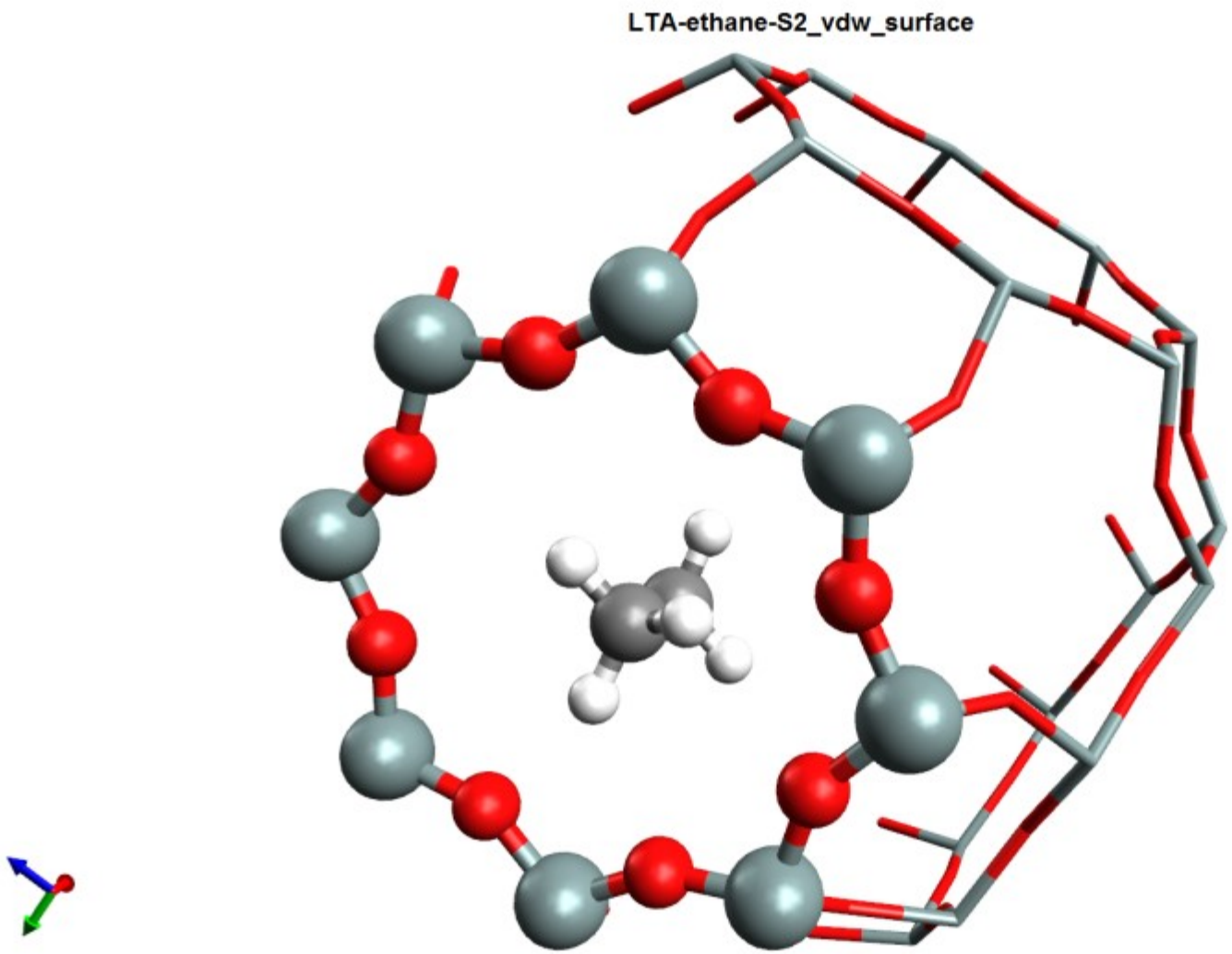
LTA-ethane-S2_vdw_surface

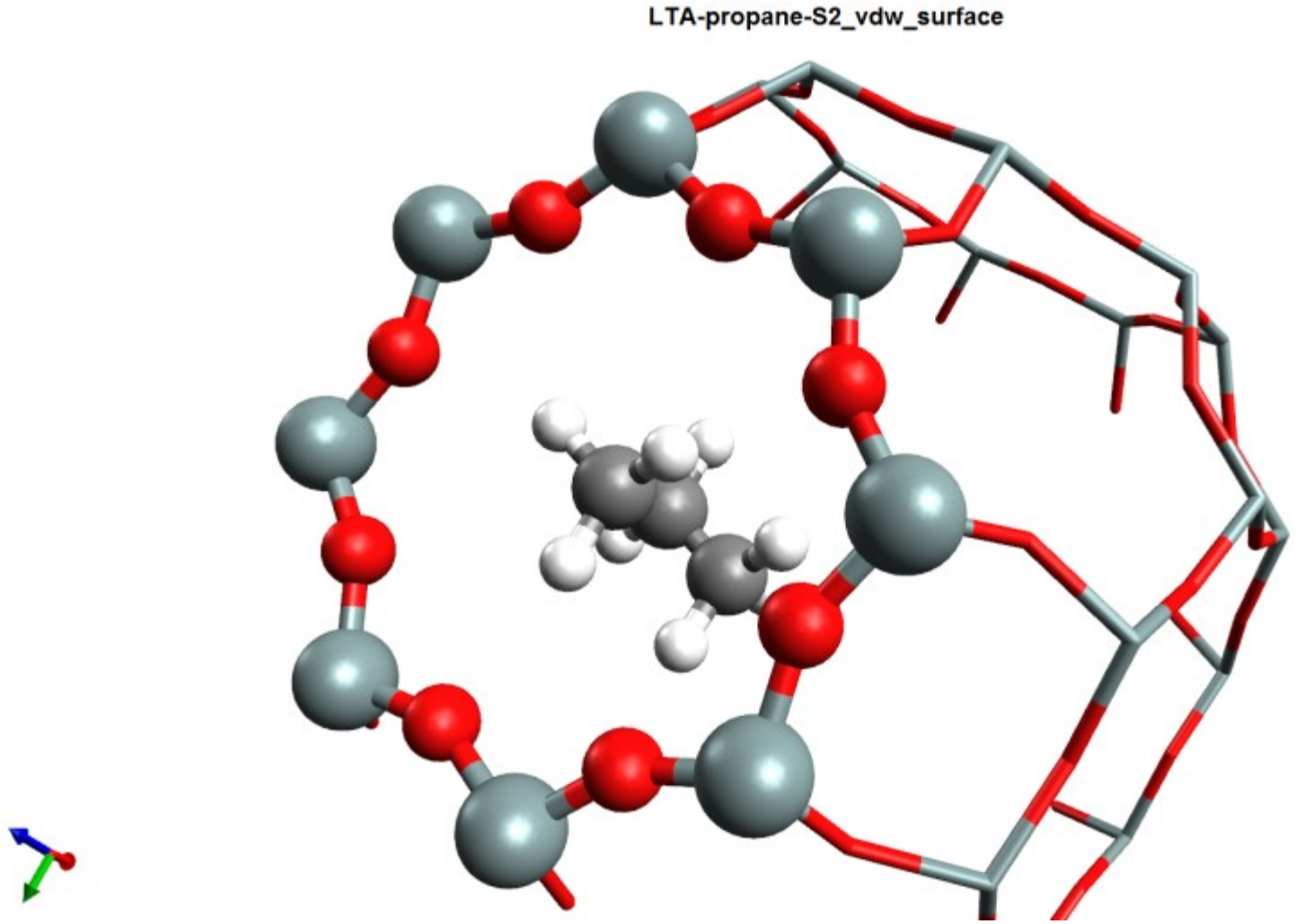
LTA-propane-S2_vdw_surface

LTA-isobutane-S2_vdw_surface

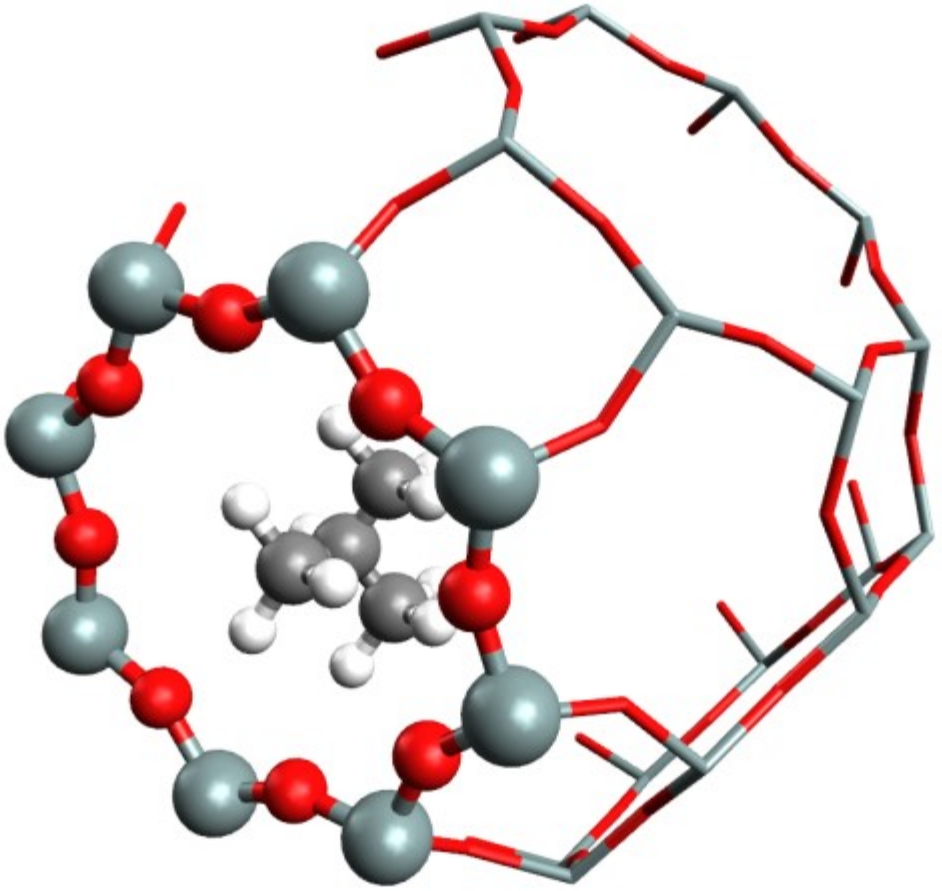

LTA-methane-S3_vdw_surface

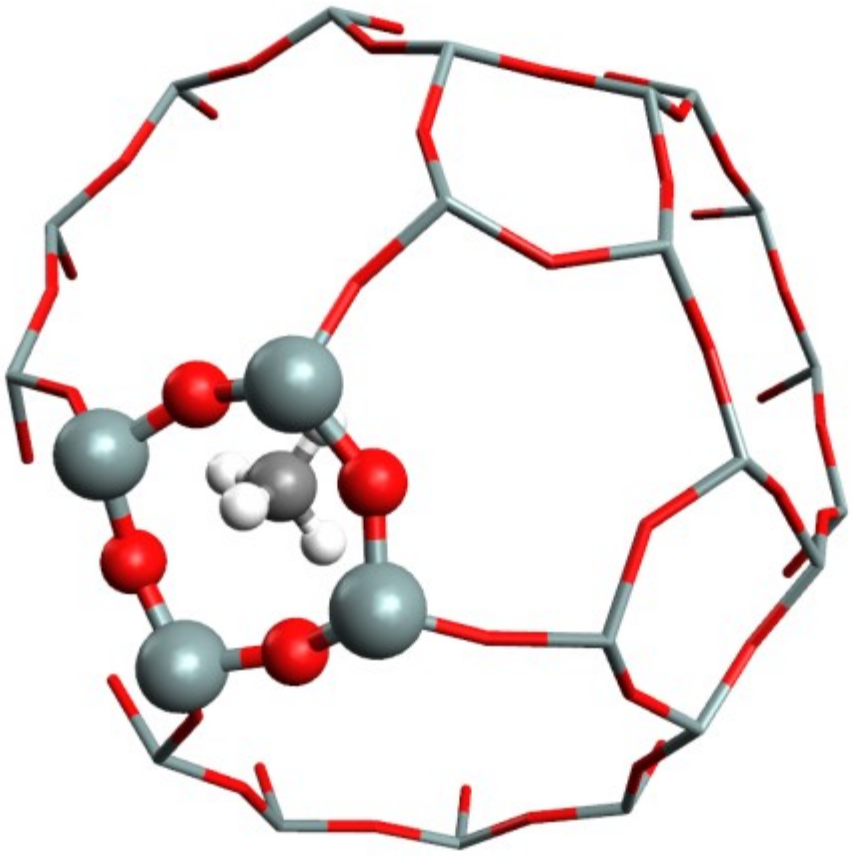

LTA-ethane-S3_vdw_surface

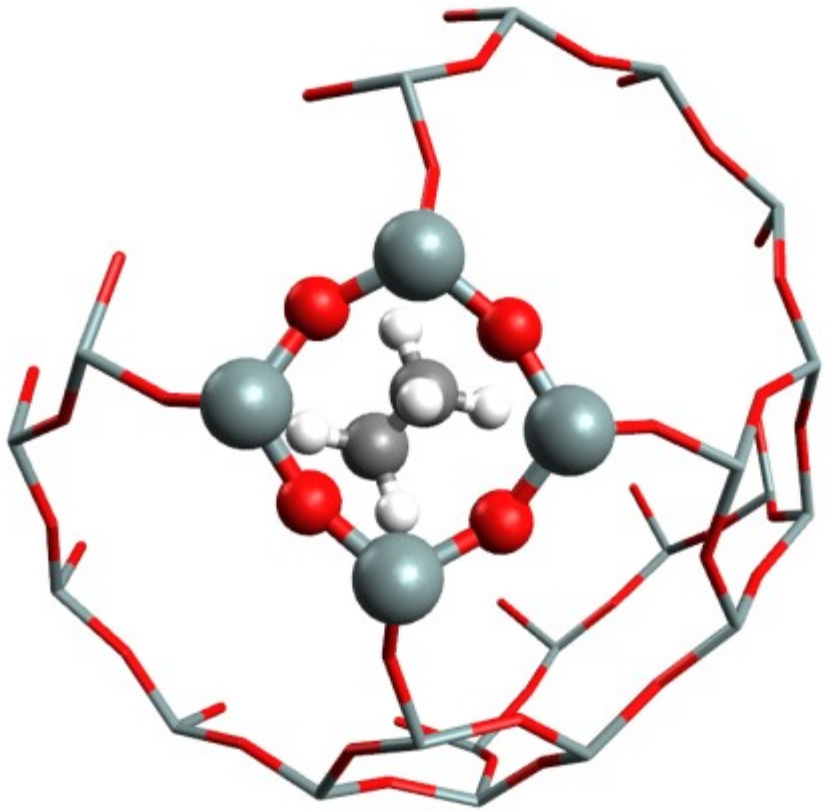

LTA-propane-S3_vdw_surface

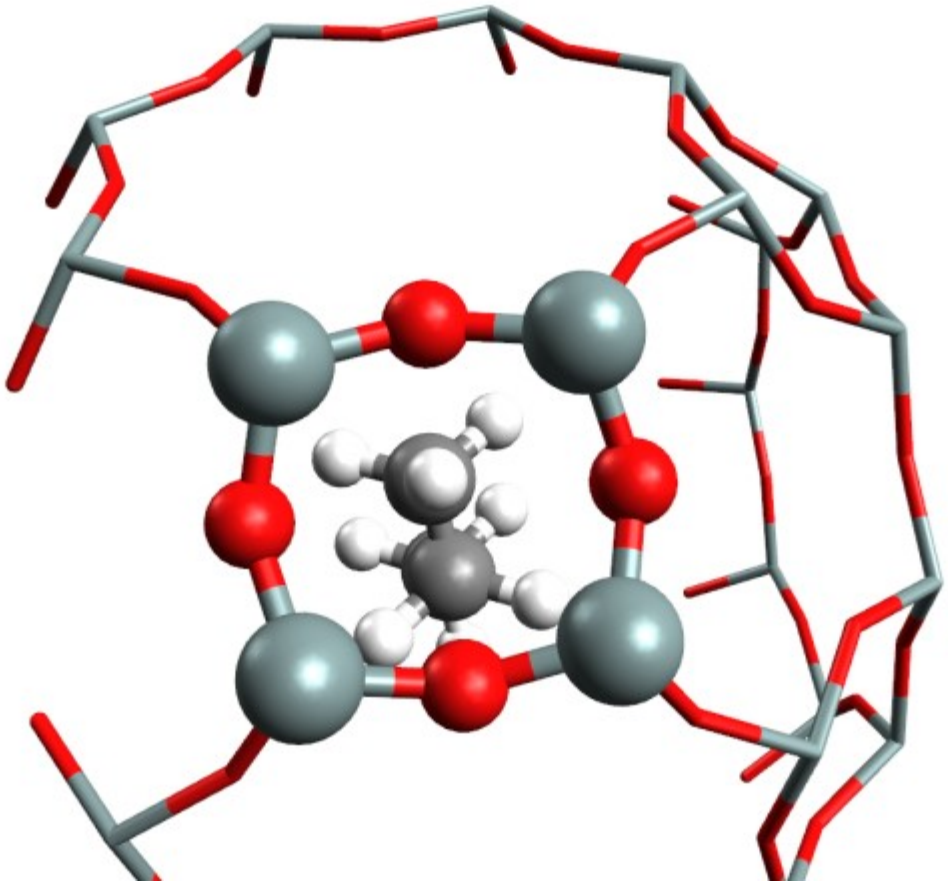

LTA-isobutane-S3_vdw_surface

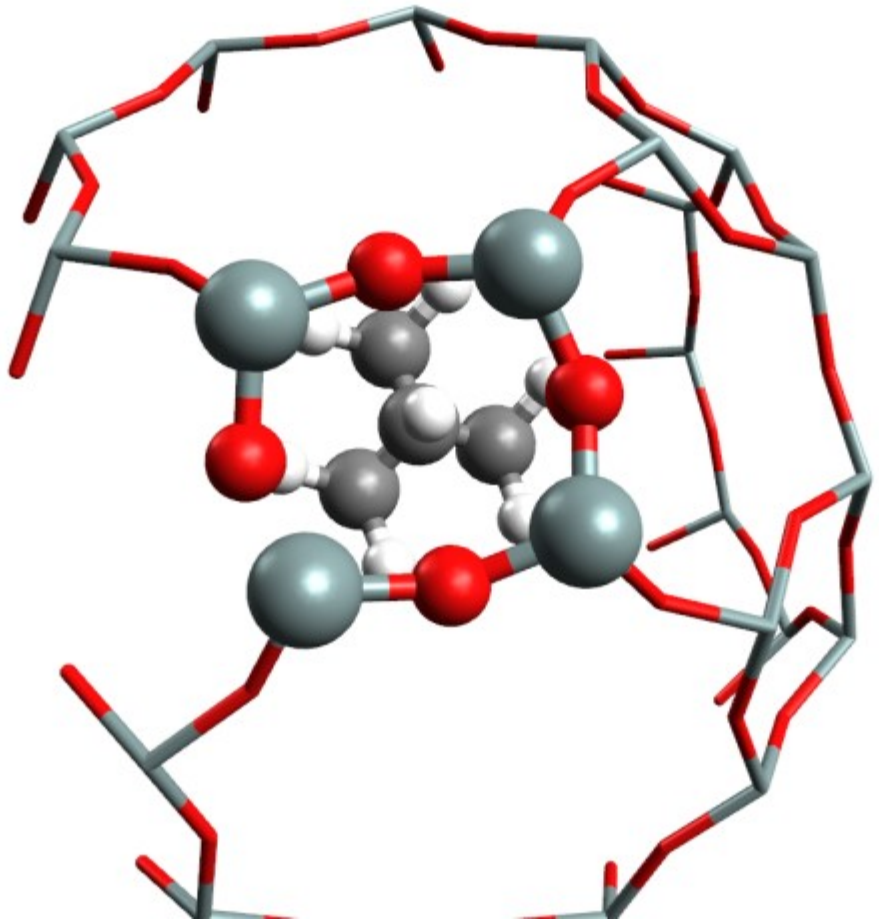

II. Alcohol geometry

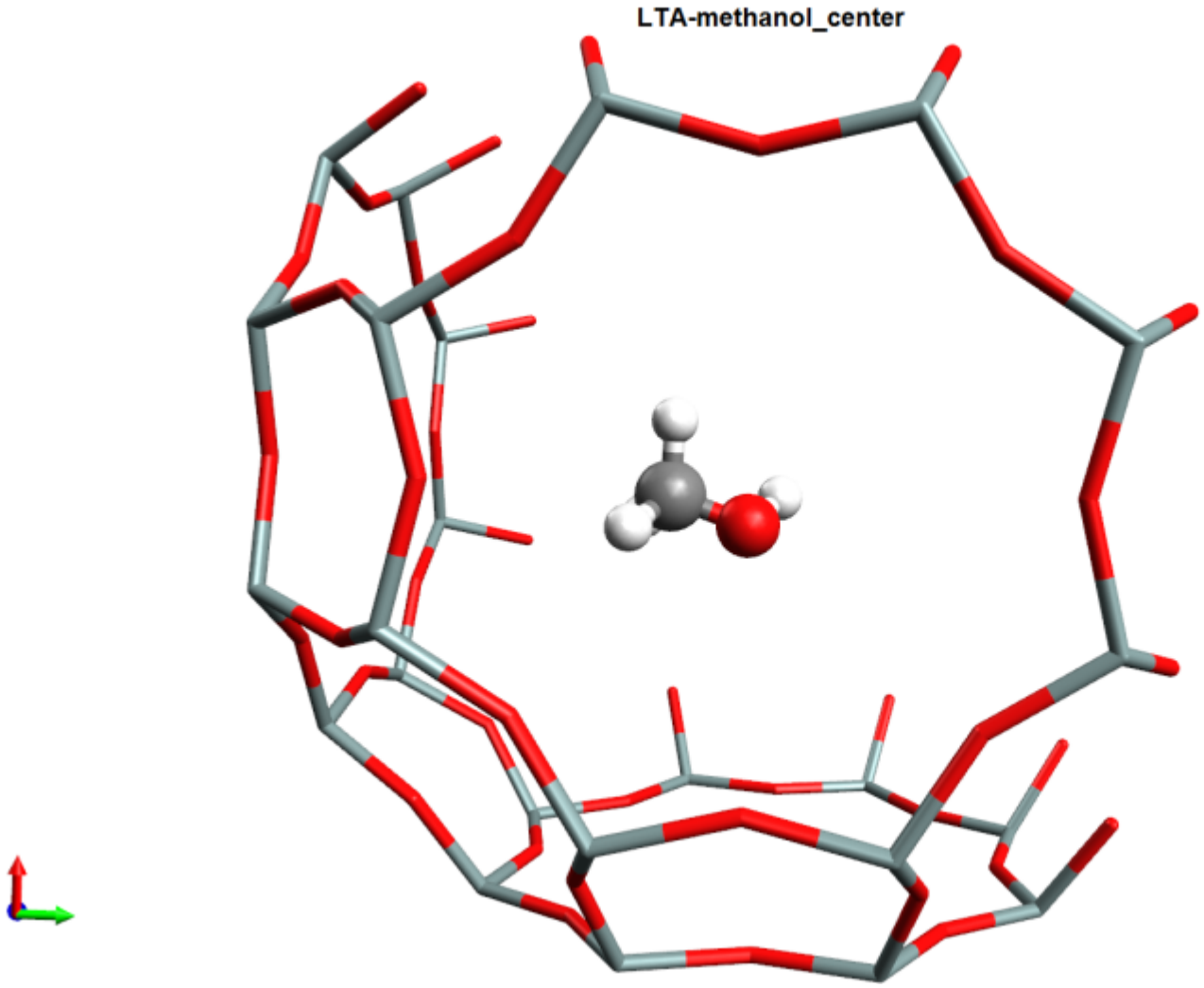

LTA-ethanol_center

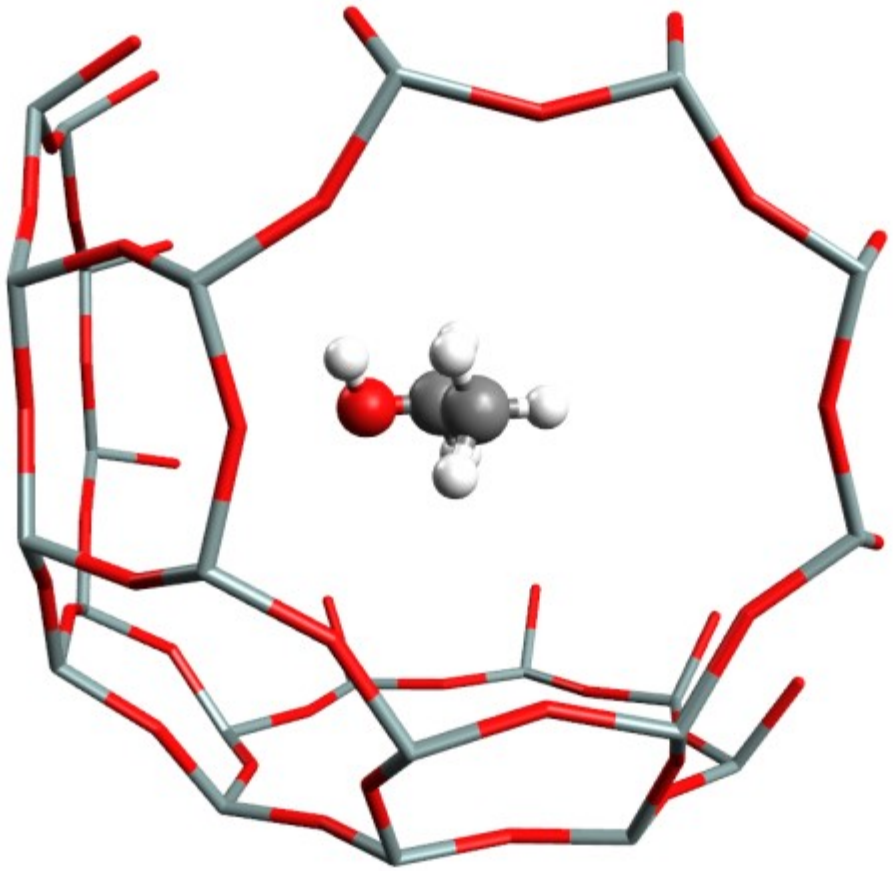

LTA-1-propanol_center

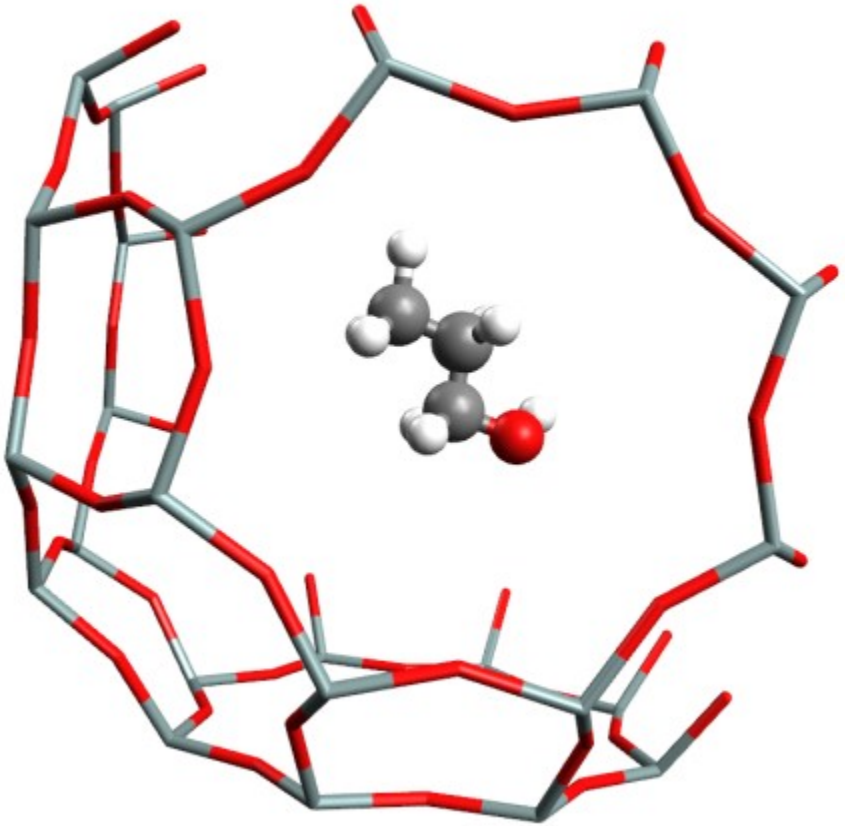

LTA-isobutanol_center

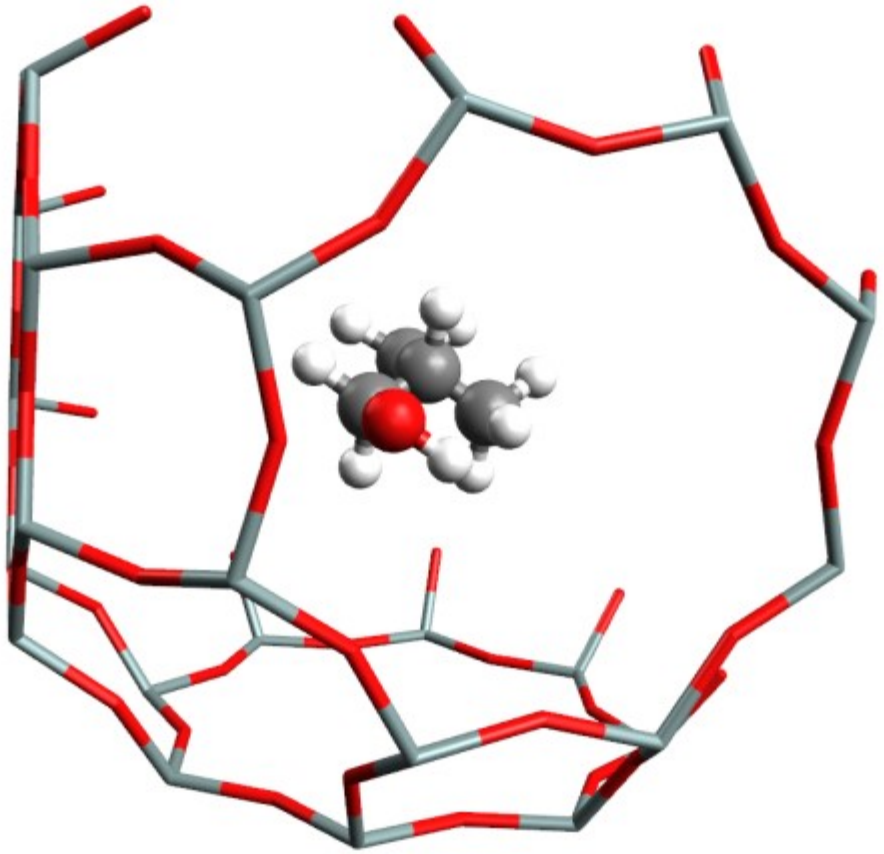

LTA-methanol-S1_vdw_surface-OH

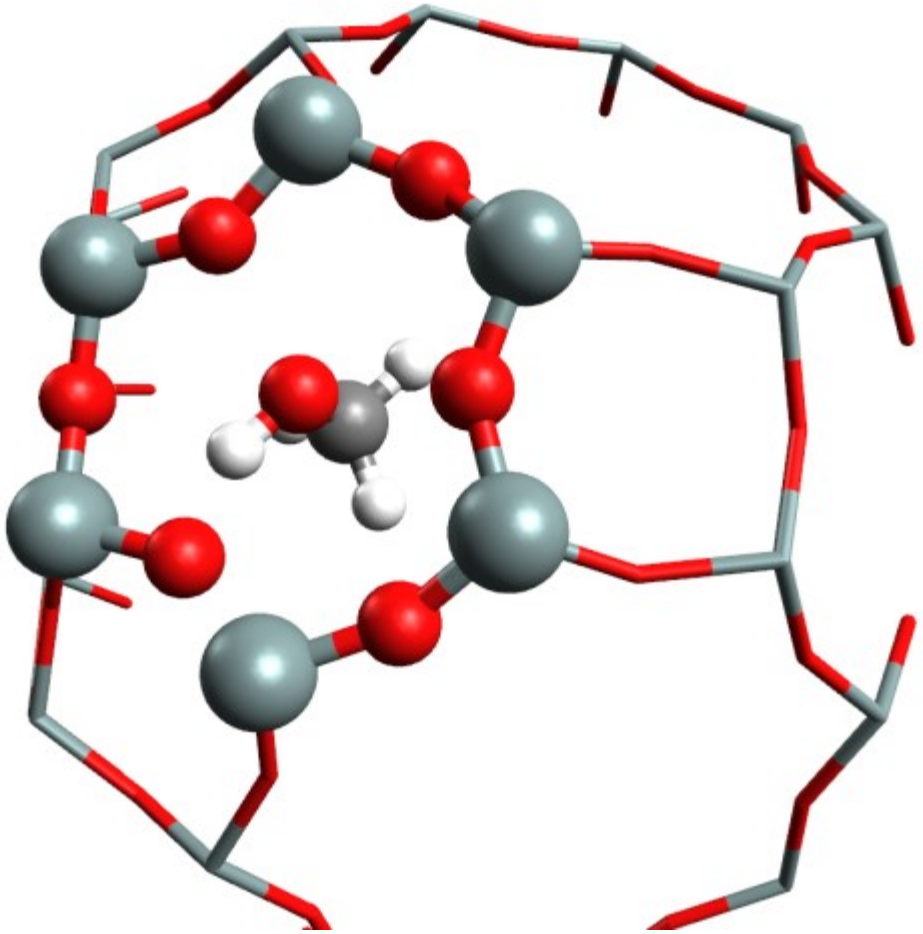

LTA-methanol-S1_vdw_surface-3H

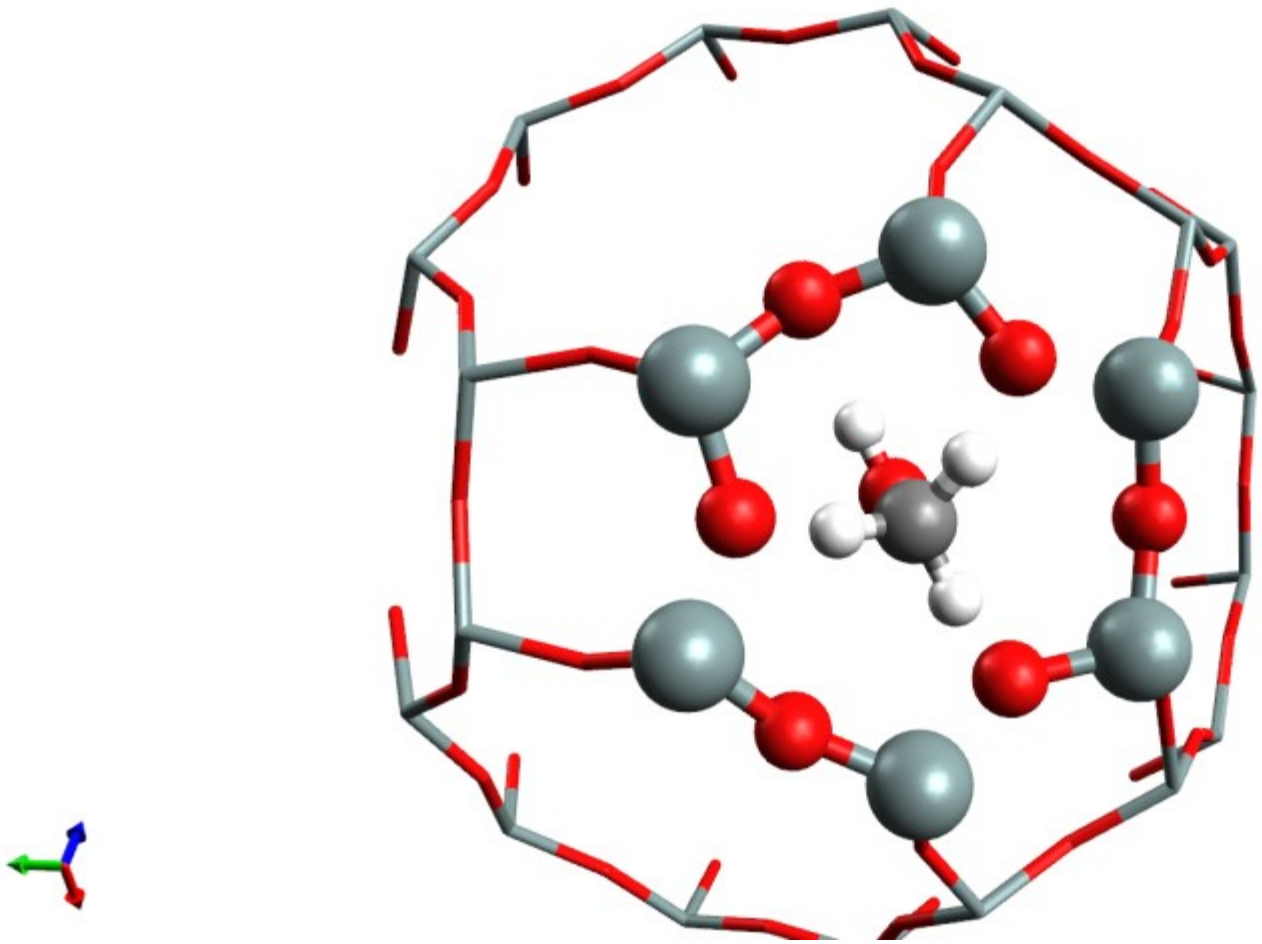

LTA-ethanol-S1_vdw_surface-OH

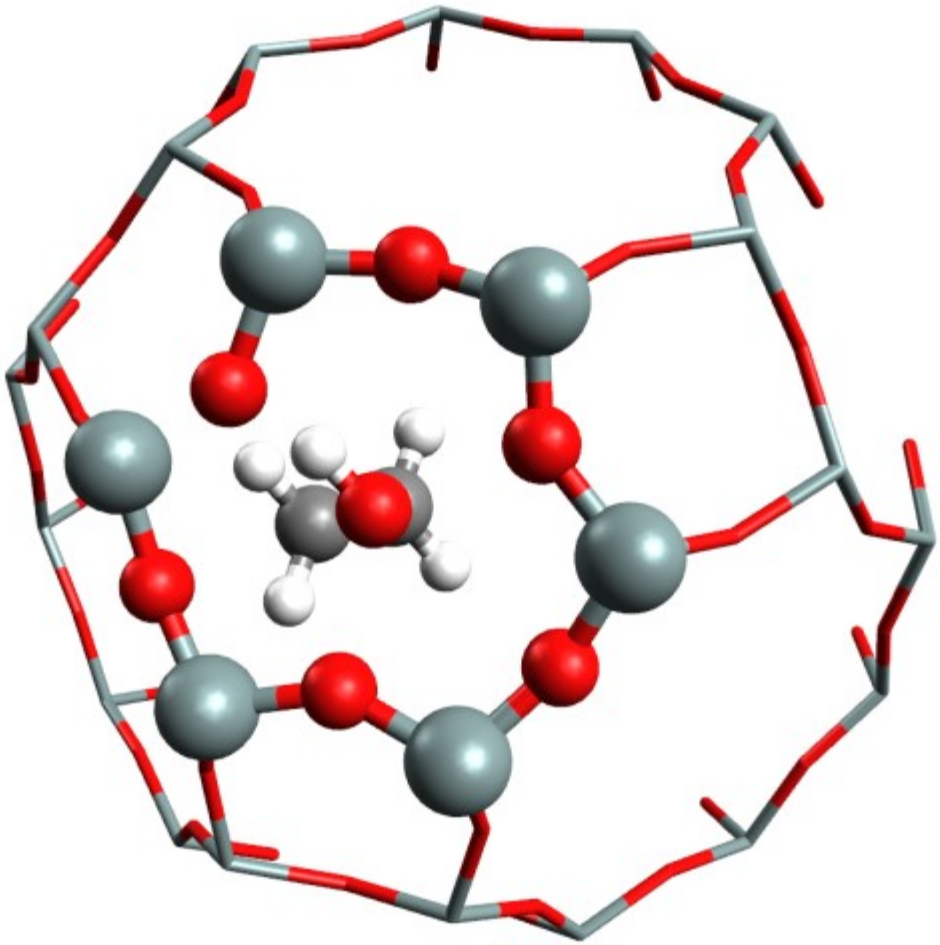

LTA-ethanol-S1_vdw_surface-3H

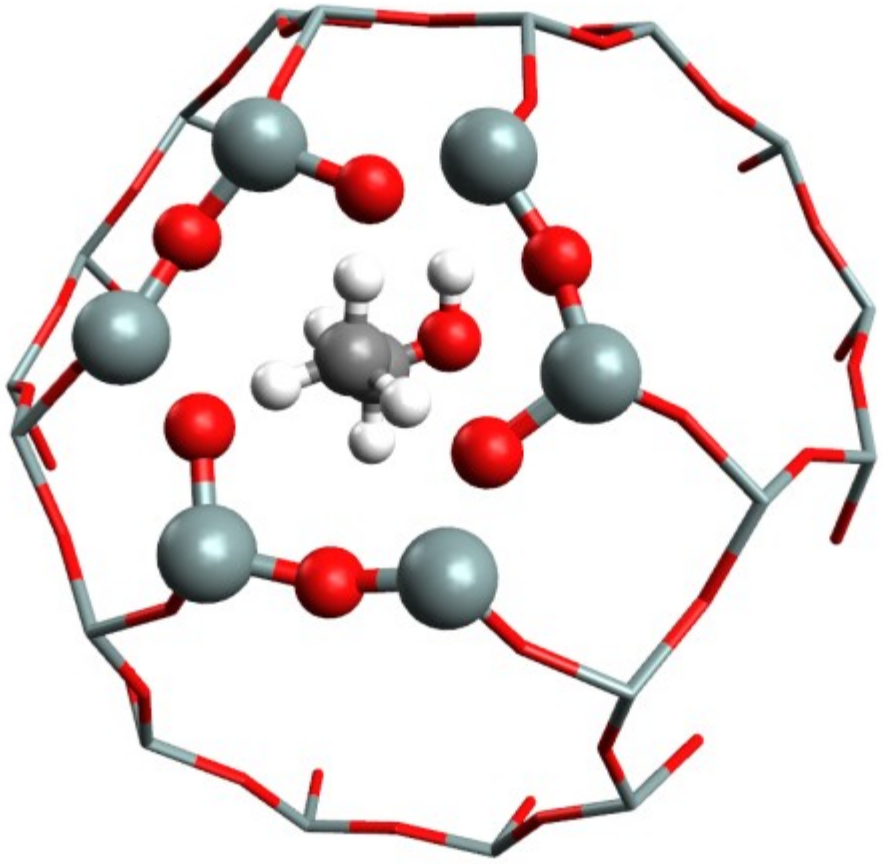

LTA-1-propanol-S1_vdw_surface-OH

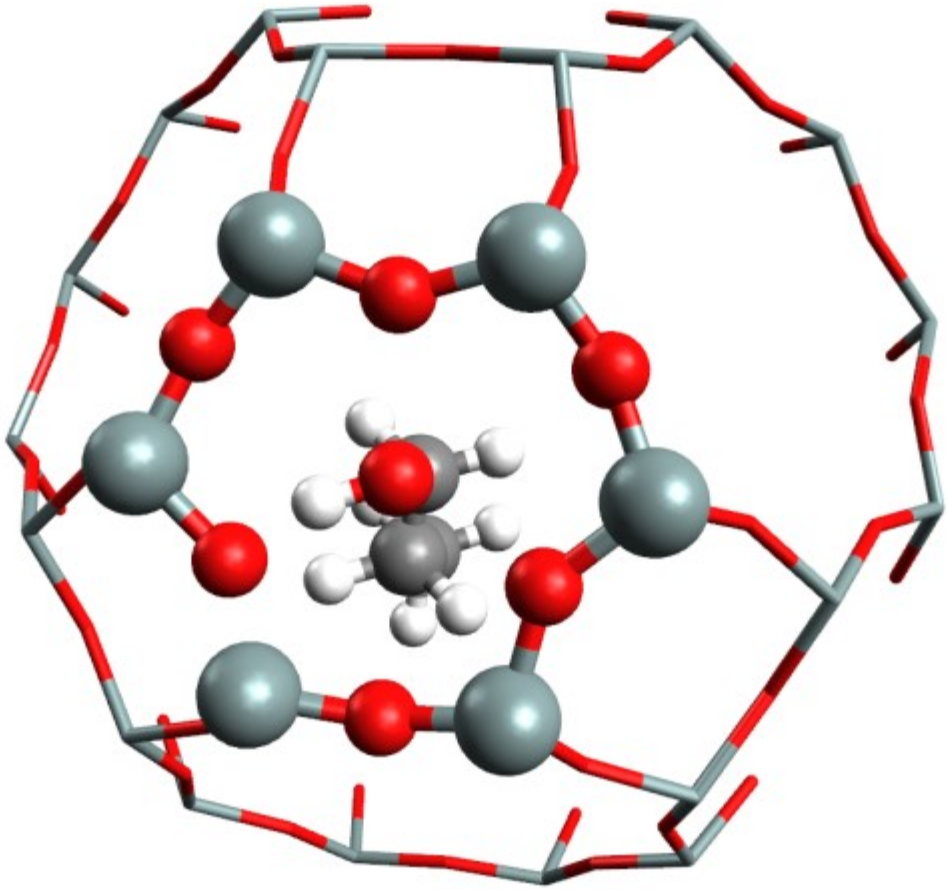

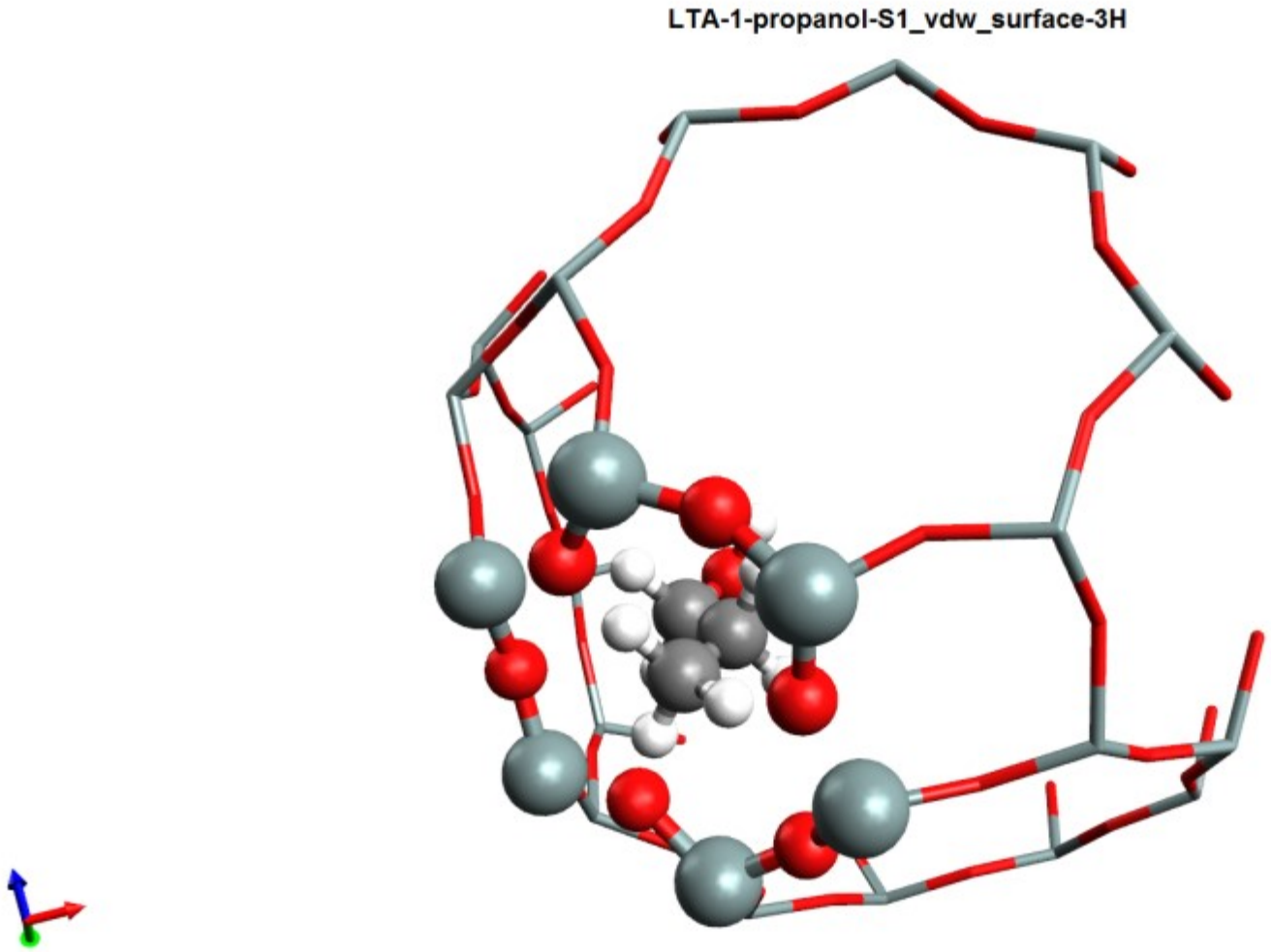
LTA-1-propanol-S1_vdw_surface-3H

LTA-1-propanol-S1_vdw_surface-OH

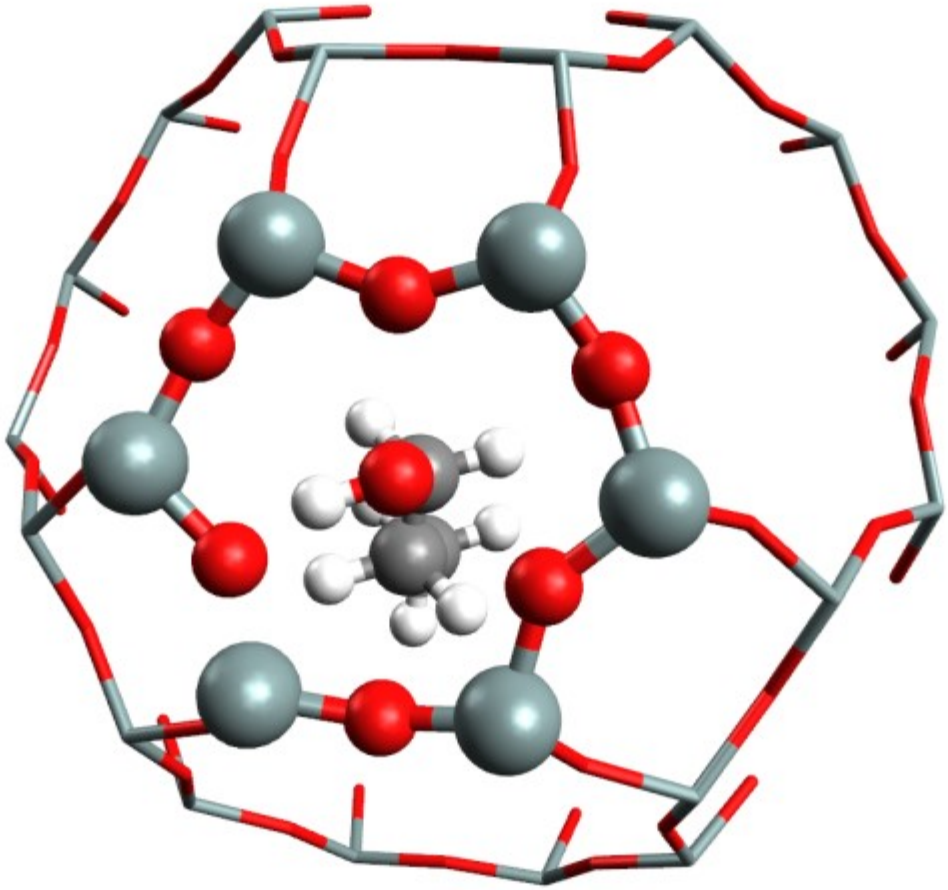

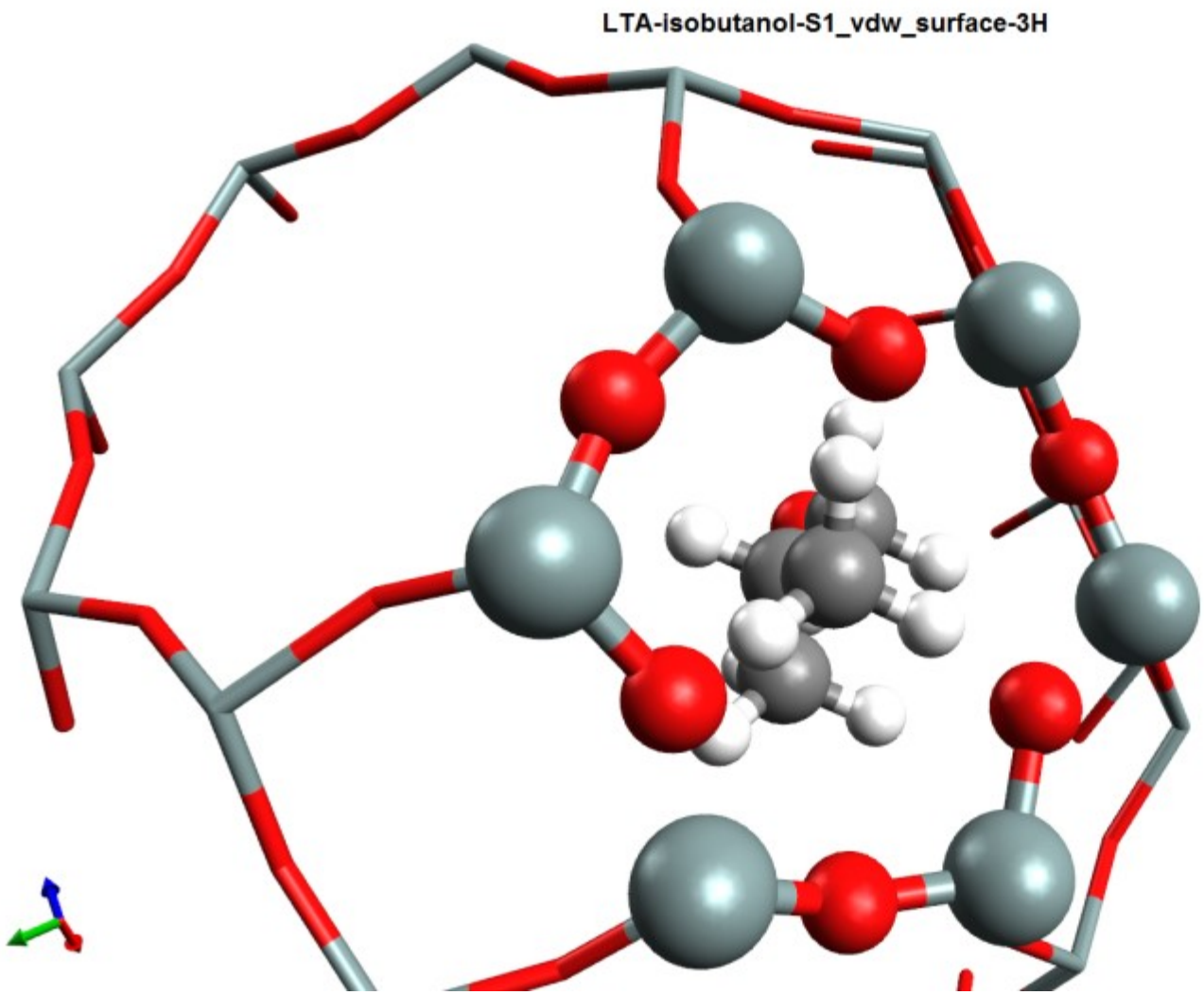
LTA-isobutanol-S1_vdw_surface-3H

LTA-methanol-S2_vdw_surface-OH

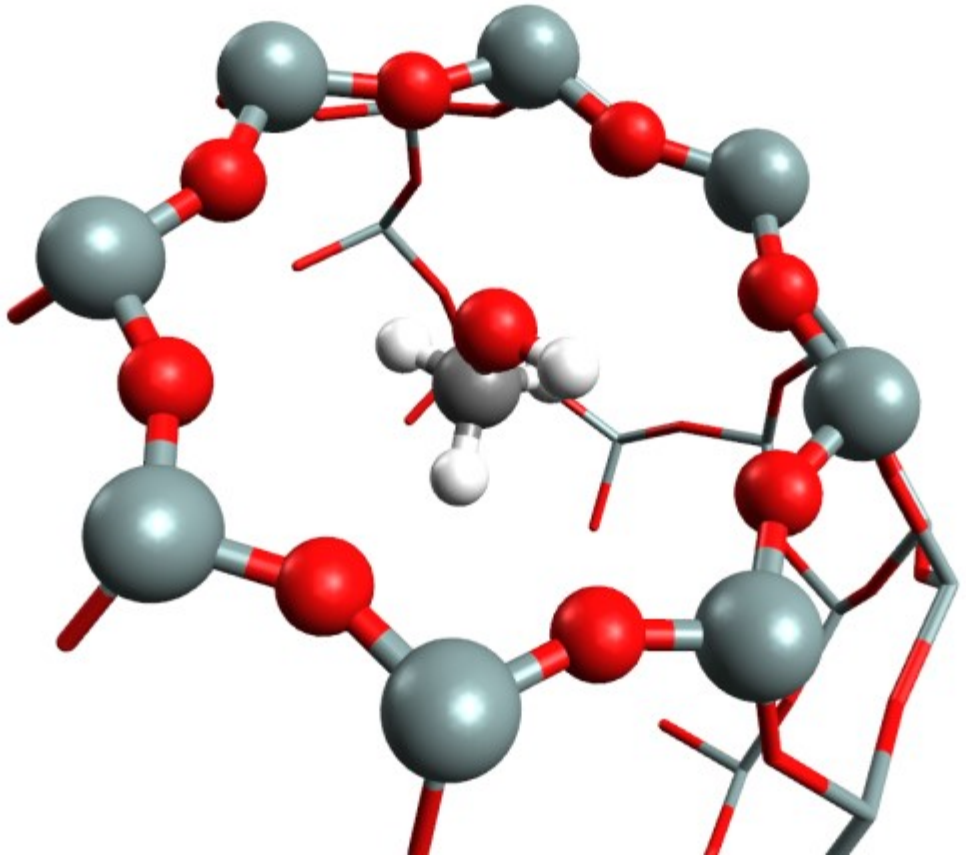

LTA-methanol-S2_vdw_surface-3H

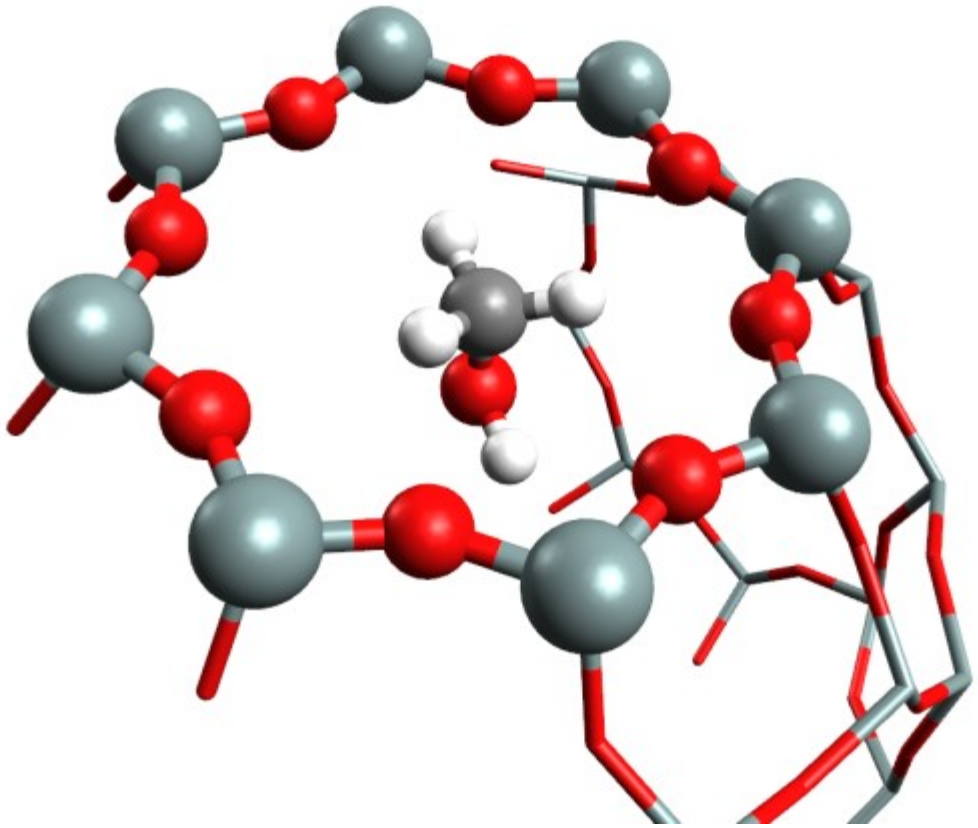

LTA-ethanol-S2_vdw_surface-OH

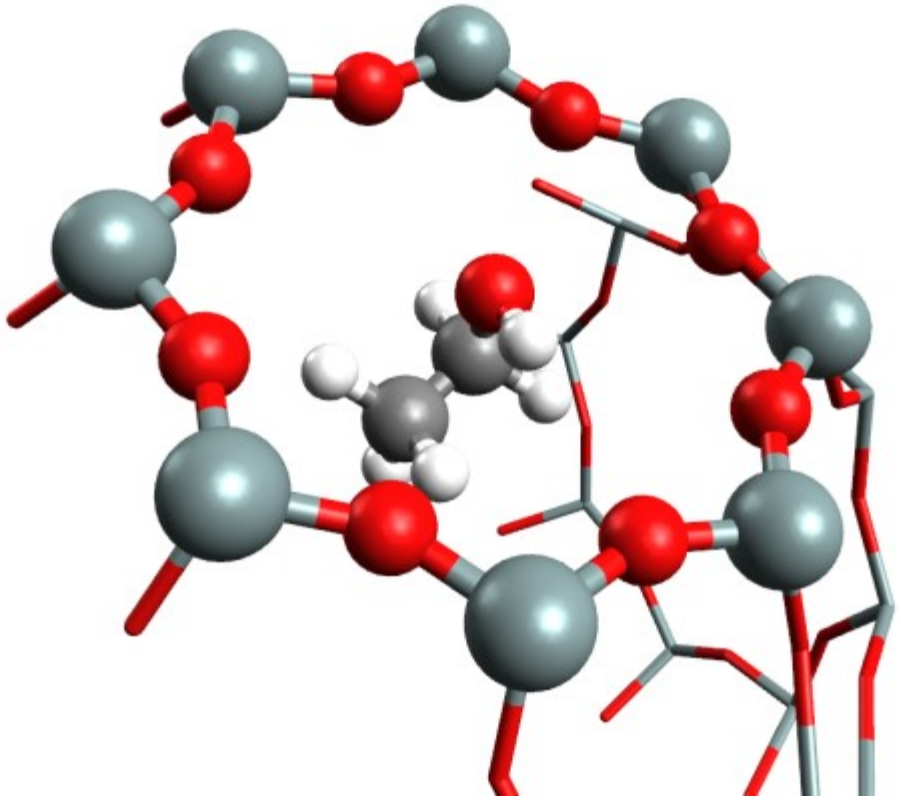

LTA-ethanol-S2_vdw_surface-3H

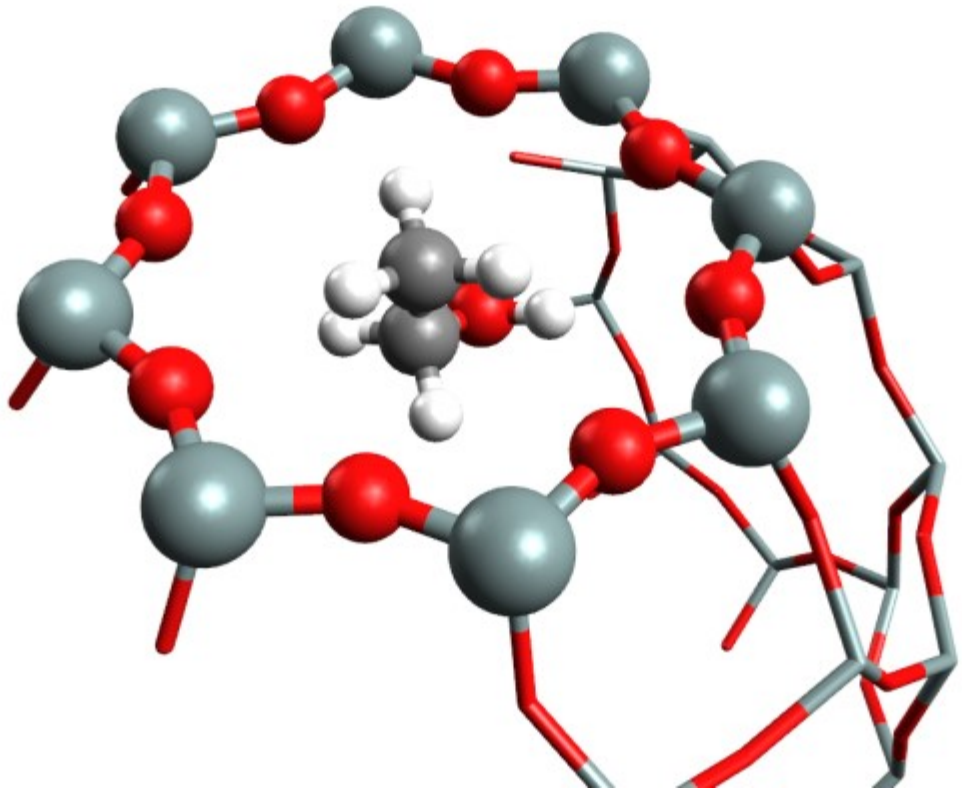

LTA-1-propanol-S2_vdw_surface-OH

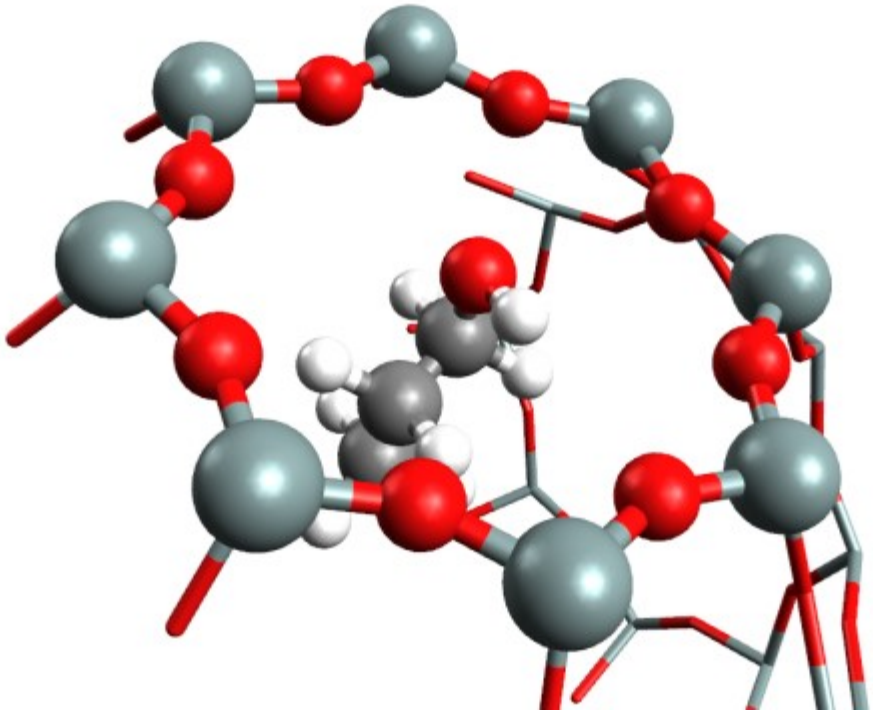

LTA-isobutanol-S2_vdw_surface-OH

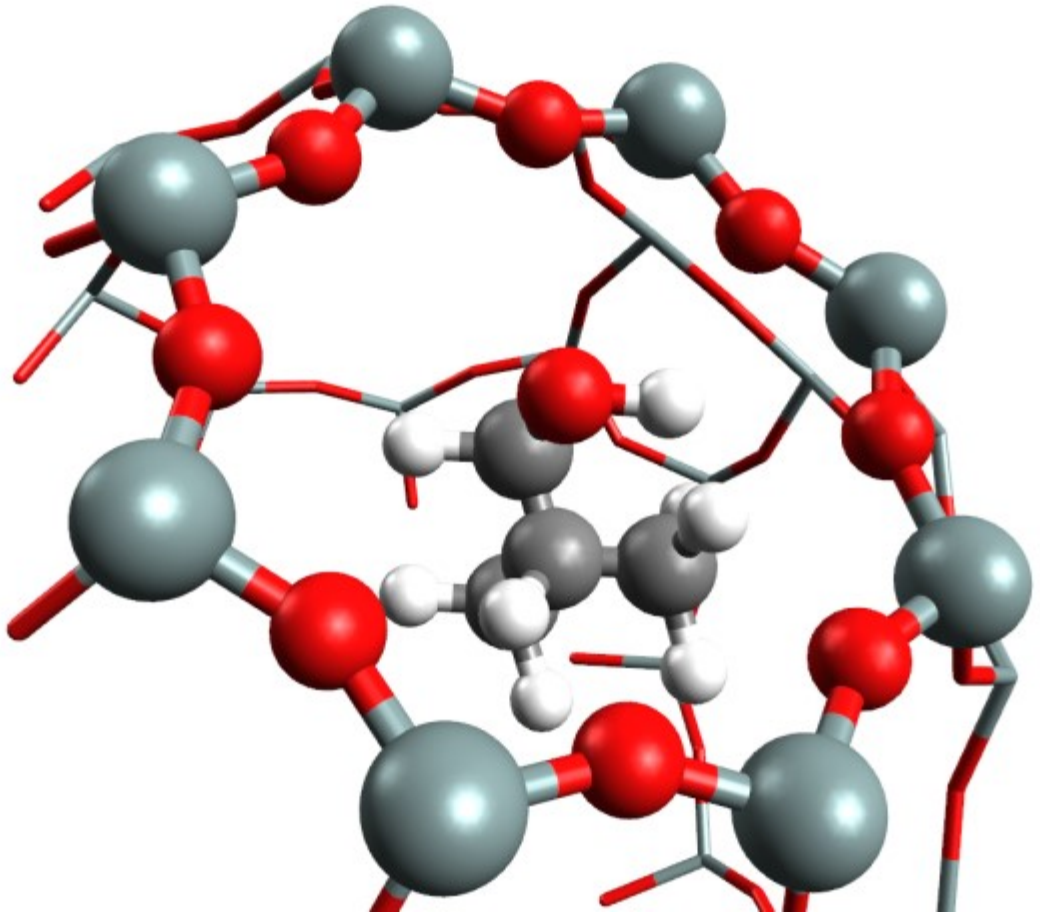

LTA-isobutanol-S2_vdw_surface-3H

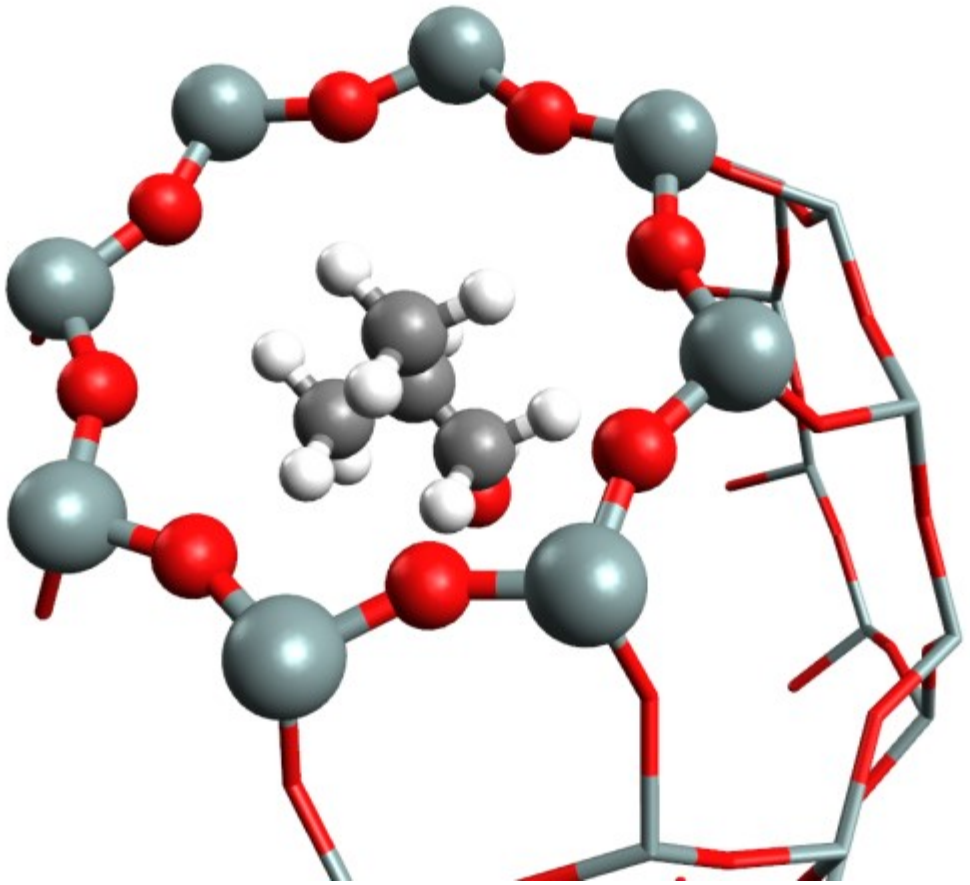

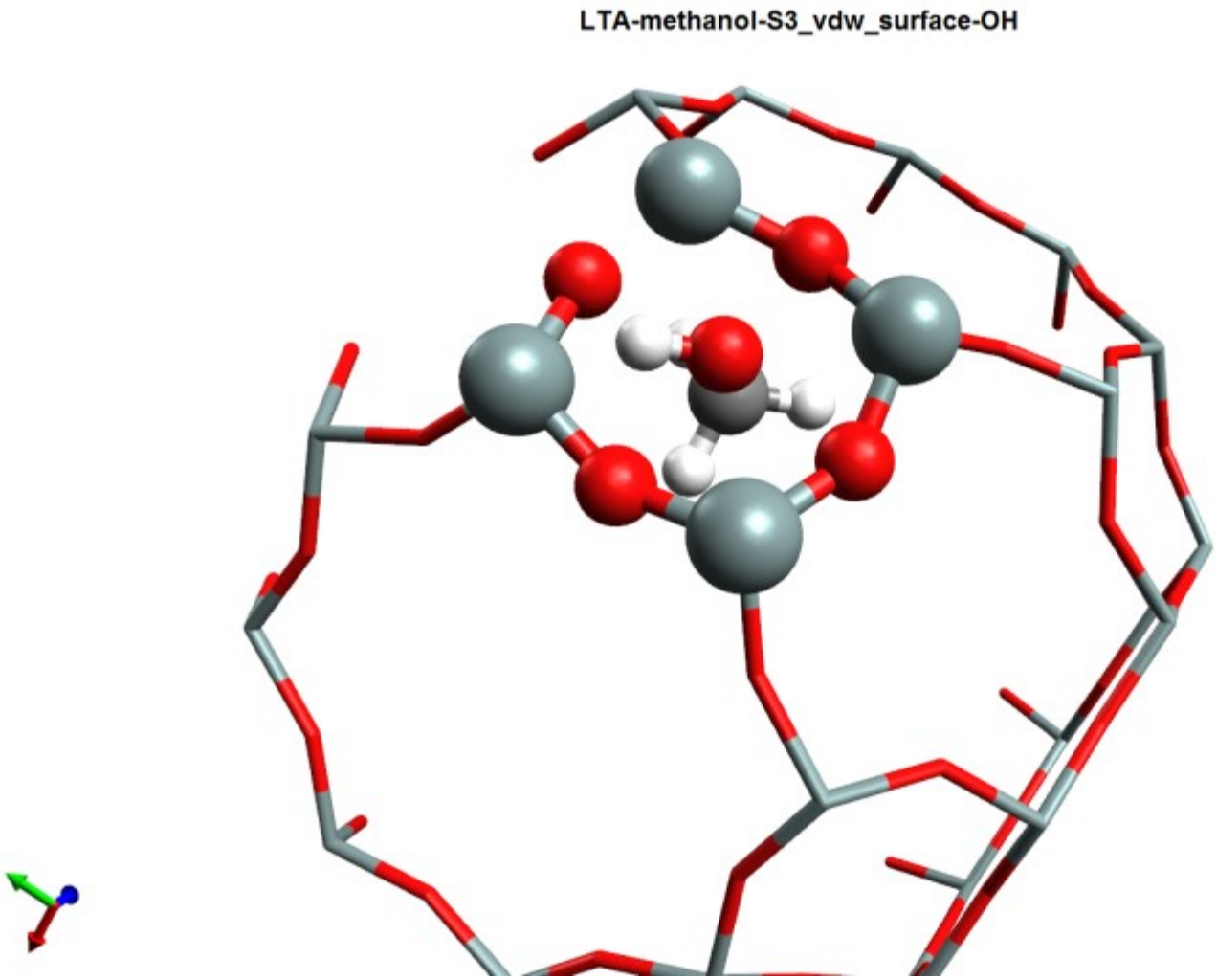
LTA-methanol-S3_vdw_surface-OH

LTA-methanol-S3_vdw_surface-3H

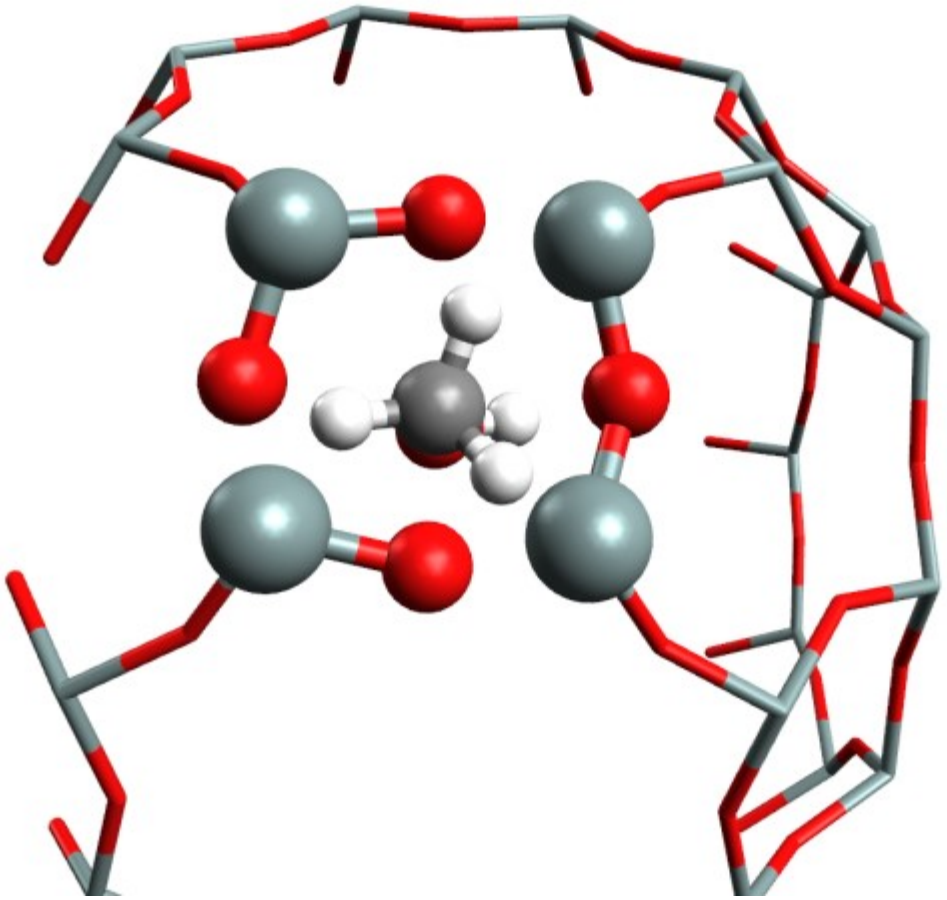

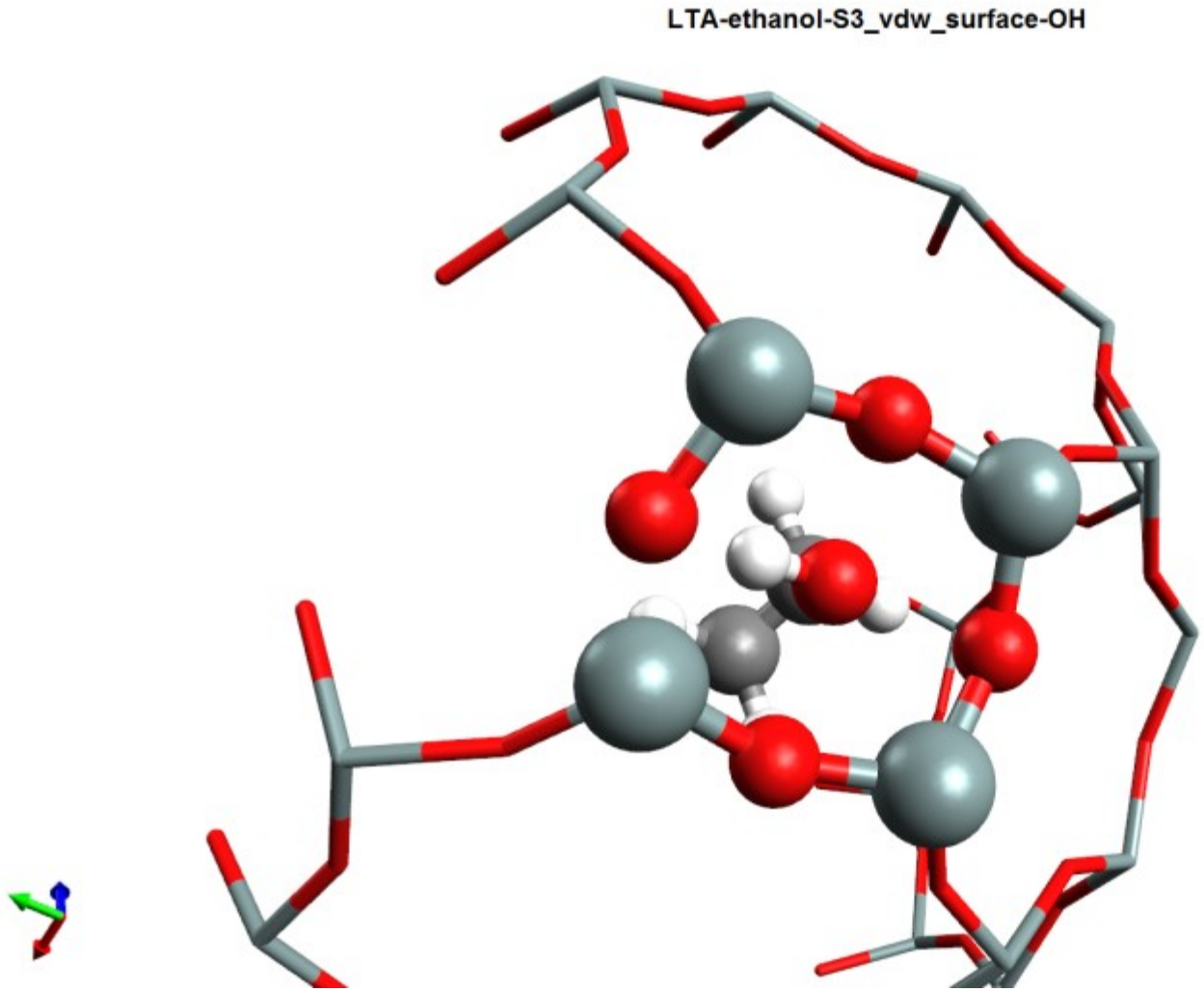
LTA-ethanol-S3_vdw_surface-OH

LTA-ethanol-S3_vdw_surface-3H

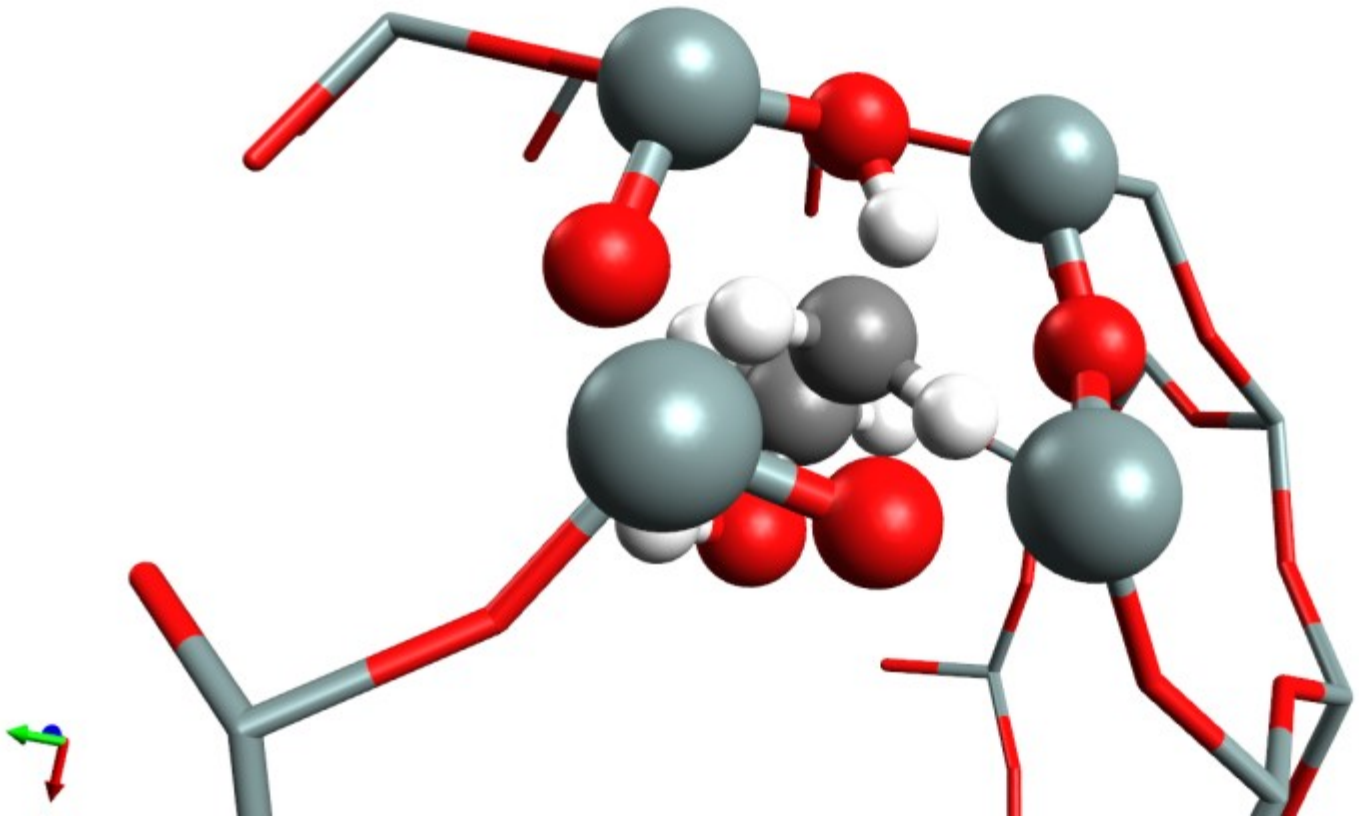

LTA-1-propanol-S3_vdw_surface-OH

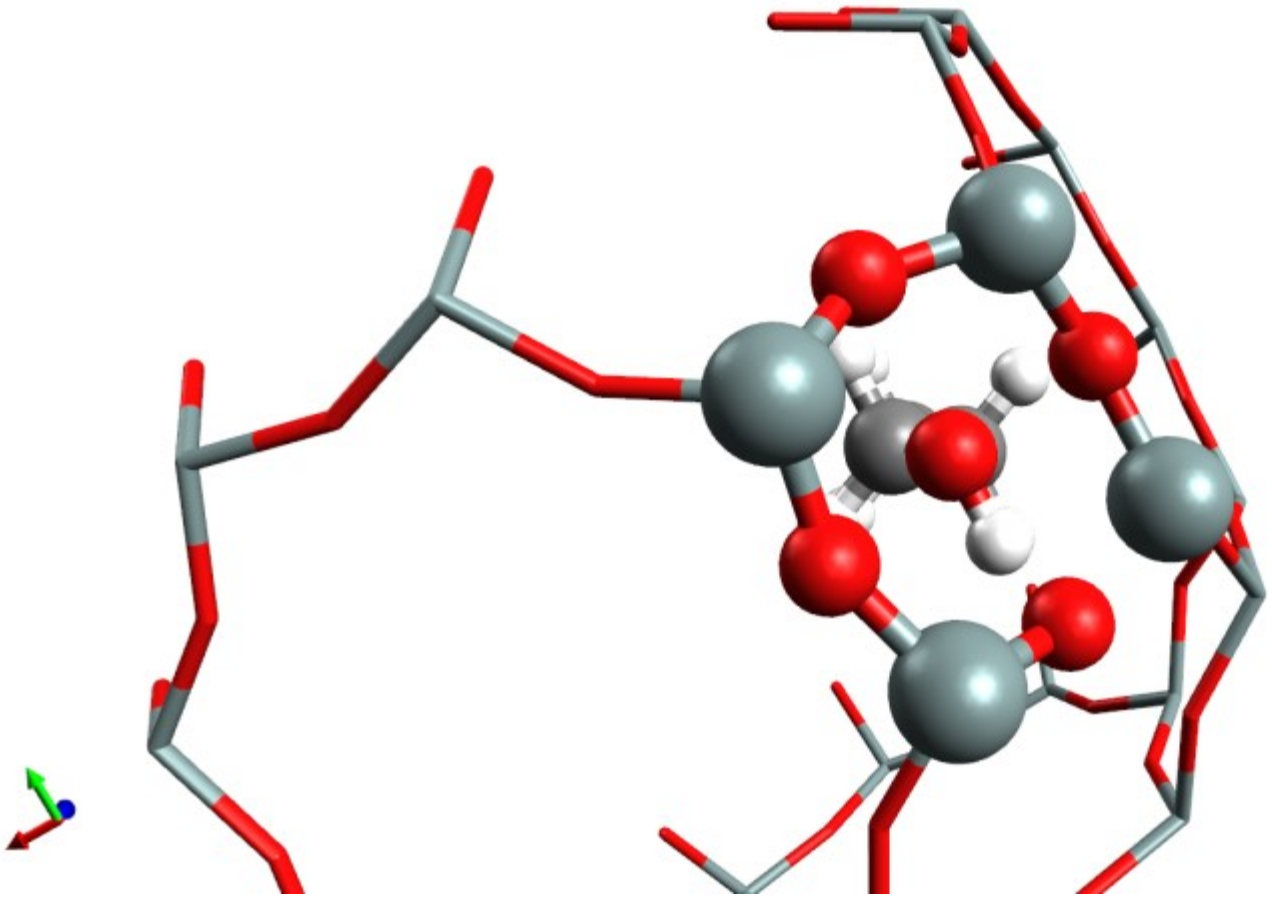

LTA-ethanol-S3_vdw_surface-3H

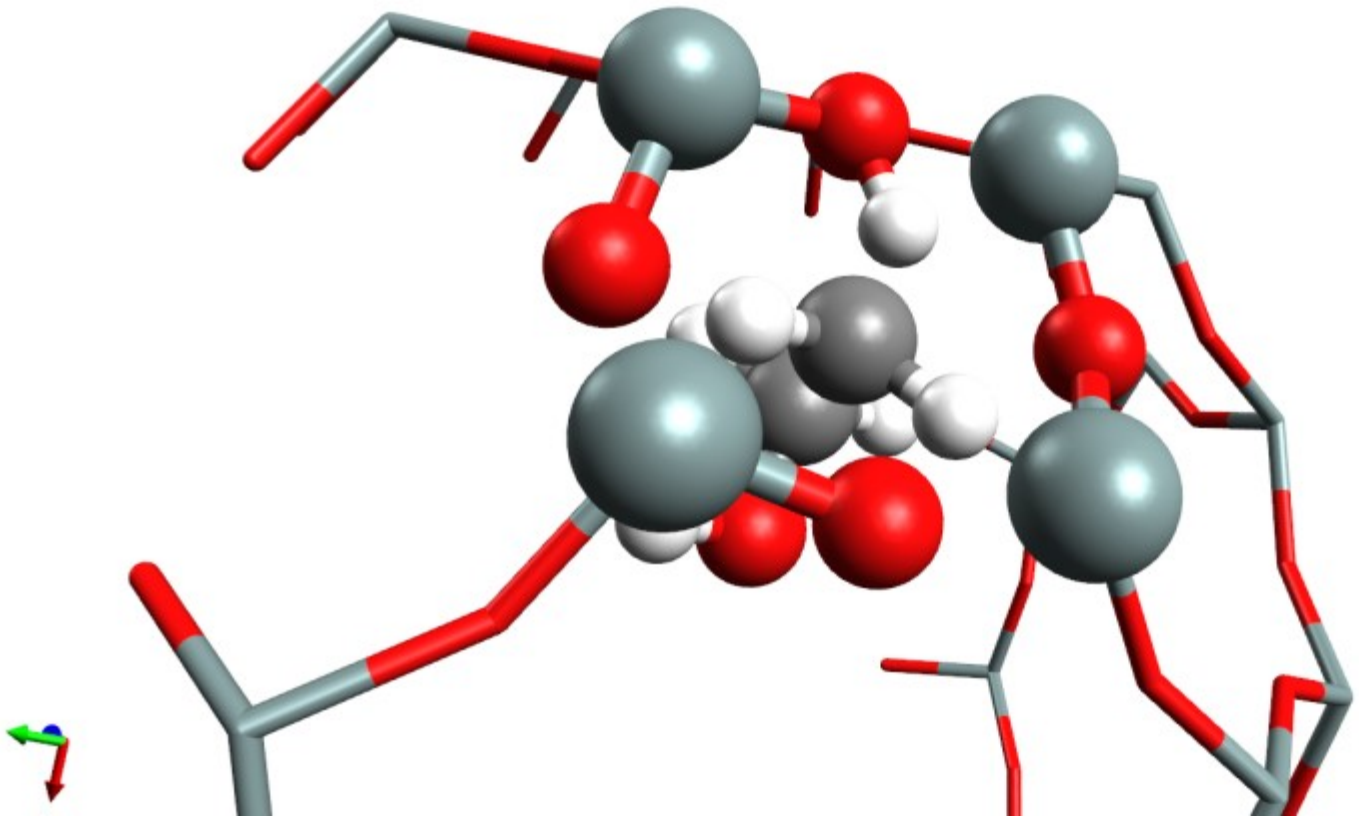

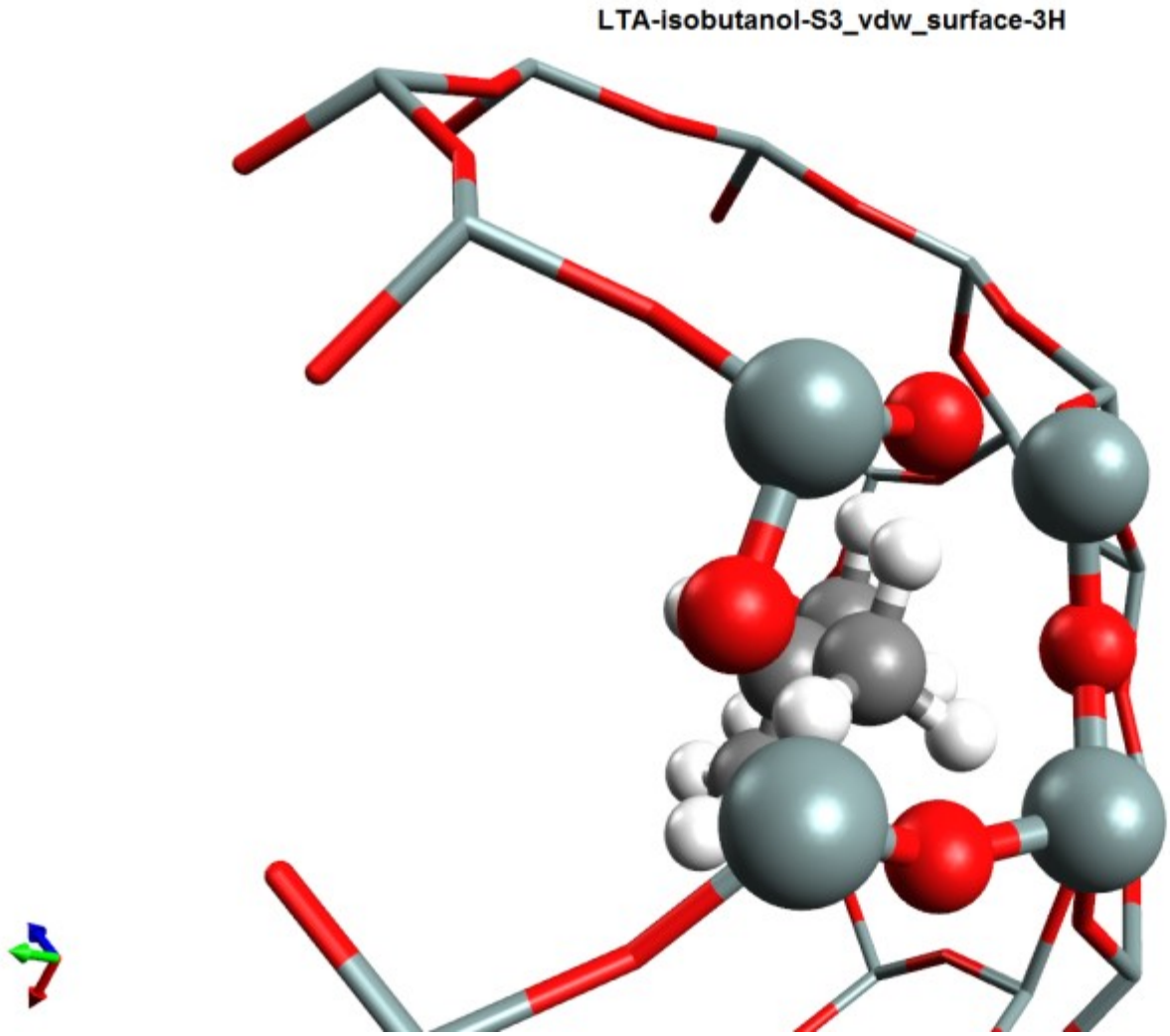
LTA-isobutanol-S3_vdw_surface-3H